1-1-1992

The influence of high voltage discharge on flat plate drag at low Reynolds number air flow

Frans Soetomo
Iowa State University

The influence of high voltage discharge on flat plate drag at low Reynolds number air flow

by

Frans Soetomo

A Thesis Submitted to the
Graduate Faculty in Partial Fulfillment of the
Requirements for the Degree of
MASTER OF SCIENCE

Major: Mechanical Engineering

Iowa State University
Ames, Iowa
1992

TABLE OF CONTENTS

LIST OF TABLES

LIST OF FIGURES

ACKNOWLEDGEMENTS

I would like to thank Dr. Gerald M. Colver, my major professor, who patiently guided and assisted me during the course of this study. I have learned a lot from him. I am also indebted to my committee, Dr. Howard N. Shapiro and Dr. Ambar K. Mitra, for their interest and invaluable suggestions.

Next, I would like to extend my gratitude to Mr. Robert D. Steed, Mr. Gaylord N. Scandrett, Mr. James J. Dautremont and Mr. Brian T. Espeland, Department of Mechanical Engineering, and also Mr. Thomas J. Elliott of Engineering Science and Mechanics, who helped me throughout the experiment. Thanks to my colleagues in the Particulates Laboratory, Tsai Hsin-chuan and David R. Tucholski, who made my time at Iowa State University enjoyable. I would also like to acknowledge partial financial support from the International Fine Particle Research Institute.

Finally, I would like to offer my sincere appreciation to my loving families, biological and adopted, for their continuous encouragement and support. Special appreciation goes to my dearest sister, Sara Leighanne Norris. Without her, this project would not be finished.

I can do all things through Christ who strengthens me.

(Phillippians 4:13)

ABSTRACT

Attempts to reduce the drag of a solid surface immersed in a fluid flow have previously been investigated both experimentally and theoretically, and various techniques have resulted. The present study enriches these results by utilizing a high voltage discharge (ionic wind) to affect the boundary layer on a flat plate made of glass in a subsonic, low speed wind tunnel, with Reynolds number ranging from 1.1×10^3 to 3.6×10^3.

The experimental apparatus used was developed in previous research in the Particulate Laboratory in the Mechanical Engineering Department and was further perfected here. The first study presented is a measurement of the plate drag without a discharge. This result is compared to theoretical drag calculations based on formulas available in the literature. The results of high voltage discharge implementation on the drag measurement indicate that the discharge has a significant effect on the plate drag. The results are supported by statistical analysis giving a comparison of the uniformities and analysis of variance.

NOMENCLATURE

A	Area
C_D	Drag coefficient
C_{DW}	Drag coefficient of the wire
$C_D{}'$	Alternative form of drag coefficient
D	Height of finite flat plate
E	Modulus of elasticity (Young's modulus)
F	Load, Random variable of F distribution
F_D	Plate's drag force
$F_D{}'$	Plate's drag sensed by only one beam
F_T	Total drag force
$F_T{}'$	Total drag sensed by only one beam
F_W	Wire's drag force
F_{ion}	Ionic wind force
I	Current, Moment of inertia
I'	Ion current per unit width
J	Current density
K	Ion mobility
L	Length of finite flat plate, Length of beam

M	Bending moment
P	Probability
R	External resistor
R_i	Total impedance
Re	Reynolds number
Re_L	Reynolds number based on length of plate
Re_x	Reynolds number based on entrance length of wind tunnel
T_{room}	Room temperature
U	Free stream velocity
V	Velocity, Voltage
V_q	Drift velocity
V_{rms}	Root mean square value of the voltage
W	Distributed load
W_1, W_2	Wire drag force

a	Length of part of a beam
b	Width of finite flat plate
c	Distance from neutral axis to the surface of a beam
f	Electrostatic body force per unit volume within the boundary layer
f'	Electrostatic body force per unit volume outside the boundary layer
$\bar{f}$	Mean body force
g	Gravity
j	Ion current
n	Number of data, Ion number density

p	Pressure
q	Charge
rh	Relative humidity
s^2	Sample variance
u	Velocity
w	Width of the plate across the flow
x	Entrance length, Individual data
y_{max}	Maximum beam deflection

Greek

α	Probability that a variable will exceed a certain value
β	A constant
δ	Boundary-layer thickness
δ'	Minimum distance from tunnel wall to glass plate
μ	Dynamic viscosity
ν	Degree of freedom
ρ	Air density
σ	Stress
σ^2	Total variance
χ^2	Random variable of χ^2 distribution

Superscript

*	Dimensionless variable

Subscript

∞	Related to the free-stream
W	Related to the wire
f	Related to the skin-friction
p	Related to the pressure or form
w	Related to the wall

CHAPTER 1. INTRODUCTION

Overview

In most applications of fluid mechanics, the drag force created by fluid flowing over a solid surface is a very important aspect of the performance of the system, whether it be a transport vehicle, weapon, or flow through a long distance pipeline. Unlike the first two cases, where the drag force is comprised of *pressure* and *viscous* drag, the flow through a pipe is purely *viscous* drag.

Pressure drag is caused by the pressure difference between upstream and downstream flow over the body due to its geometry. This drag can be reduced or eliminated by streamlining or fairing the body shape[13][1], and is not considered in the present study. Viscous drag on the other hand, is present in a zero pressure gradient, being caused by the shear stress distribution due to the skin friction. This drag is currently considered a major barrier to the further optimization of most aerodynamics and hydrodynamics bodies[5]. For this reason, intense research to reduce this drag is still in progress.

So far, the results of these research efforts have found applications in broad areas such as high speed aircraft and missiles (order of 30-40% skin-friction drag); transport aircraft, cruise missiles, and tankers/other surface ships operated at low Froude

[1] In automobile design it is called *bobtailing*[28].

number (order of 50% skin-friction drag); most underwater bodies (70% or greater skin-friction drag); long distance pipelines; liquid lithium blankets of fusion reactors; and some prestigious applications such as the America's Cup Races or the Olympics; where even a small viscous drag reductions can have large impacts. Economically, 5-10% viscous drag changes can produce savings in the order of half a billion dollars per year[5].

Several classes of transport, notably automobiles, trucks, and helicopters, are still impacted to zeroth order by pressure drag, and therefore these devices would not benefit materially from viscous drag reduction at the present time as viscous drag is a small portion of their overall drag budget.

Viscous Drag Reduction

Depending on the application, viscous drag can be observed in three different regimes [5]. The first one is laminar boundary layer regime, where the body Reynolds number is relatively low ($Re_L < 10^6$). In this case the drag-reduction problem is reducing laminar skin friction. Previous researchers proposed several techniques on this problem, including:

- Reducing the tangential momentum accommodation coefficient, e.g., introducing a slip velocity at the surface
- Use of convex longitudinal curvature
- Adverse longitudinal pressure gradients
- Fluid injection through the wall

In the second problem—where the range of the Reynolds number is generally from 1×10^6 to 10×10^6 (or greater)— the boundary layer is transitional. The drag-reduction problem is to delay the start of this transition process for as long as possible. The techniques—also called laminar flow control (LFC)—implemented so far include:

- Wall suction
- Favorable pressure gradient (on two-dimensional or axisymmetric bodies at small incidence)
- Wall heating (in water) or cooling (in air)
- Compliant surfaces (in water)

The third problem is the turbulent boundary layer regime, where the Reynolds number is greater than 10×10^6. This regime is of a great interest since it has many technological applications including high speed airplanes, spacecrafts, and missiles. Several applicable techniques include:

- Passive turbulent drag reduction:
  - Riblets
  - Outer-layer manipulators
  - Convex curvature concept
- Active turbulent drag reduction:
  - MHD flow drag reduction

- Gas injection
- Polymer and surfactants applications
- Particle addition
- Surface mass injection

- Interactive wall turbulence control [5] (or flexible wall [33])

In the present study the range of interest of the Reynolds number is from 1.1×10^3 to 3.6×10^3 (based on the length of a flat plate); therefore, it is obvious that we are dealing with laminar flow. Unlike the techniques noted above, the method used in the present study utilized a high voltage electric discharge (ionic wind) driven by high voltage power source to manipulate momentum in the boundary layer. The electric discharge method may be applicable to low speed drag reduction as with helicopter rotors by reducing drag due to separation.

Corona Discharge

The first recorded form of corona was probably the *Saint Elmo's Fire*[2], which appears as a flamelike reddish or bluish lights on the tops of masts and on the ends of yardarms during stormy weather at sea[1]. Because the rounded head of the mast wore this light like a crown or halo, it was later referred to as *corona* by the Latin-oriented scholars of that day. To this day, the term *corona* is used to describe electrical discharge phenomena occurring either internally or externally, in or on electrical apparatus or devices.

[2]Saint Elmo was the sailors' patron saint; therefore, the sailors believed they were being protected by the corona. Actually, the masts were acting as lightning rods and were indeed protecting them.

The ASTM Standard Method for Detection and Measurement of Discharge (Corona) Pulses in Evaluation of Insulation Systems (D 1868-73) defines *corona* or *partial discharge* as a type of localized discharge resulting from transient gaseous ionization in an insulation system when the voltage stress exceeds a critical value[1]. Cobine [6] defines the term *corona* in a more specific way as a glow discharge at atmospheric pressure which results from gas breakdown near a surface at a voltage less than the spark-breakdown voltage for a given gap length. Leob (cited by Malik, et al. [22]) describes corona as the general class of luminous phenomena associated with the current jump to microamperes at the highly stressed electrode preceding a spark breakdown of the gap.

The appearance of corona is always accompanied by a hissing sound (especially in a high humidity environment) together with the generation of ultraviolet radiation and a strong oxidizing agent, such as ozone, which is poisonous. It also causes chemical and mechanical destruction of adjacent material's surfaces by ion bombardment and interferes with radio communication within the usual broadcast band frequency spectrum. These characteristics often make corona discharges undesirable—especially in electrical equipment—because of their destructive effects. However, with these very same properties, corona discharges perform important commercial services in many areas ranging from xerography to ore separations[1].

Another important effect of corona discharge is the generation of electric or ionic wind. It is known that a charged needle electrode that produces corona also generates a wind that blows parallel to the needle and in the direction indicated by the point, as shown in Figure 1.1. It will blow a flame on a Bunsen burner to one side if the point is positively charged. A negatively charged point has the effect of wind partly

reduced by the fact that the flame carries positive ions. The concept of ionic wind has also found several engineering applications in heat and mass transfer problems. For instance, it has been observed that proper generation of ionic wind could augment heat transfer up to 200 % [22].

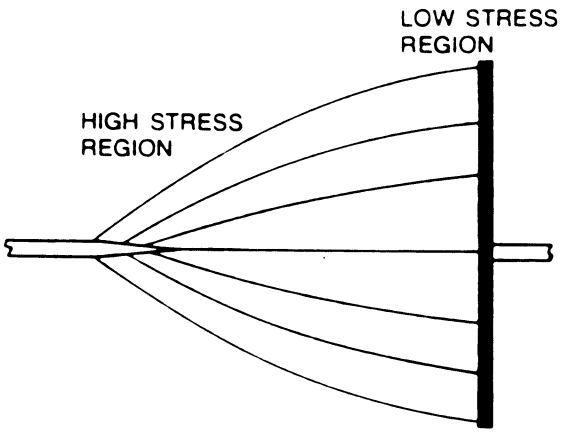

Figure 1.1: Point-to-plane electrode system

Lawton [20] and Weinberg [32], together and individually, have conducted investigations on high voltage discharge in combustion and flame control. They found that the wind effects can be used, for example, to modify flame shape and stability (Figure 1.2), rates of flame propagation, entrainment of air into fuel, combustion intensity, heat transfer from flames to solid surfaces, and rates of flame spread in solid propellants.

Colver and Nakai [7] have qualitatively investigated the effect of a corona discharge on a boundary layer near a semi-insulating wall, such as hot glass, using a

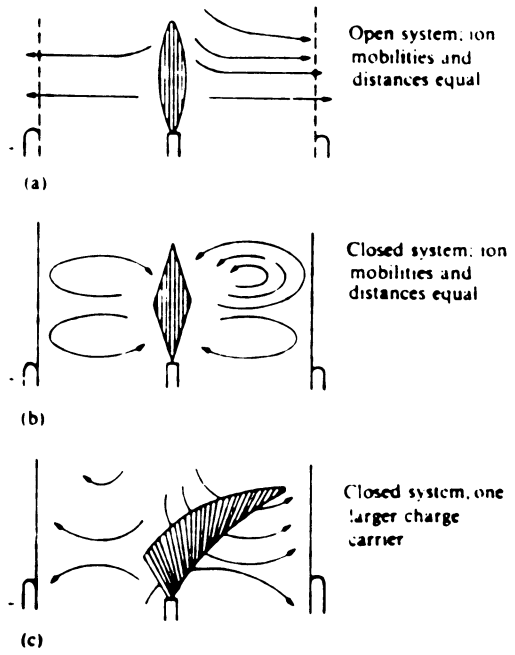

Figure 1.2: Flow patterns and flame shape

flame as a visual indicator. They observed that the electrical conductivity of the wall has a significant influence on the discharge and therefore on the momentum added to the boundary layer. Application of these ionic wind-wall effects may be useful where control of the boundary layer or of the flame is desirable.

Present Study

It is known that a solid surface coating with a magnetic fluid layer on the free-stream flow structure has an effect on the hydrodynamic drag by controlling the flow separation[23]. Based on previous research, it was hypothesized [Colver, personal

communication] that a discharge of corona over the contour of a sphere may be used as a method of separation control since separation is the main contributor to the drag force. In order to provide evidence to support his hypothesis, a wind tunnel was built in the Particulate Laboratory of the Mechanical Engineering Department, Iowa State University[12].

It was demonstrated earlier in laboratory tests that a glass sphere, when heated, will allow a corona discharge to wrap around its contour. Figure 1.3 illustrates the phenomenon. It was suggested that if this *induced electrical boundary layer* is intense enough, it actually can create a no-slip condition and thus either move the separation point further downstream (delay the separation) or even prevent it. This hypothesis was also supported by Malik et al. [22] However, due to the difficulties in the mounting method, the idea of testing a glass sphere was changed to a glass plate. Razor blades were used as *line* electrodes to produce a scattered distribution over the plate, rather than needles as *point* electrodes which are able only to produce a concentrated corona distribution. Figure 1.4 illustrates the final configuration. Figures 1.5 through 1.8 show photographs of corona discharge from blade-electrodes with and without the glass plate.

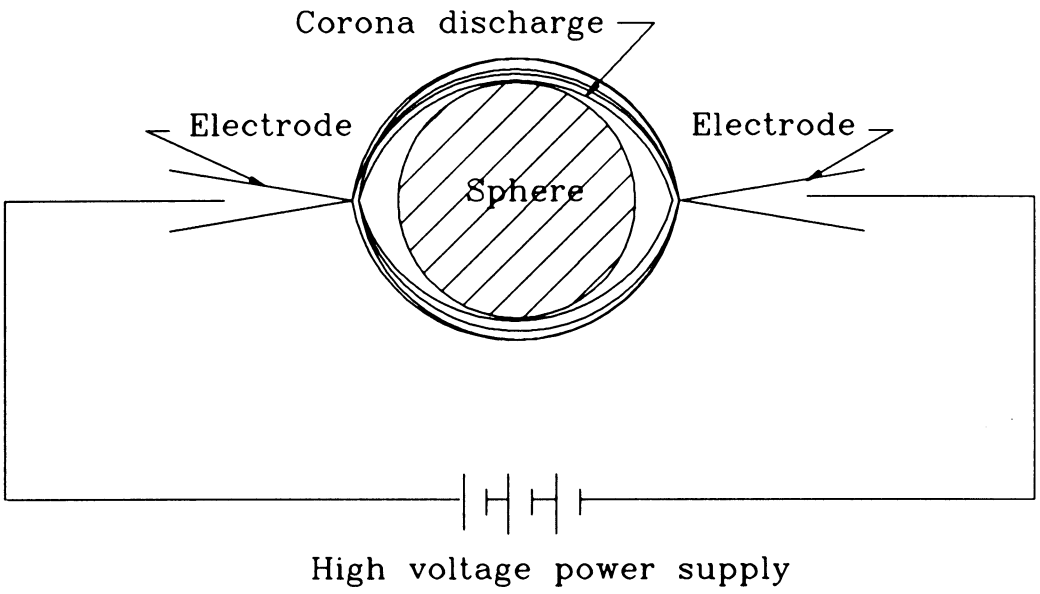

Figure 1.3: Induced electrical boundary layer

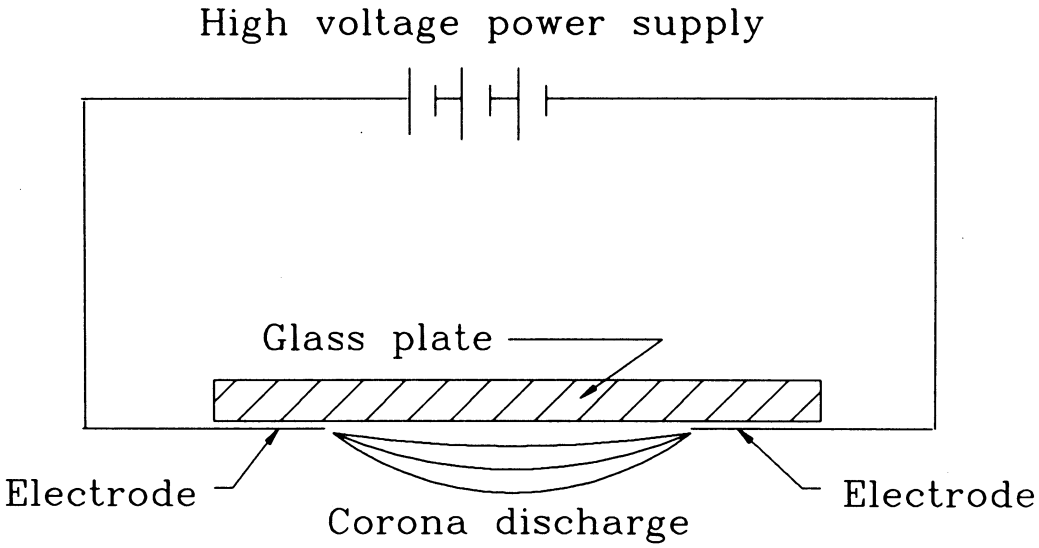

Figure 1.4: Induced electrical boundary layer over a plate

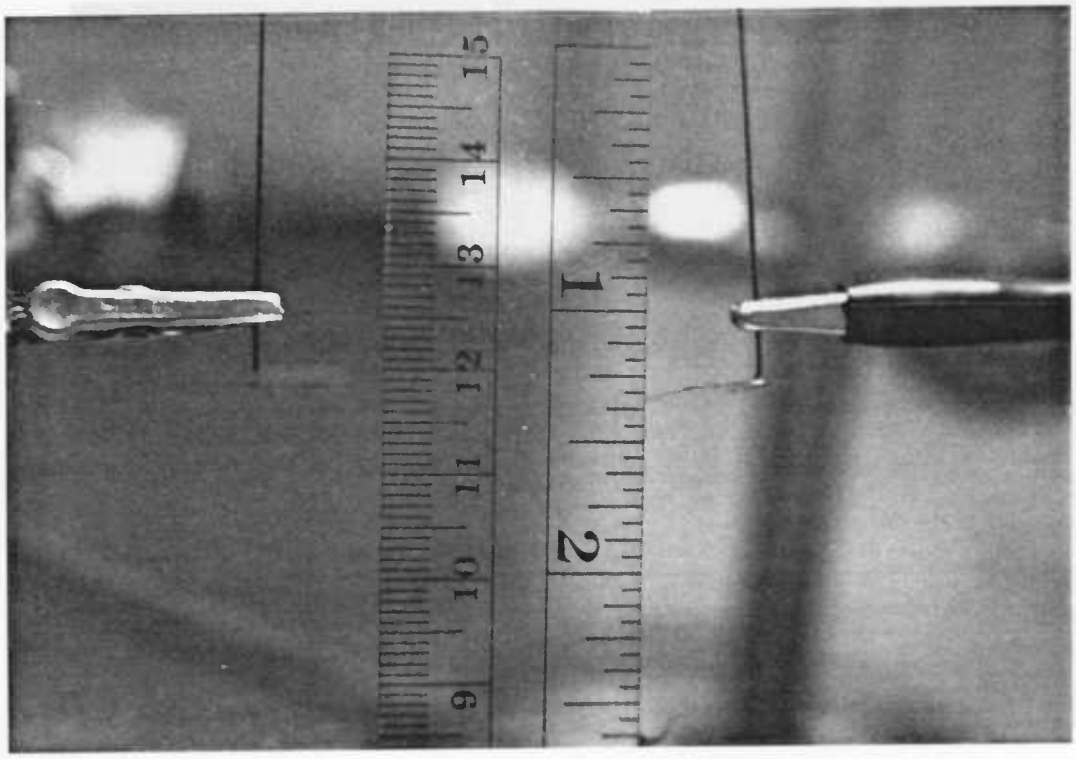

Figure 1.5: Blade-electrodes without glass plate: set up

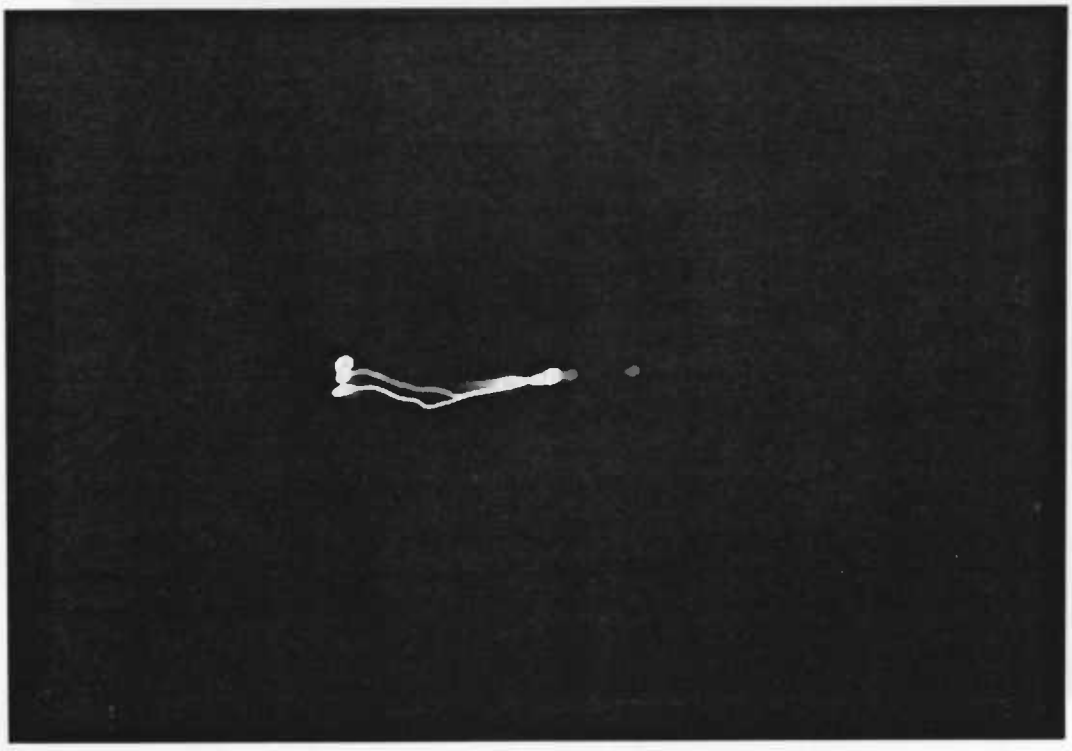

Figure 1.6: Blade-electrodes without glass plate: corona discharge

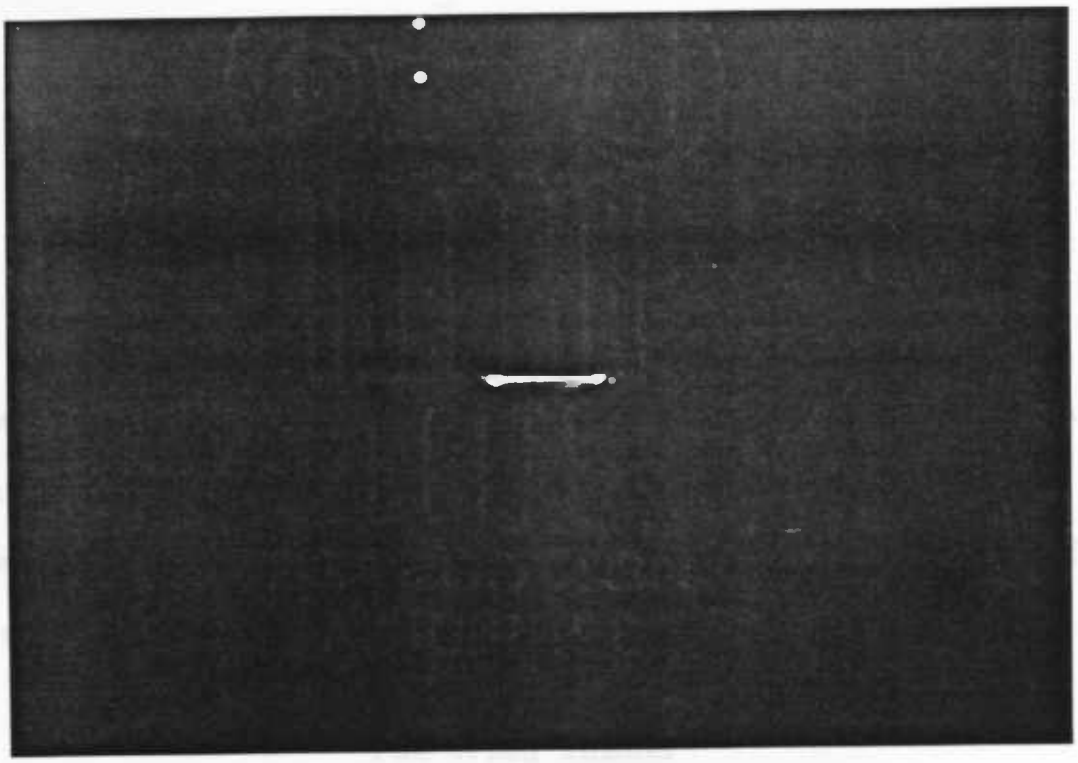

Figure 1.7: Blade-electrodes with glass plate: side view

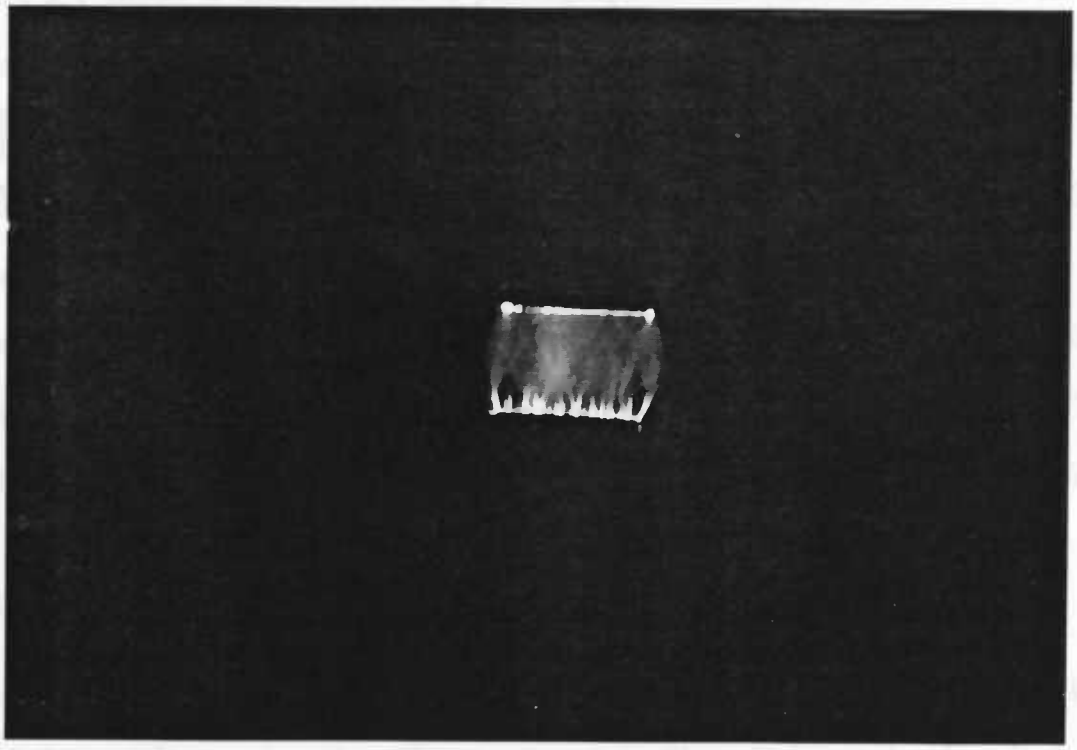

Figure 1.8: Blade-electrodes with glass plate: top view

CHAPTER 2. EXPERIMENTAL APPARATUS

The basic equipment used in this experiment was built by Kaveh Forouraghi[12], and consists of the wind tunnel and the force sensor. This equipment was later developed to be used specifically for measuring plate drag under the influence of high voltage electric discharge.

The Wind Tunnel

Figure 2.1 shows a diagram and a photograph of the wind tunnel used in this experiment. It is an open circuit air tunnel with a rectangular test section measuring $18\frac{1}{4} \times 6\frac{3}{8} \times 4\frac{1}{8}$ inches with two transparent windows on top and on the front. The air is pulled by a squirrel cage fan of radial vanes by an ac motor of $\frac{1}{2}$ hp. This centrifugal fan is mounted in a round sheet metal housing.

Air speed was measured by a pitot-static tube which was mounted on the front side of the test section with the aid of a pressure transducer and a manometer. This air speed was regulated by a variable transformer connected to the centrifugal fan.

Pitot-static tube

The pitot-static probe used was of the round nose type with static and total pressure holes on the sensing tip. The sensing stem diameter was $\frac{1}{16}$ of an inch and

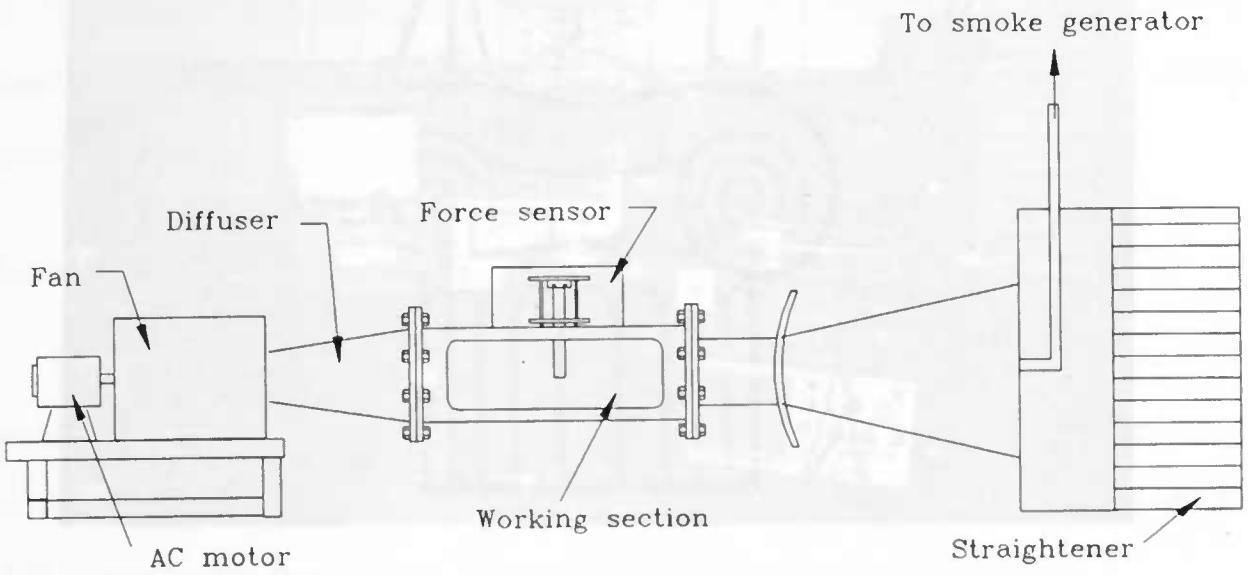

Figure 2.1: The Wind Tunnel

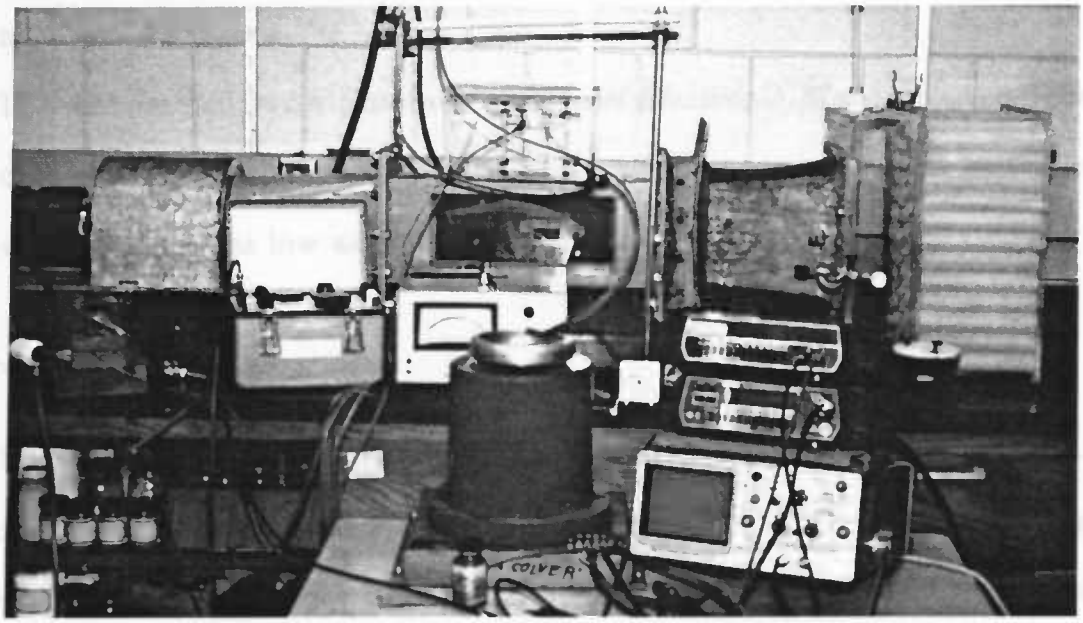

Figure 2.2: Photograph of the wind tunnel with measuring instruments

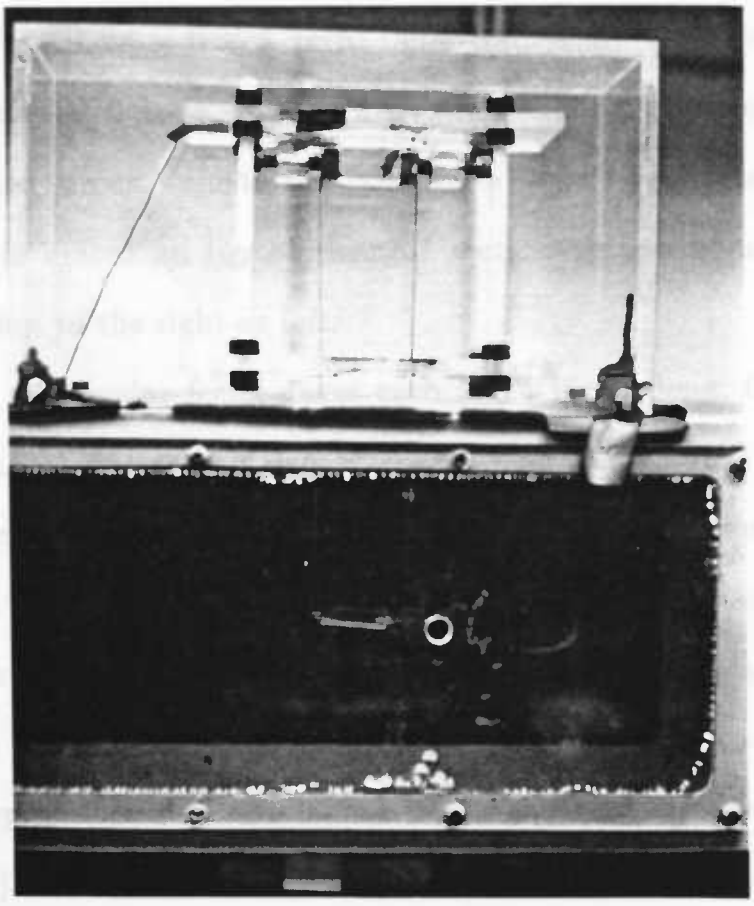

Figure 2.3: Photograph of the force sensor

its length was 12 inches.

The manometer was a *Datametric Barocel Electronic Manometer* equipped with Barocel Pressure Sensor with 100-torr range. The system is capable of measuring pressure differences as low as 0.002 torr.

Force sensor

Figure 2.4 shows the sensor designed for measuring the drag of a flat plate. The device consists of a threaded rod-support mechanism which holds two sensing beams to be connected to the plate-wire suspension system. Figure 2.3 shows a photograph of the force sensor mounted on top of wind tunnel's test section.

The threaded rod-support assembly consists of two upper and lower frames made out of plexiglass each $2\frac{3}{8} \times 6 \times \frac{1}{4}$ inch. The frames are connected to each other by four plastic threaded rods which are five inches long. The upper plate has a support protrusion which adjusts the separation of the two sensing beams. The whole assembly is bolted on top of the test section by two adjusting screws that allow linear motion to the right or left.

The beams are regular feeler gages each 2.875 inches long, 0.5 inch wide and 0.005 inch thick, which are soldered to music wire, 0.0184 inch in diameter and 3.9375 inches long to obtain good electrical conductivity. The wires pass through 0.5 inch holes in the cover of a transparent window on top of the test section. This cover was necessary to prevent air leaking through the window. The drag is sensed by the left beam which has two precision strain gages mounted at its base. The gages are of a general purpose family of constantan strain gages widely used in experimental stress analysis[3].

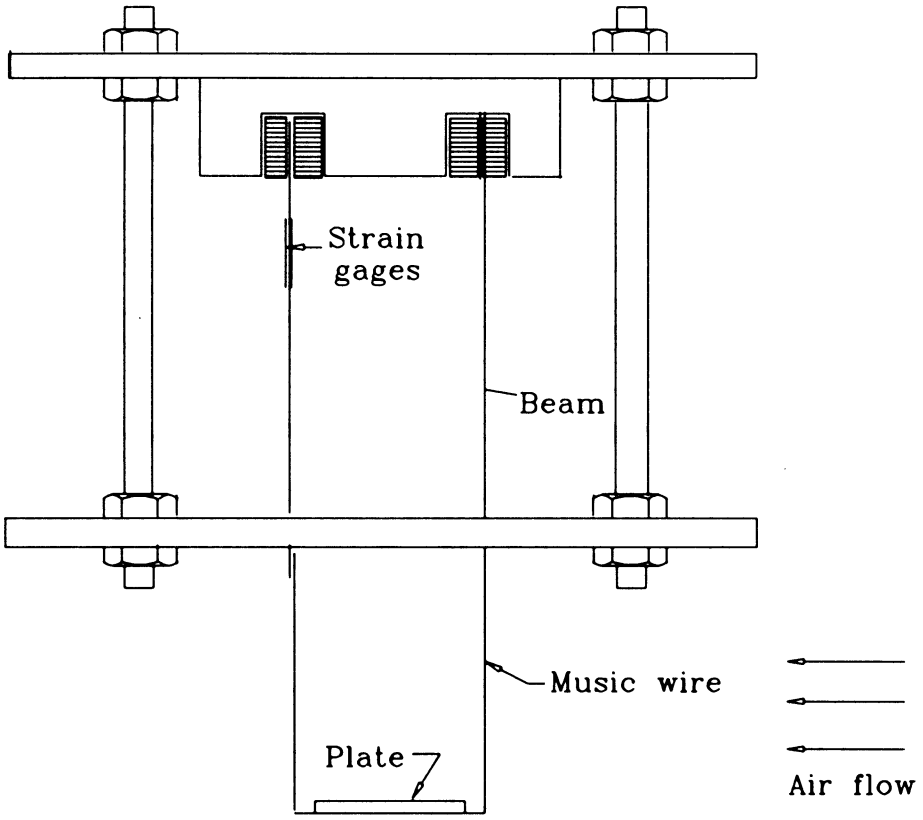

Figure 2.4: Force Sensor

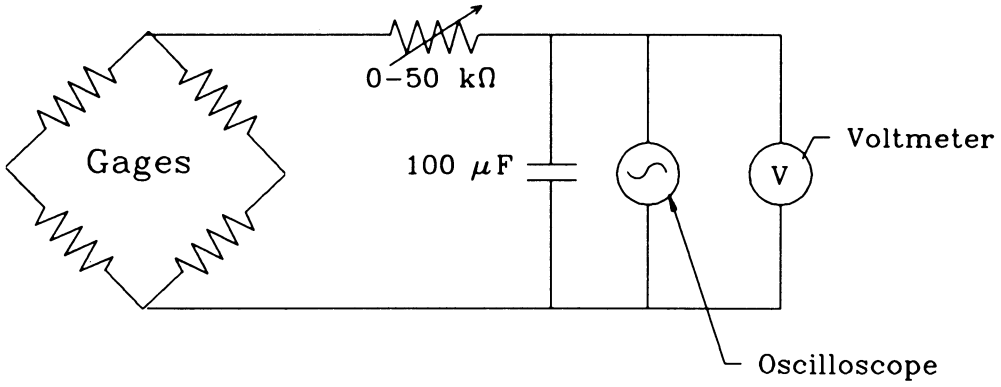

Figure 2.5: RC circuit

The output of the gages is sensed by a null-balance type of static strain indicator connected to an RC circuit to produce smooth and readable signal and to reduce noise. This circuit has two outputs. One goes to a *Keithley* digital multimeter and the other to a *Tektronix* oscilloscope. The sensor was calibrated versus the millivolts read on the voltmeter and the scope[1].

High Voltage Power Source

The AC power supply used in this research was a *Hipotronics AC Dielectric Test Set*, capable of providing high voltage up to 30 kV AC and current up to 20 mA. The output frequency of this device was 60 Hz. The DC power supply was a *Hipotronics HV DC Power Supply*, capable of providing high voltage up to 50 kV DC and current up to 5 mA. Since corona discharge requires both a high voltage and a low current[1], a 15 MΩ resistor was mounted on the charged line and was capable of limiting the current reading to approximately 0.3 mA for 20 kV output voltage under shorting condition. The current was measured using a digital voltmeter and oscilloscope with the aid of two resistors 10 kΩ (nominal) and a switch box, enabling some readings to be taken at the same time[2].

Two razor blades, 0.004 inch thick and $\frac{7}{8}$ inch wide, were used as the *line*-electrodes to produce a uniform corona distribution over the plate. These blades were soldered[3] to the tips of the wires and glued to a piece of precleaned microscope slide 75 × 25 × 1 mm.

---

[1] See Appendix A for details of calibration.

[2] See Appendix C for details.

[3] See Figure 1.4 for the final configuration of plate-wire suspension system.

CHAPTER 3. THEORETICAL DRAG CALCULATION

To verify the validity of drag measurement on a flat plate, a *standard drag curve* was used as a comparison to the experimental value. The purpose of this chapter is to discuss how such a curve was developed.

Unlike spheres and circular cylinders, flat plates do not have a standard drag curve. One of the reasons is because the exact solutions for flat plate drag have been developed. For purposes of this research it was considered necessary to approximate a *standard* drag curve based on these solutions. Unfortunately, most available solutions were intended to calculate skin-friction drag of an infinite flat plate[13][24][27][34], based on the Blasius boundary layer solution. As an approximation, the plate's drag was divided into two parts: skin-friction drag for the surfaces parallel to the flow, and pressure drag for the surface normal to the flow.

(a) (b) (c)

Figure 3.1: Approximation to the finite-flat-plate drag: (a) skin-friction drag, (b) pressure drag, (c) combination drag

Plate Parallel to The Flow

Based on an exact solution to the boundary-layer equations corresponding to a uniform flow over a flat surface developed by Blasius [9], the *skin-friction drag* on one side of a flat plate is defined to be:

$$C_D = \frac{1.328}{\sqrt{Re_L}} \tag{3.1}$$

where $Re_L = \rho U_\infty L/\mu$ denotes the Reynolds number based on the length of the plate and U_∞ is the free-stream velocity.

Equation 3.1 was developed for an infinite flat plate, without taking into consideration the leading- and trailing-edge effect and is valid only in the region of laminar flow, i.e. for $Re_L < 5 \times 10^5$ to 10^6[27].

Boundary-layer equations of higher order have been developed extensively to solve difficulties on the leading- and trailing-edge region. Imai [17] solved the leading-edge problem based on an asymptotic expansions of the solutions of the Navier-Stokes equations. The result to the second order is

$$C_D \sim \frac{1.328}{\sqrt{Re_L}} + \frac{2.326}{Re_L} \tag{3.2}$$

for one side of the plate. Van Dyke[30] proposed a revision on the skin-friction coefficient based on the work by Kuo [19]:

$$C_D \sim \frac{1.328}{\sqrt{Re_L}} + \frac{5.3}{Re_L} \tag{3.3}$$

Later on, it was discovered that the flow near the trailing edge of a finite-length flat plate has a *triple-deck* structure[35], illustrated in Figure 3.2. The triple-deck region is of size $Re^{-3/8}$, centered about the trailing edge, merging upstream with

two-layer flow and downstream with a two-layer wake. Near the wall, dominated by viscous effects, is the *lower* deck, of size $Re^{-5/8}$, which enforces the no-slip condition at the inner boundary. This is patched by velocity and pressure to the *main* deck, of size $Re^{-1/2}$, in which viscous effects are secondary. Finally, there is an *upper* deck, of purely potential flow, which is controlled by changes in the main deck. Centered in a radius of size $Re^{-3/4}$ about the trailing edge is a small region where the full equations of motion are needed.

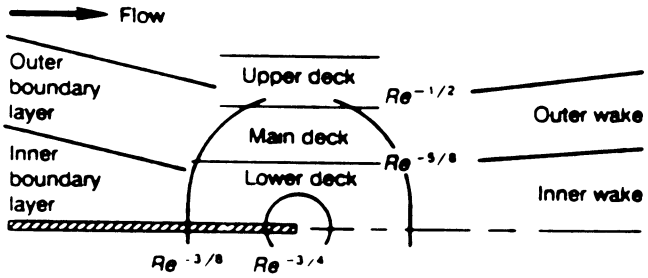

Figure 3.2: Sketch of the triple-deck region at the trailing edge of a flat plate, merging into two-layer upstream and downstream regions

The friction drag from triple-deck theory predicts a new contribution from the trailing edge:

$$C_D = \frac{1.328}{{Re_L}^{1/2}} + \frac{2.661}{{Re_L}^{7/8}} \tag{3.4}$$

This analysis applies not only to low-speed flat-plate flow but also to various body shapes and compressible flows.

Plate Normal to The Flow

There is no theoretical solution available for the *pressure* or *form* drag, therefore, this drag was determined using an empirical value.

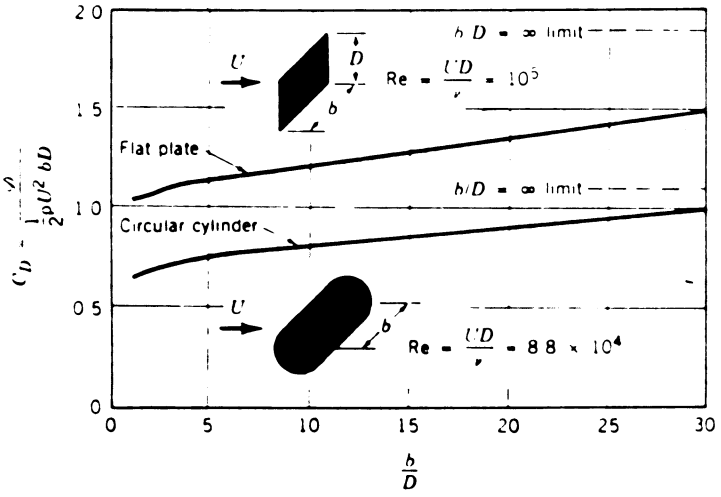

Figure 3.3: Drag coefficient as a function of aspect ratio for a flat plate normal to the upstream flow and a circular cylinder [24]

From Figure 3.3[24], with $b/D = 7.5$ (see Figure 3.4),the value of C'_D is approximately 1.9, which is in agreement with Blevins [4] and Hughes[16].

Finite Flat-plate Drag Approximation

The finite flat-plate used in this study was a precleaned microscope slide 75 mm wide, 25 mm long and 1 mm thick.

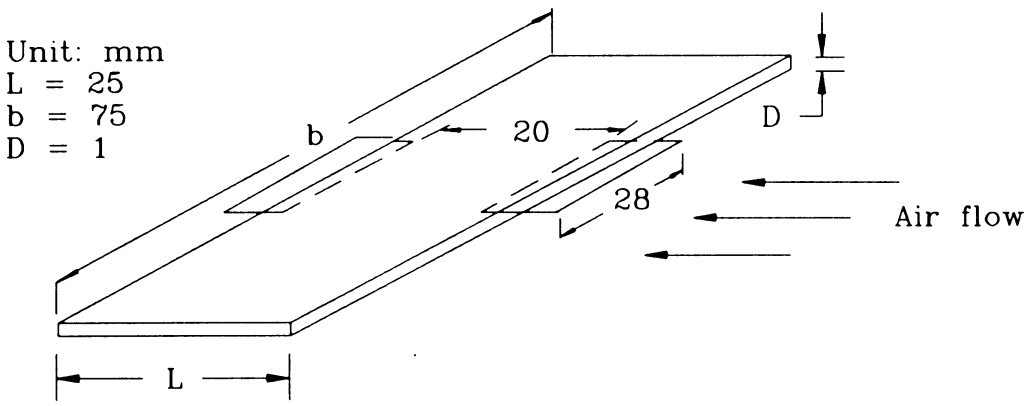

Figure 3.4: Flat plate dimension

The total drag force of the flat plate, according to the above approximation, is:

$$F_T = \frac{1}{2}\rho V^2 \left(C_{D_f} A_f + C_{D_p} A_p \right) \tag{3.5}$$

where A_f is area of the plate subjected to skin-friction drag, and A_p is the area subjected to pressure drag:

$$A_f = 2 \times b \times L$$

$$A_p = b \times D$$

Recalling that the drag force is:

$$F_D = \frac{1}{2}\rho V^2 A C_D$$

where A is the *total* area affected by the drag, i.e. $A_f + A_p$, Equation 3.5 can be rewritten as:

$$F_T = \frac{1}{2}\rho V^2 \left(\frac{C_{D_f} A_f + C_{D_p} A_p}{A_f + A_p} \right) (A_f + A_p) \tag{3.6}$$

thus, a new drag coefficient is introduced:

$$C_D{}' = \left(\frac{C_{D_f} A_f + C_{D_p} A_p}{A_f + A_p} \right) \tag{3.7}$$

In determining the above equation, a question arose: *How important is form drag compared to skin-friction drag? Can't we just neglect it?* To answer this question one can perform a simple calculation comparing the two forms of drag force.

$$\frac{F_{D_p}}{F_{D_f}} = \frac{\frac{1}{2}\rho V^2 b D C_{D_p}}{2\left(\frac{1}{2}\rho V^2 L b C_{D_f}\right)}$$

With air density, $\rho = 1.225 kg/m^3$, and dynamic viscosity, $\mu = 1.79 \times 10^{-5} N.s/m^2$ at STP[13][24], and $C_{D_p} = 1.9$, C_{D_f} from Equation 3.1 the range of interest of the Reynolds number in this study was 1129–3570, gives:

$$for\ Re_L = 1129 \rightarrow \frac{F_{D_p}}{F_{D_f}} = 0.96$$

$$for\ Re_L = 3570 \rightarrow \frac{F_{D_p}}{F_{D_f}} = 1.71$$

Both results are of $O(1)$! Therefore, it was obvious that the form drag cannot be neglected and must be included in the drag calculation.

One final consideration is that even though the actual plate drag is definitely higher than the theoretical flat-plate calculation, this approximation would overestimate the total drag, since the drag of a plate normal to the flow (Figure 3.1 (b)) will be slightly higher than that of the *cornered-surface* (Figure 3.1 (c)) due to the wake on the rear surface of the plate. Moreover, cornered-surface will have a smoothing effect on the boundary layer. Therefore, the actual drag curve would lie in

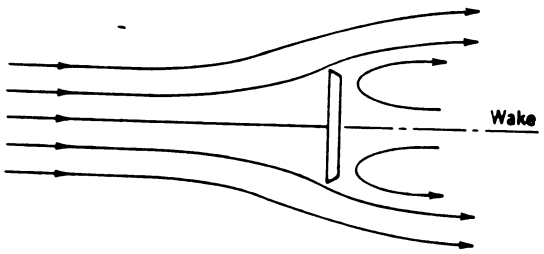

Figure 3.5: Flow over a flat plate normal to the flow

between the flat-plate and the combination flat-plate and plate normal to the flow approximation.

All skin-friction drag coefficient, Equation 3.1, 3.2, 3.3 and 3.4, were used in Equation 3.7 to produce a *standard* drag curve for a finite flat plate. A computer program was developed for this purpose (see Appendix F), where the drag coefficient was plotted against the Reynolds number in Figure 3.6. In addition, the basic equation—without taking the form drag term into consideration—were also plotted in the same figure as a comparison.

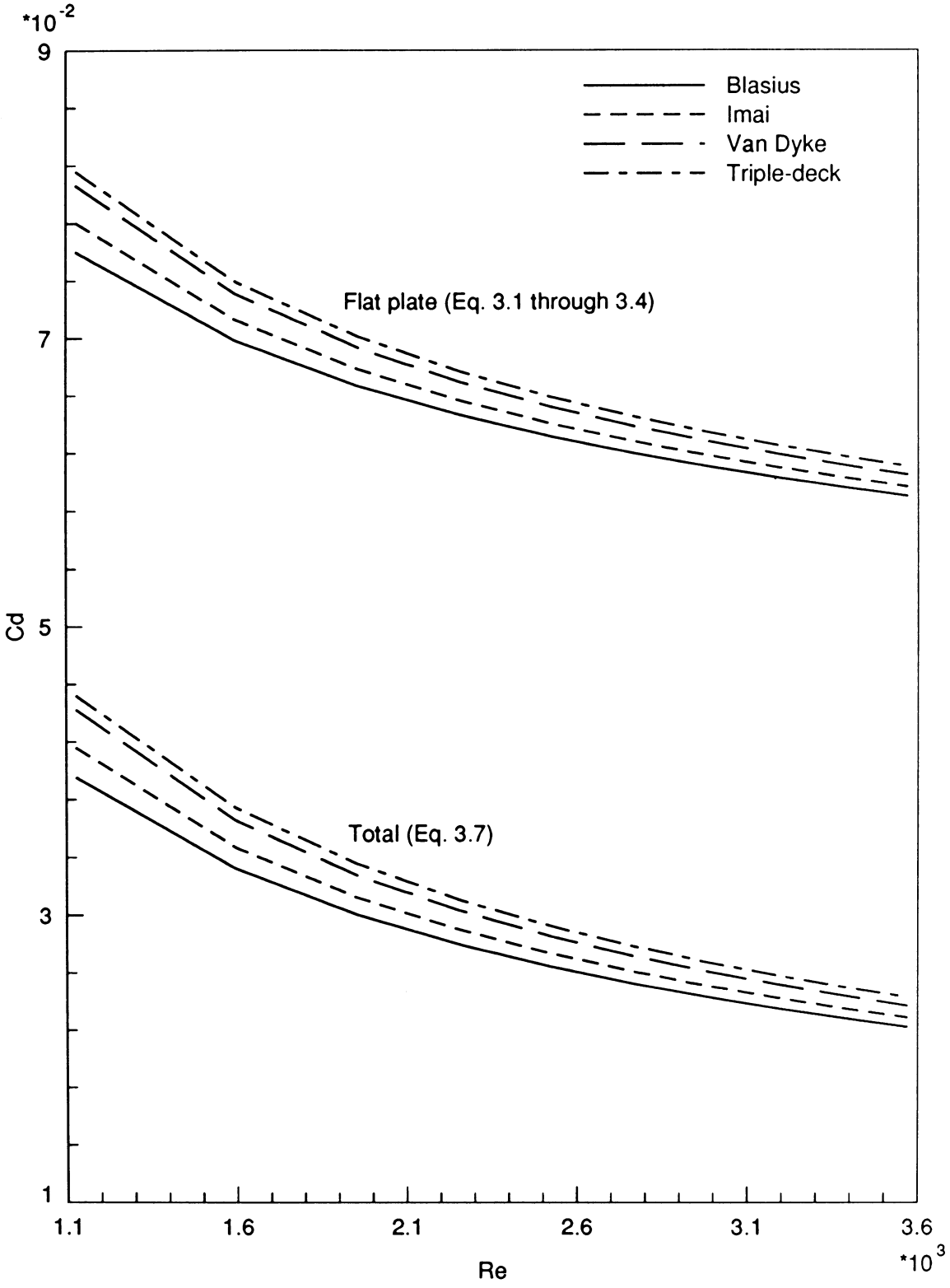

Figure 3.6: Standard drag curve for a finite flat plate

CHAPTER 4. THE EXPERIMENT

The experiment was divided into two parts. The first part was to measure the drag coefficient of a flat plate and compare the result with a theoretical standard drag calculation. The second part was to add a high voltage electrical discharge to the plate's surface and compare the result with the previous one.

Plate drag measurement

The purpose of this experiment was to measure the plate drag over the widest range of air speeds that the tunnel's capabilities permitted.

The speed of air flow was controlled by a variable transformer supplying voltage to the ac fan motor. The speed measurements were carried out by the dynamic readings of the pitot-static tubes. The velocity was calculated based on the Bernoulli equation:

$$V = \sqrt{\frac{2\Delta p}{\rho}} \tag{4.1}$$

where Δp is the manometer reading (in $torr$, equal to 133.322 Pa), and ρ is the air density = 1.225 kg/m^3.

The sensor could detect the forces over a wide range of the speeds quite satisfactorily. The device was easily nulled by the voltmeter before each run. The drag force was calculated using Equations A.1 and A.4 for a positive direction and A.3 and A.5

for a negative direction[1]. And the drag coefficient, C_D was

$$C_D = \frac{F_D}{\frac{1}{2}\rho V^2 A} \tag{4.2}$$

where A is the *total area* of the body, i.e. the area subjected to the pressure and skin friction[2].

Attempts were made to carry out all the force readings at one run at a time. However, the tunnel had to be stopped at times to null the sensor and to switch the range multiplier of the manometer.

The amount of noise in the scope's signal was found to be high. This was the noise inherent in the strain indicator. An RC circuit was placed on the output side of the strain indicator to short out the noise. There were also other ac signals picked up by the scope whose frequency were not appreciable in the measurement process.

Wire drag

The drag of the plate was integrated from the total drag of the plate-wire suspension system. Therefore, the drag of the wires had to be measured separately; then these resistances were subtracted from the total drag to find the plate drag.

Because one wire was in the wake of the other wire, it was considered necessary to run an experiment measuring both the wire drag with and without the wake influence, then compare the results. First, a single wire was subjected to air flow and the drag of this single wire was recorded. Then, another wire was placed upstream to create a wake effect on the wire being measured. Figure 4.1 illustrates the configuration. The raw data for both conditions are shown in Figure 4.2 and Table 4.1.

---

[1] See Appendix A.

[2] See Chapter 3.

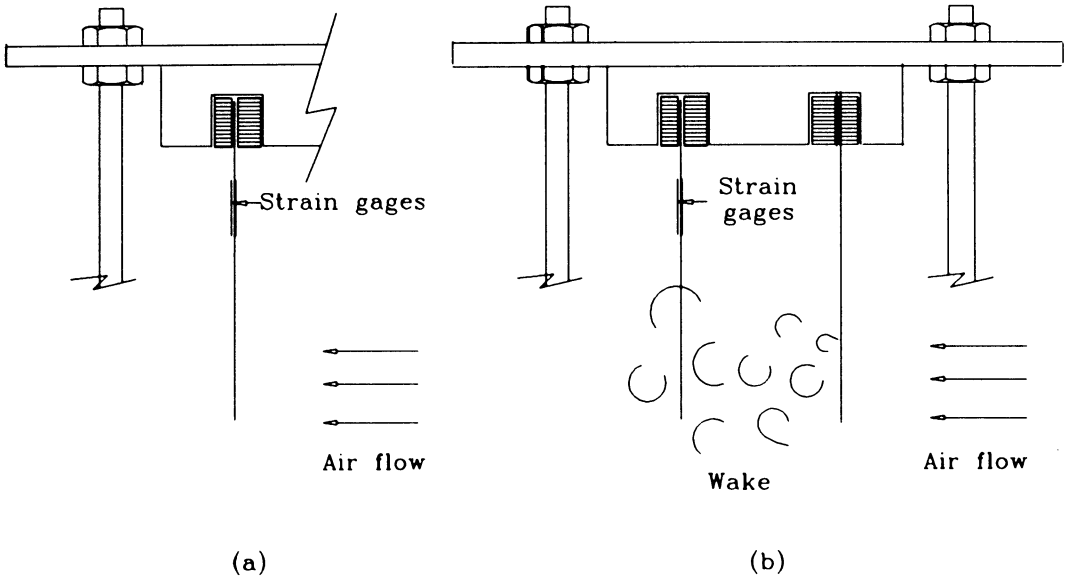

Figure 4.1: Wire drag measurement: (a) single wire, (b) wire in the wake of another wire

Table 4.1: Wire drag measurement: raw data

Air speed	Force (Voltage reading)	
Pressure reading	without wake effect	with wake effect
torr	mV	mV
0.20E-02	3.817	2.800
0.40E-02	5.500	4.033
0.60E-02	6.250	5.400
0.80E-02	7.667	6.767
0.10E-01	9.917	8.400
0.12E-01	11.333	10.150
0.14E-01	12.633	11.683
0.16E-01	14.017	12.883
0.18E-01	14.800	14.183
0.20E-01	16.833	15.800

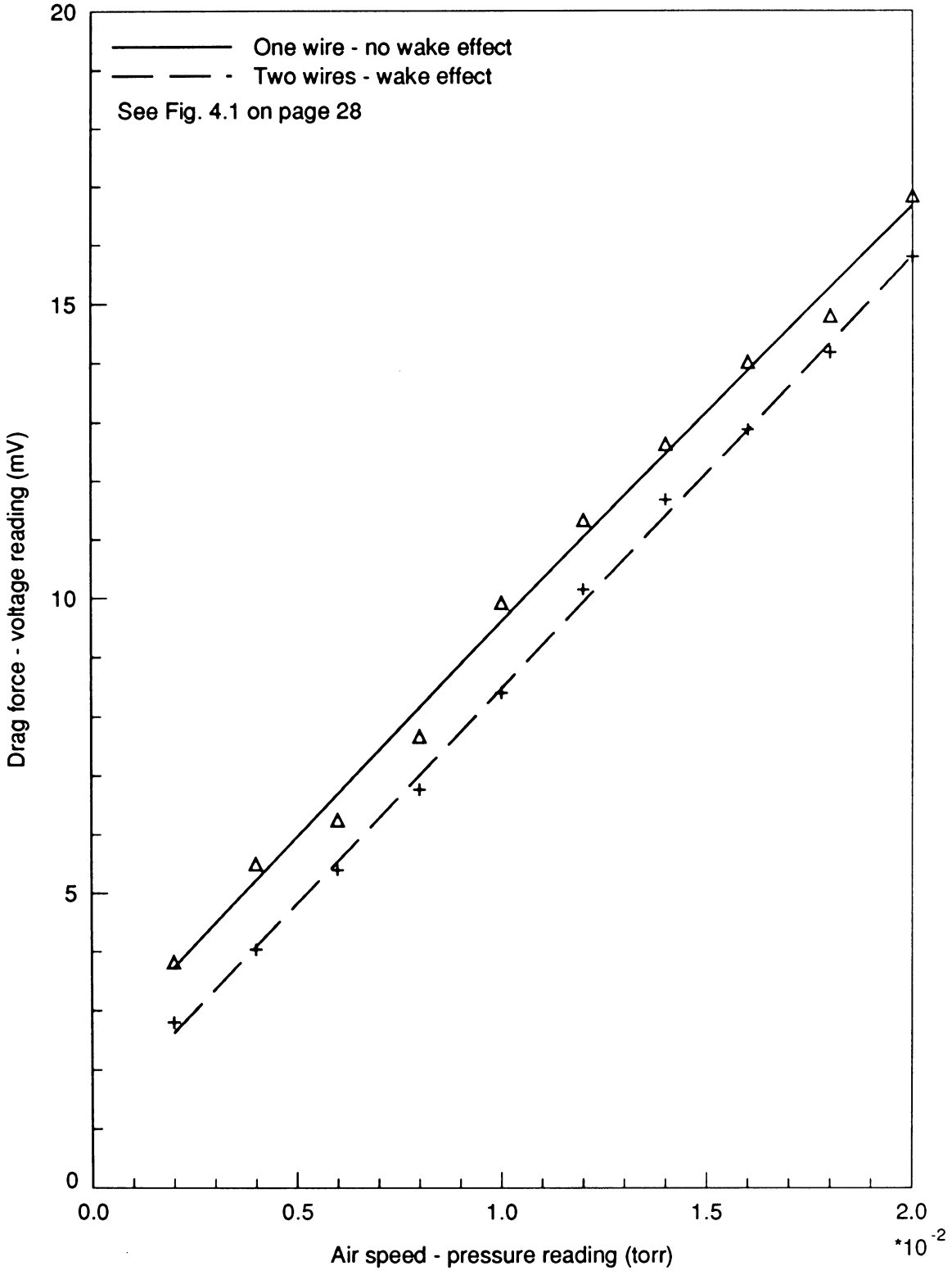

Figure 4.2: Wire drag: air speed (pressure reading) vs. drag force (voltage reading)

For a single wire without a wake effect, the line equation is:

$$Voltage = -1.5786 \times 10^3 p^2 + 7.5410 \times 10^2 p + 2.2247 \tag{4.3}$$

For a single wire in the wake of another wire:

$$Voltage = 1.8847 \times 10^2 p^2 + 7.2907 \times 10^2 p + 1.1611 \tag{4.4}$$

When calculating the wire drag, we have to take into consideration that the wire was calibrated by placing some weights on its tip, whereas in the drag force measurement, the wind creates drag force on the entire length of the wire. Therefore, a formula to calculate the actual wire drag force was derived from beam theory:

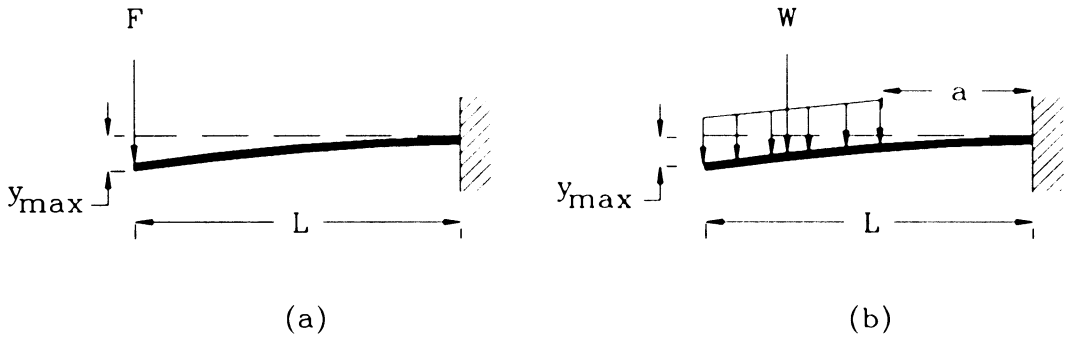

Figure 4.3: Beam representation of wire drag calculation: (a) calibration condition: Load on beam tip, (b) actual condition: Distribution load on part of the beam

For the condition of Figure 4.3 (a), the maximum deflection, resulted from calibration, is [26]

$$ymax = \frac{FL^3}{3EI} \tag{4.5}$$

and for condition (b) [26],

$$y_{max} = \frac{W}{24EI}(3a^2L + 3aL^2 + 3L^3 - a^3) \tag{4.6}$$

where F is the concentrated load (in this case: the weights), W is the integrated distributed load (in this case: drag force from the wind), E and I are the Young's modulus and the moment of inertia for the entire beam, respectively.

Equating Equations 4.5 and 4.6 we have:

$$\frac{FL^3}{3EI} = \frac{W}{24EI}(3a^2L + 3aL^2 + 3L^3 - a^3)$$

Eliminating the EI and simplifying, we have:

$$FL^3 = \frac{W}{8}(3a^2L + 3aL^2 + 3L^3 - a^3)$$

$$F = \frac{W}{8}\left(\frac{3a^2}{L^2} + \frac{3a}{L} + 3 - \frac{a^3}{L^3}\right)$$

The diameter of the wire was 0.0184 inch; however, to prevent corona discharge on the wire, a *TV Corona Dope* coating was applied to the entire beam-wire length, which made the diameter of the wire $\approx$ 0.02164 inch.[3] The length of the wire subjected to air flow $(L - a)$ was approximately 3.23 in. and the total length of the *beam*, L was 6.8125 in[4].

With the above data,

$$F = W \times 0.657881$$

or

$$W = \frac{F}{0.657881} \approx 1.52F \tag{4.7}$$

[3] Average of 10 measurements with a micrometer.

[4] See Chapter 2.

Equation 4.7 was used in a computer program[5] to calculate drag force and in turn, the drag coefficient (C_{DW}) of the wire. Table 4.2 shows the result, for a single wire both with and without the wake effect.

Table 4.2: Wire drag data

		without wake effect		with wake effect	
Air speed (m/sec)	Re_D	Force (N)	C_{DW}	Force (N)	C_{DW}
0.6598	24.819	0.2700E-04	2.298	0.1573E-04	1.338
0.9331	35.100	0.4216E-04	1.794	0.3060E-04	1.302
1.1428	42.988	0.5720E-04	1.623	0.4549E-04	1.291
1.3196	49.638	0.7212E-04	1.534	0.6039E-04	1.285
1.4754	55.497	0.8690E-04	1.479	0.7532E-04	1.282
1.6162	60.794	0.1016E-03	1.440	0.9025E-04	1.280
1.7457	65.665	0.1161E-03	1.411	0.1052E-03	1.279
1.8662	70.199	0.1305E-03	1.388	0.1202E-03	1.278
1.9794	74.457	0.1447E-03	1.369	0.1352E-03	1.278
2.0865	78.485	0.1589E-03	1.352	0.1501E-03	1.278

As can be seen from the above result, there is a slight difference between the two conditions. Therefore, it was considered necessary to include both conditions (Equations 4.3 and 4.4) in the plate drag force calculation.

Plate drag

In the experiment, the total drag of the plate-wire suspension system was measured by reading the millivolts from the strain gages attached to *one* of the beams.

The total drag is:

$$F_T = F_D + W_1 + W_2 \tag{4.8}$$

[5]See Appendix F.

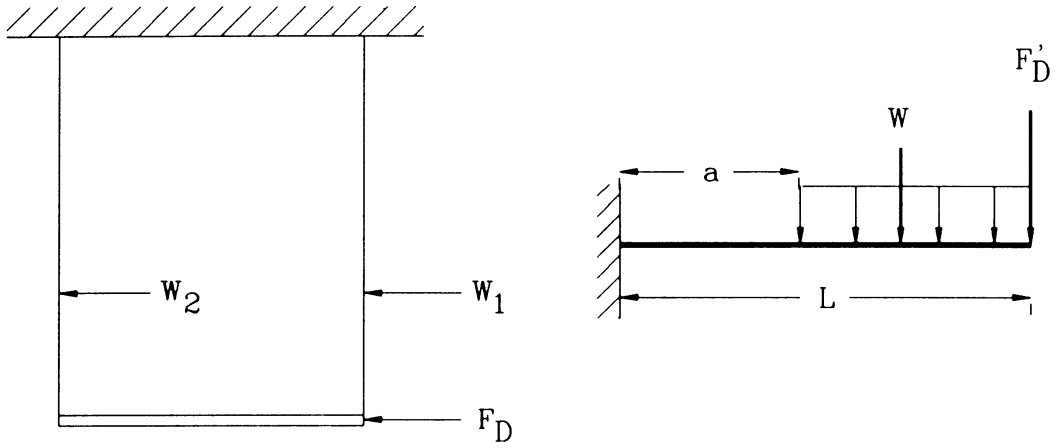

Figure 4.4: Plate-wire drag measurement: (a) actual measurement, (b) beam representation

where W_1 and W_2 are the drag force on the wires. Then, the drag of the plate alone

$$F_D = F_T - (W_1 + W_2) \tag{4.9}$$

It should be noticed, however, that the system was calibrated by putting some weights on the tip of the whole system, i.e., the beam-wire system[6]; therefore, the wire drag forces have to be shifted to the tip. Figure 4.4 (b) shows the beam representation of this system. For one beam:

$$\frac{F_T' L^3}{3EI} = \frac{F_D' L^3}{3EI} + \frac{W}{24EI}(3a^2 L + 3aL^2 + 3L^3 - a^3)$$

[6]See Figure A.4 of Appendix A.

simplifying, we have

$$F_T{}' = F_D{}' + \frac{W}{8}\left(\frac{3a^2}{L^2} + \frac{3a}{L} + 3 - \frac{a^3}{L^3}\right)$$

or

$$F_D{}' = F_T{}' - 0.657881(W)$$

And for the whole system:

$$F_D = F_T - 0.657881(W_1 + W_2) \tag{4.10}$$

where F_T comes from the raw data (voltage reading) converted to force using Equation A.4 for the normal orientation experiment, and Equation A.5 for the reversed strain gages experiment. Note that although Equation 4.10 becomes independent of the value of the coefficient (0.657881) when Equation 4.7 is used to eliminate W_1 and W_2, the final calibration procedure (Appendix A) is independent of any beam theory.

The steps of calculation can be summarized as follows:

1. The voltage reading of the strain gages for a certain air speed was converted to its corresponding force using either Equation A.4 or A.5.

2. The wire drag were obtained from Equation 4.3 and 4.4 which were then converted to their corresponding force using Equation A.1 and A.3 and Equation 4.7.

3. The drag force acting on the plate was calculated using Equation 4.10.

4. The overall drag coefficient was calculated on the total area, $(A_f + A_p)$ using Equation 4.2.

Table 4.3: Plate drag measurement: raw data—normal and reversed strain gages position

Air speed (Pressure reading) (torr)	Force (Voltage reading) Normal orientation (mV)	Reversed orientation (mV)
0.00E+00	0.000	0.000
0.20E-02	2.850	3.200
0.40E-02	5.350	5.267
0.60E-02	7.650	7.400
0.80E-02	9.550	9.450
0.10E-01	11.500	12.217
0.12E-01	12.717	14.283
0.14E-01	14.733	16.250
0.16E-01	16.550	18.367
0.18E-01	18.700	20.933
0.20E-01	20.500	22.867

Table 4.4: Plate drag data: normal and reversed strain gages position

		Normal orientation		Reversed orientation	
Air speed (m/sec)	Re_L	Force (N)	C_D	Force (N)	C_D
0.6598	1129	0.4393E-04	0.4307E-01	0.4455E-04	0.4368E-01
0.9331	1596	0.9123E-04	0.4472E-01	0.7255E-04	0.3557E-01
1.1428	1955	0.1333E-03	0.4355E-01	0.1020E-03	0.3333E-01
1.3196	2258	0.1647E-03	0.4036E-01	0.1297E-03	0.3180E-01
1.4754	2524	0.1975E-03	0.3872E-01	0.1725E-03	0.3383E-01
1.6162	2765	0.2107E-03	0.3444E-01	0.2007E-03	0.3280E-01
1.7457	2987	0.2455E-03	0.3438E-01	0.2269E-03	0.3178E-01
1.8662	3193	0.2749E-03	0.3370E-01	0.2563E-03	0.3141E-01
1.9794	3387	0.3134E-03	0.3414E-01	0.2951E-03	0.3215E-01
2.0865	3570	0.3426E-03	0.3359E-01	0.3208E-03	0.3145E-01

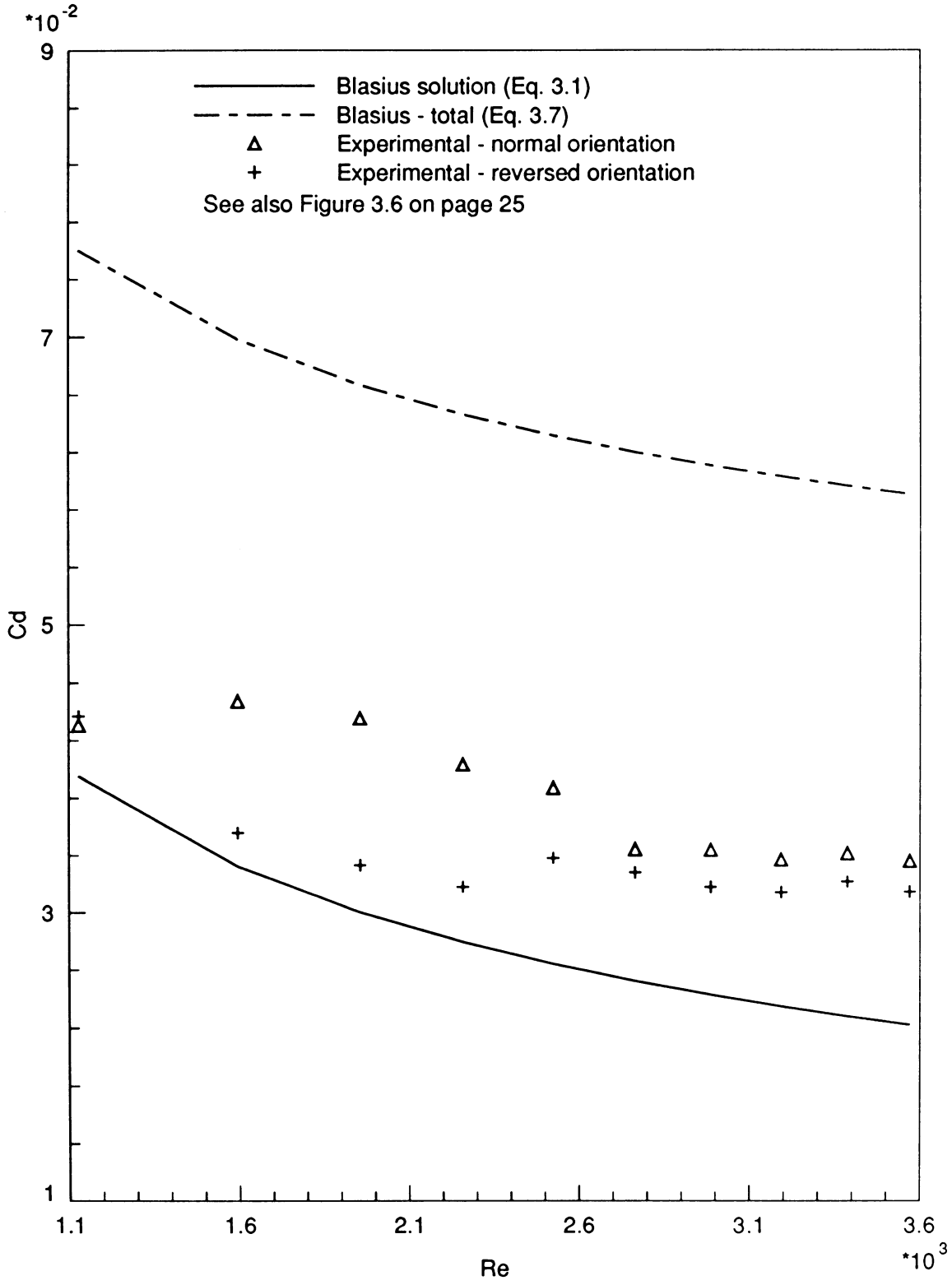

Figure 4.5: Plate drag: Reynolds number vs. Drag coefficient, in comparison with standard drag curves

Table 4.3 shows the raw data, which were converted to corresponding air speed, drag force, Reynolds number, and drag coefficient as shown in Table 4.4. All calculation was performed with the aid of computer programs listed in Appendix F.

In an attempt to examine the effect of electrostatic and/or thrust force on the plate by the high voltage discharge (see Chapter 6), it was necessary conduct another experiment where the threaded rod-support force sensor was *flipped* so that the strain gages are on the upstream position of the working section. This position is called *reversed strain gages orientation.* The drag force and coefficient of this position were also presented in Figure 4.5 and Tables 4.3 and 4.4.

Figure 4.6 summarizes the terms used in this chapter, such as position of the plate-wire system relative to the air flow, dimension of the glass plate; and the variables in the tables.

Plate Drag With High Voltage Discharge

The plate drag with high voltage discharge was performed by fixing the air speed in the wind tunnel and varying the output voltage from the high voltage electric power source. It was noticed, however, that the plate-wire system could be deflected when the high voltage discharge was applied, even without air flow[7]. This meant that the voltage readings of strain could not be simply translated to their corresponding force using the strain-force calibration curves of Appendix A. To solve this problem, the strain readings for no-air-flow condition at each voltage were recorded. These data were then used as the *reference/initial force* to be subtracted from the *absolute force*

[7]This phenomenon could be resulted from electrostatic and/or thrust force due to the high voltage discharge itself, and will be discussed further in Chapter 6.

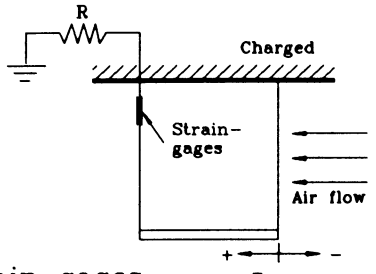 Strain gages orientation	AC – Normal orientation DC – Positive polarity DC – Negative polarity
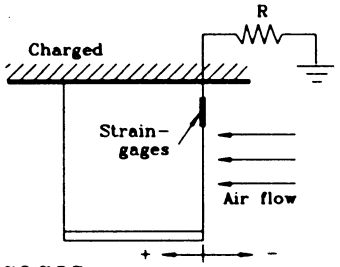 Strain gages orientation	AC – Reversed orientation
Glass plate's Dimension 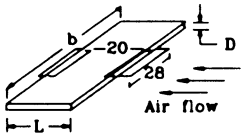	Unit: mm L = 25 b = 75 D = 1
Reynolds number, Re_L	Calculated based on plate's length, L
Absolute force	Voltage reading converted to force, subtracted by wire drag
Net force	Absolute force at certain high voltage and air speed sub-tracted by the corresponding force at the same high voltage but without any air flow
Current	Voltage drop accross the resistor divided by its resistance

Figure 4.6: Description of terms used in the experiments

obtained from a given air speed and voltage. Then the drag coefficient was calculated from the *net force*. Therefore, the steps of calculation on page 34 should be modified as follows:

1. The voltage reading of strain gages for the first data (no air flow condition) was converted to its corresponding force using Equations A.4 or A.5. This was called the *reference force*.

2. The voltage reading of subsequent data (at certain air flow) was converted as in page 34. This was called the *absolute force*.

3. The *net force* on the plate was equal to the *absolute force* minus the *reference force*; and was then used to calculate the drag coefficient (C_D).

4. In addition, the current for every test was also calculated by measuring the voltage drop across a resistor and dividing it by the resistance.

Four different types of experiments are subsequently presented: AC, normal and reversed strain gages orientation, DC-positive polarity, and DC-negative polarity. All experimental results will be presented in the forms of tables, plots of Reynolds number vs. drag force, and plots of Reynolds number vs. drag coefficient.

Some photographs of actual corona discharge on the glass plate are also shown, for AC, DC-positive and negative polarity, respectively. These pictures were taken with the glass plate outside the wind tunnel.

AC source—normal strain gages orientation

Table 4.5: AC Source—normal orientation: with 2 kV high voltage discharge

Air speed (m/s)	Re_L	Net Force (N)	C_D	Absolute Force (N)	Current (mA)
0.6598	1129.	0.4182E-04	0.04100	0.3101E-04	0.1227E-02
0.9331	1596.	0.8821E-04	0.04324	0.7740E-04	0.1227E-02
1.1428	1955.	0.1298E-03	0.04242	0.1190E-03	0.1227E-02
1.3196	2258.	0.1603E-03	0.03929	0.1495E-03	0.1227E-02
1.4754	2524.	0.1913E-03	0.03752	0.1805E-03	0.1227E-02
1.6162	2765.	0.2042E-03	0.03336	0.1934E-03	0.1227E-02
1.7457	2987.	0.2407E-03	0.03371	0.2299E-03	0.1227E-02
1.8662	3193.	0.2688E-03	0.03295	0.2580E-03	0.1227E-02
1.9794	3387.	0.3095E-03	0.03372	0.2987E-03	0.1227E-02
2.0865	3570.	0.3360E-03	0.03294	0.3252E-03	0.1227E-02

Table 4.6: AC Source—normal orientation: with 4 kV high voltage discharge

Air speed (m/s)	Re_L	Net Force (N)	C_D	Absolute Force (N)	Current (mA)
0.6598	1129.	0.3146E-04	0.03085	-0.2414E-05	0.2454E-02
0.9331	1596.	0.7517E-04	0.03685	0.4130E-04	0.2454E-02
1.1428	1955.	0.1154E-03	0.03773	0.8156E-04	0.2454E-02
1.3196	2258.	0.1442E-03	0.03534	0.1103E-03	0.2454E-02
1.4754	2524.	0.1756E-03	0.03444	0.1418E-03	0.2454E-02
1.6162	2765.	0.1898E-03	0.03101	0.1559E-03	0.2454E-02
1.7457	2987.	0.2201E-03	0.03083	0.1862E-03	0.2454E-02
1.8662	3193.	0.2513E-03	0.03080	0.2174E-03	0.2454E-02
1.9794	3387.	0.2884E-03	0.03142	0.2546E-03	0.2454E-02
2.0865	3570.	0.3140E-03	0.03079	0.2802E-03	0.2454E-02

Table 4.7: AC Source—normal orientation: with 6 kV high voltage discharge

Air speed (m/s)	Re_L	Net Force (N)	C_D	Absolute Force (N)	Current (mA)
0.6598	1129.	0.1776E-04	0.01741	-0.4303E-04	0.3681E-02
0.9331	1596.	0.5486E-04	0.02690	-0.5928E-05	0.3681E-02
1.1428	1955.	0.8929E-04	0.02918	0.2850E-04	0.3681E-02
1.3196	2258.	0.1220E-03	0.02991	0.6124E-04	0.3681E-02
1.4754	2524.	0.1522E-03	0.02984	0.9137E-04	0.3681E-02
1.6162	2765.	0.1672E-03	0.02733	0.1064E-03	0.3681E-02
1.7457	2987.	0.1993E-03	0.02791	0.1385E-03	0.3681E-02
1.8662	3193.	0.2279E-03	0.02793	0.1671E-03	0.3681E-02
1.9794	3387.	0.2610E-03	0.02843	0.2002E-03	0.3681E-02
2.0865	3570.	0.2879E-03	0.02823	0.2271E-03	0.3681E-02

Table 4.8: AC Source—normal orientation: with 8 kV high voltage discharge

Air speed (m/s)	Re_L	Net Force (N)	C_D	Absolute Force (N)	Current (mA)
0.6598	1129.	0.2768E-04	0.02714	-0.1206E-03	0.5011E-02
0.9331	1596.	0.5107E-04	0.02504	-0.9720E-04	0.5011E-02
1.1428	1955.	0.9921E-04	0.03243	-0.4906E-04	0.5011E-02
1.3196	2258.	0.1404E-03	0.03442	-0.7842E-05	0.5011E-02
1.4754	2524.	0.1804E-03	0.03537	0.3211E-04	0.5011E-02
1.6162	2765.	0.1883E-03	0.03077	0.4001E-04	0.5011E-02
1.7457	2987.	0.2132E-03	0.02986	0.6495E-04	0.5011E-02
1.8662	3193.	0.2387E-03	0.02925	0.9041E-04	0.5011E-02
1.9794	3387.	0.2678E-03	0.02917	0.1195E-03	0.5011E-02
2.0865	3570.	0.2916E-03	0.02859	0.1433E-03	0.5011E-02

Table 4.9: AC Source—normal orientation: with 10 kV high voltage discharge

Air speed (m/s)	Re_L	Net Force (N)	C_D	Absolute Force (N)	Current (mA)
0.6598	1129.	-0.5640E-05	-0.00553	-0.2189E-03	0.6647E-02
0.9331	1596.	0.1902E-04	0.00932	-0.1943E-03	0.6647E-02
1.1428	1955.	0.3510E-04	0.01147	-0.1782E-03	0.6647E-02
1.3196	2258.	0.5093E-04	0.01248	-0.1624E-03	0.6647E-02
1.4754	2524.	0.6299E-04	0.01235	-0.1503E-03	0.6647E-02
1.6162	2765.	0.6776E-04	0.01107	-0.1456E-03	0.6647E-02
1.7457	2987.	0.7769E-04	0.01088	-0.1356E-03	0.6647E-02
1.8662	3193.	0.9601E-04	0.01177	-0.1173E-03	0.6647E-02
1.9794	3387.	0.1202E-03	0.01310	-0.9310E-04	0.6647E-02
2.0865	3570.	0.1431E-03	0.01403	-0.7016E-04	0.6647E-02

Table 4.10: AC Source—normal orientation: with 12 kV high voltage discharge

Air speed (m/s)	Re_L	Net Force (N)	C_D	Absolute Force (N)	Current (mA)
0.6598	1129.	0.2224E-04	0.02180	-0.2862E-03	0.9204E-02
0.9331	1596.	0.1869E-04	0.00916	-0.2898E-03	0.9204E-02
1.1428	1955.	0.3991E-04	0.01304	-0.2686E-03	0.9204E-02
1.3196	2258.	0.6856E-04	0.01681	-0.2399E-03	0.9204E-02
1.4754	2524.	0.6779E-04	0.01329	-0.2407E-03	0.9204E-02
1.6162	2765.	0.7737E-04	0.01264	-0.2311E-03	0.9204E-02
1.7457	2987.	0.8350E-04	0.01170	-0.2250E-03	0.9204E-02
1.8662	3193.	0.9770E-04	0.01197	-0.2108E-03	0.9204E-02
1.9794	3387.	0.9115E-04	0.00993	-0.2173E-03	0.9204E-02
2.0865	3570.	0.1197E-03	0.01174	-0.1887E-03	0.9204E-02

Table 4.11: AC Source—normal orientation: with 14 kV high voltage discharge

Air speed (m/s)	Re_L	Net Force (N)	C_D	Absolute Force (N)	Current (mA)
0.6598	1129.	-0.1014E-04	-0.00994	-0.3667E-03	0.6821E-01
0.9331	1596.	0.7555E-06	0.00037	-0.3558E-03	0.6821E-01
1.1428	1955.	0.1764E-05	0.00058	-0.3548E-03	0.6821E-01
1.3196	2258.	0.2594E-04	0.00636	-0.3306E-03	0.6821E-01
1.4754	2524.	0.2423E-04	0.00475	-0.3323E-03	0.6821E-01
1.6162	2765.	0.1040E-04	0.00170	-0.3461E-03	0.6821E-01
1.7457	2987.	0.1300E-04	0.00182	-0.3435E-03	0.6821E-01
1.8662	3193.	0.1247E-04	0.00153	-0.3441E-03	0.6821E-01
1.9794	3387.	0.2259E-04	0.00246	-0.3340E-03	0.6821E-01
2.0865	3570.	0.1162E-04	0.00114	-0.3449E-03	0.6821E-01

Table 4.12: AC Source—normal orientation: with 16 kV high voltage discharge

Air speed (m/s)	Re_L	Net Force (N)	C_D	Absolute Force (N)	Current (mA)
0.6598	1129.	-0.2744E-04	-0.02691	-0.3388E-03	0.1602E+00
0.9331	1596.	-0.4187E-04	-0.02053	-0.3532E-03	0.1602E+00
1.1428	1955.	-0.4726E-04	-0.01545	-0.3586E-03	0.1602E+00
1.3196	2258.	-0.6283E-04	-0.01540	-0.3742E-03	0.1602E+00
1.4754	2524.	-0.7896E-04	-0.01548	-0.3903E-03	0.1602E+00
1.6162	2765.	-0.9597E-04	-0.01568	-0.4073E-03	0.1602E+00
1.7457	2987.	-0.1120E-03	-0.01568	-0.4233E-03	0.1602E+00
1.8662	3193.	-0.1199E-03	-0.01469	-0.4312E-03	0.1602E+00
1.9794	3387.	-0.1219E-03	-0.01328	-0.4333E-03	0.1602E+00
2.0865	3570.	-0.1303E-03	-0.01278	-0.4417E-03	0.1602E+00

Table 4.13: AC Source—normal orientation: with 18 kV high voltage discharge

Air speed (m/s)	Re_L	Net Force (N)	C_D	Absolute Force (N)	Current (mA)
0.6598	1129.	-0.1108E-04	-0.01086	-0.2901E-03	0.1602E+00
0.9331	1596.	-0.4187E-04	-0.02053	-0.3209E-03	0.1602E+00
1.1428	1955.	-0.5814E-04	-0.01900	-0.3371E-03	0.1602E+00
1.3196	2258.	-0.7179E-04	-0.01760	-0.3508E-03	0.1602E+00
1.4754	2524.	-0.9145E-04	-0.01793	-0.3705E-03	0.1602E+00
1.6162	2765.	-0.9276E-04	-0.01516	-0.3718E-03	0.1602E+00
1.7457	2987.	-0.1190E-03	-0.01667	-0.3980E-03	0.1602E+00
1.8662	3193.	-0.1410E-03	-0.01728	-0.4200E-03	0.1602E+00
1.9794	3387.	-0.1466E-03	-0.01597	-0.4256E-03	0.1602E+00
2.0865	3570.	-0.1540E-03	-0.01510	-0.4330E-03	0.1602E+00

Table 4.14: AC Source—normal orientation: with 20 kV high voltage discharge

Air speed (m/s)	Re_L	Net Force (N)	C_D	Absolute Force (N)	Current (mA)
0.6598	1129.	-0.1783E-04	-0.01748	-0.2888E-03	0.1738E+00
0.9331	1596.	-0.2778E-04	-0.01362	-0.2988E-03	0.1738E+00
1.1428	1955.	-0.4661E-04	-0.01523	-0.3176E-03	0.1738E+00
1.3196	2258.	-0.7052E-04	-0.01729	-0.3415E-03	0.1738E+00
1.4754	2524.	-0.7736E-04	-0.01517	-0.3483E-03	0.1738E+00
1.6162	2765.	-0.9086E-04	-0.01485	-0.3618E-03	0.1738E+00
1.7457	2987.	-0.1104E-03	-0.01546	-0.3813E-03	0.1738E+00
1.8662	3193.	-0.1343E-03	-0.01646	-0.4053E-03	0.1738E+00
1.9794	3387.	-0.1479E-03	-0.01611	-0.4189E-03	0.1738E+00
2.0865	3570.	-0.1723E-03	-0.01689	-0.4433E-03	0.1738E+00

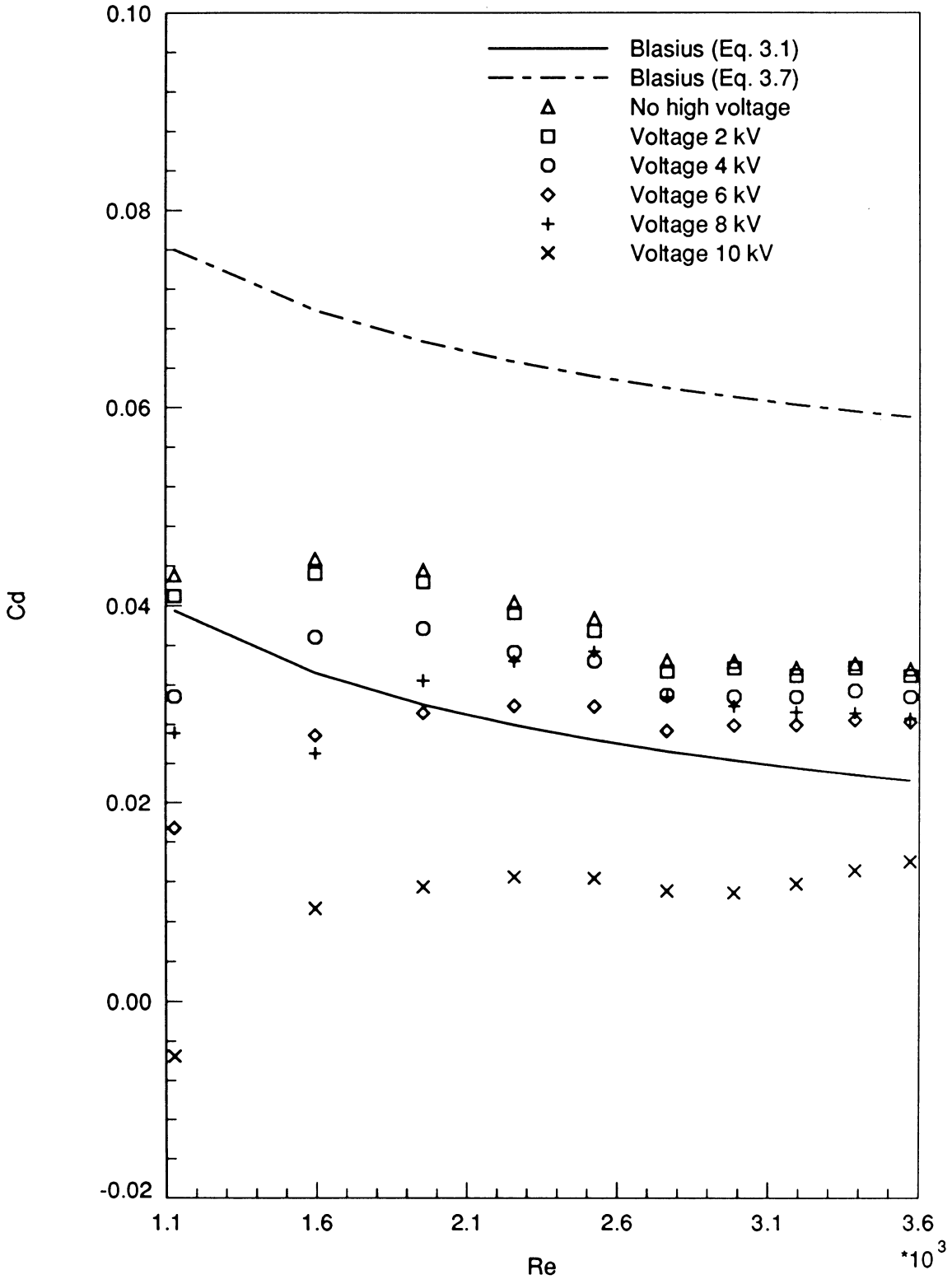

Figure 4.7: AC Source—normal orientation: Re vs. C_D, with 2 kV–10 kV high voltage discharge

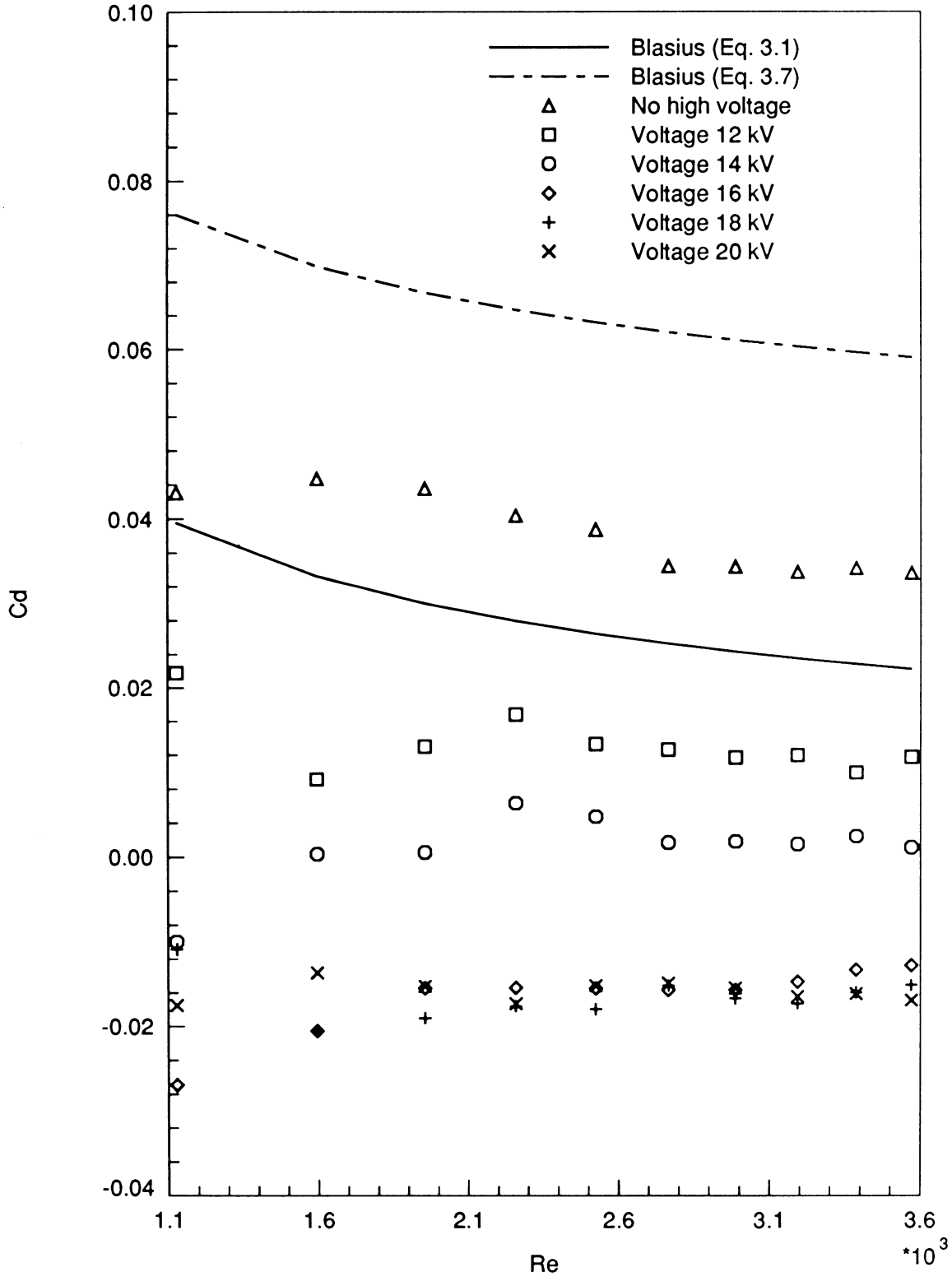

Figure 4.8: AC Source—normal orientation: Re vs. C_D, with 12 kV–20 kV high voltage discharge

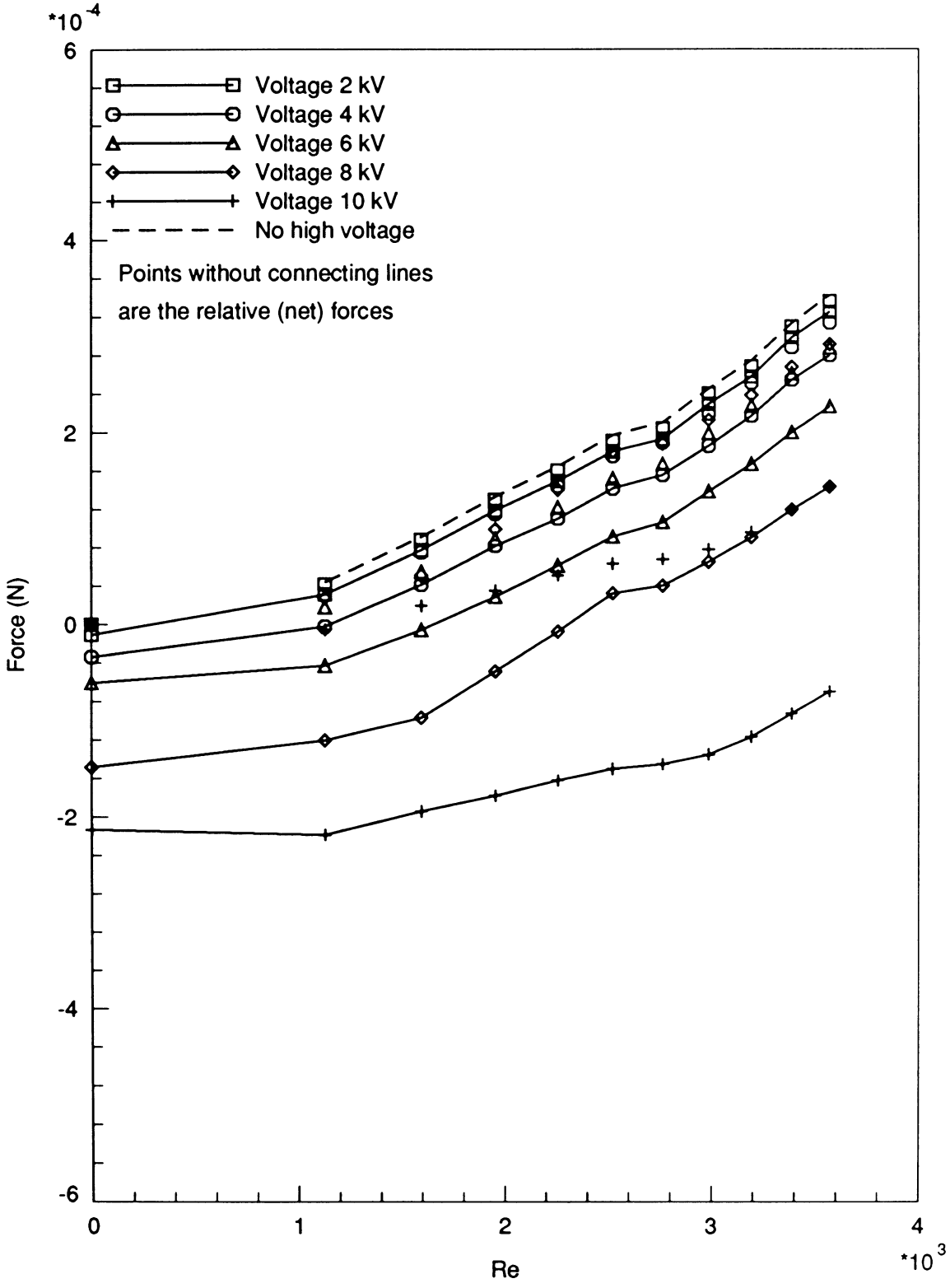

Figure 4.9: AC Source—normal orientation: Re vs. Force, with 2 kV–10 kV high voltage discharge

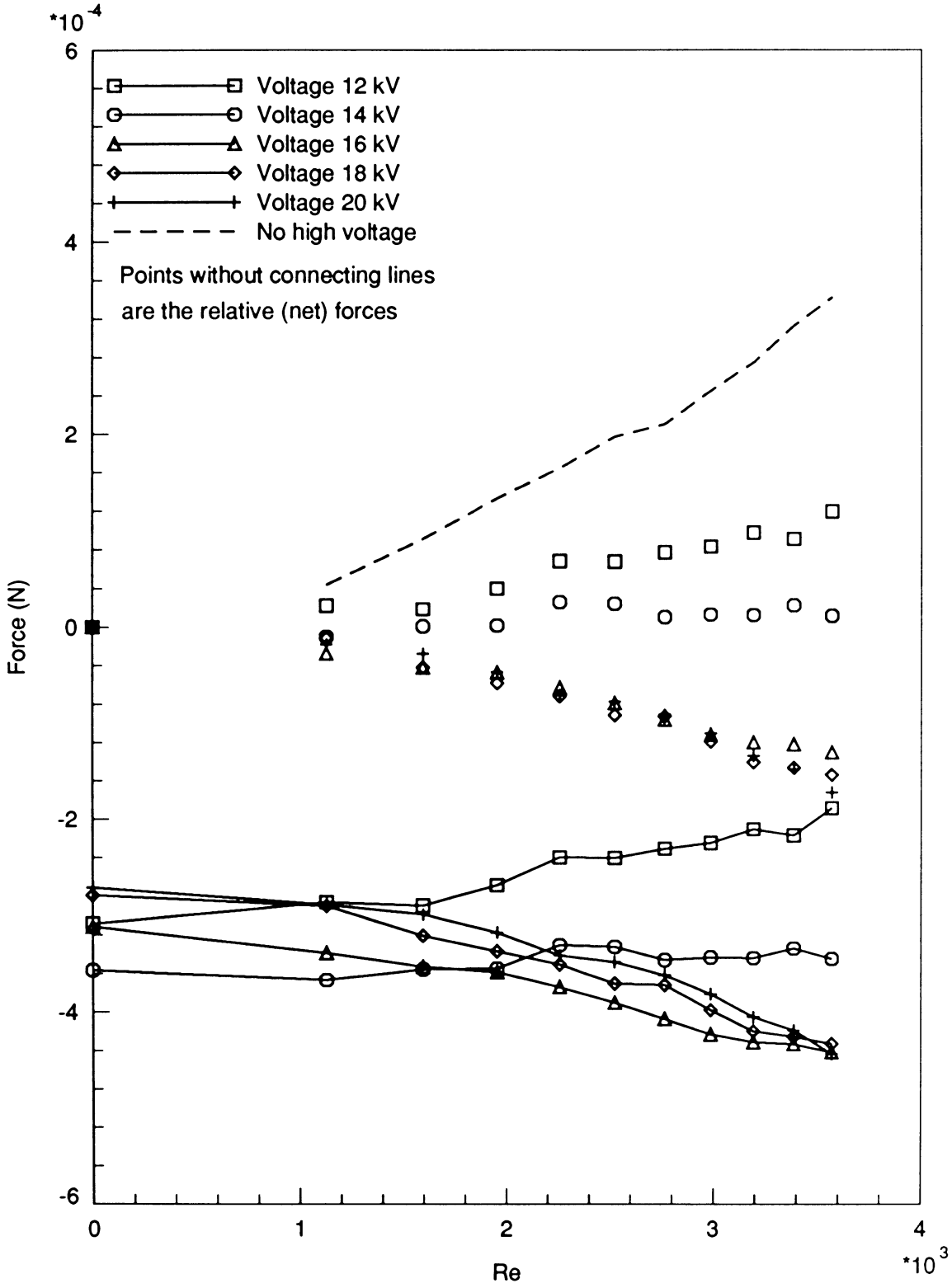

Figure 4.10: AC Source—normal orientation: Re vs. Force, with 12 kV–20 kV high voltage discharge

AC source—reversed strain gages orientation

Table 4.15: AC Source—reversed orientation: with 2 kV high voltage discharge

Air speed (m/s)	Re_L	Net Force (N)	C_D	Absolute Force (N)	Current (mA)
0.6598	1129.	0.4035E-04	0.03957	0.6124E-04	0.1432E-02
0.9331	1596.	0.7044E-04	0.03453	0.9132E-04	0.1432E-02
1.1428	1955.	0.1006E-03	0.03286	0.1214E-03	0.1432E-02
1.3196	2258.	0.1280E-03	0.03137	0.1489E-03	0.1432E-02
1.4754	2524.	0.1634E-03	0.03205	0.1843E-03	0.1432E-02
1.6162	2765.	0.1937E-03	0.03166	0.2146E-03	0.1432E-02
1.7457	2987.	0.2223E-03	0.03114	0.2432E-03	0.1432E-02
1.8662	3193.	0.2559E-03	0.03136	0.2768E-03	0.1432E-02
1.9794	3387.	0.2857E-03	0.03112	0.3066E-03	0.1432E-02
2.0865	3570.	0.3159E-03	0.03097	0.3367E-03	0.1432E-02

Table 4.16: AC Source—reversed orientation: with 4 kV high voltage discharge

Air speed (m/s)	Re_L	Net Force (N)	C_D	Absolute Force (N)	Current (mA)
0.6598	1129.	0.3841E-04	0.03766	0.1044E-03	0.2863E-02
0.9331	1596.	0.6570E-04	0.03221	0.1316E-03	0.2966E-02
1.1428	1955.	0.9653E-04	0.03155	0.1625E-03	0.2966E-02
1.3196	2258.	0.1201E-03	0.02944	0.1861E-03	0.2863E-02
1.4754	2524.	0.1566E-03	0.03071	0.2226E-03	0.2863E-02
1.6162	2765.	0.1834E-03	0.02998	0.2494E-03	0.2966E-02
1.7457	2987.	0.2093E-03	0.02931	0.2752E-03	0.2863E-02
1.8662	3193.	0.2418E-03	0.02963	0.3077E-03	0.2863E-02
1.9794	3387.	0.2695E-03	0.02936	0.3354E-03	0.2966E-02
2.0865	3570.	0.3035E-03	0.02976	0.3694E-03	0.2863E-02

Table 4.17: AC Source—reversed orientation: with 6 kV high voltage discharge

Air speed (m/s)	Re_L	Net Force (N)	C_D	Absolute Force (N)	Current (mA)
0.6598	1129.	0.2569E-04	0.02519	0.1492E-03	0.4500E-02
0.9331	1596.	0.5193E-04	0.02546	0.1755E-03	0.4500E-02
1.1428	1955.	0.7615E-04	0.02489	0.1997E-03	0.4500E-02
1.3196	2258.	0.9522E-04	0.02334	0.2187E-03	0.4500E-02
1.4754	2524.	0.1230E-03	0.02413	0.2466E-03	0.4500E-02
1.6162	2765.	0.1506E-03	0.02460	0.2741E-03	0.4500E-02
1.7457	2987.	0.1684E-03	0.02359	0.2919E-03	0.4500E-02
1.8662	3193.	0.1925E-03	0.02360	0.3161E-03	0.4500E-02
1.9794	3387.	0.2182E-03	0.02377	0.3417E-03	0.4500E-02
2.0865	3570.	0.2438E-03	0.02391	0.3673E-03	0.4500E-02

Table 4.18: AC Source—reversed orientation: with 8 kV high voltage discharge

Air speed (m/s)	Re_L	Net Force (N)	C_D	Absolute Force (N)	Current (mA)
0.6598	1129.	0.2632E-04	0.02580	0.1711E-03	0.5931E-02
0.9331	1596.	0.3865E-04	0.01895	0.1834E-03	0.5931E-02
1.1428	1955.	0.5245E-04	0.01714	0.1972E-03	0.5829E-02
1.3196	2258.	0.4579E-04	0.01122	0.1906E-03	0.5931E-02
1.4754	2524.	0.6350E-04	0.01245	0.2083E-03	0.5931E-02
1.6162	2765.	0.8791E-04	0.01437	0.2327E-03	0.6033E-02
1.7457	2987.	0.9566E-04	0.01340	0.2405E-03	0.5931E-02
1.8662	3193.	0.1045E-03	0.01281	0.2493E-03	0.5931E-02
1.9794	3387.	0.1218E-03	0.01327	0.2666E-03	0.5931E-02
2.0865	3570.	0.1370E-03	0.01343	0.2818E-03	0.5829E-02

Table 4.19: AC Source—reversed orientation: with 10 kV high voltage discharge

Air speed (m/s)	Re_L	Net Force (N)	C_D	Absolute Force (N)	Current (mA)
0.6598	1129.	0.1720E-04	0.01686	0.2521E-03	0.8386E-02
0.9331	1596.	0.9734E-05	0.00477	0.2446E-03	0.8079E-02
1.1428	1955.	0.2421E-04	0.00791	0.2591E-03	0.7874E-02
1.3196	2258.	0.9908E-05	0.00243	0.2448E-03	0.7874E-02
1.4754	2524.	0.1198E-04	0.00235	0.2469E-03	0.7772E-02
1.6162	2765.	0.3672E-04	0.00600	0.2716E-03	0.7772E-02
1.7457	2987.	0.3824E-04	0.00536	0.2731E-03	0.7670E-02
1.8662	3193.	0.4605E-04	0.00564	0.2810E-03	0.7567E-02
1.9794	3387.	0.4244E-04	0.00462	0.2774E-03	0.7670E-02
2.0865	3570.	0.5802E-04	0.00569	0.2929E-03	0.7567E-02

Table 4.20: AC Source—reversed orientation: with 12 kV high voltage discharge

Air speed (m/s)	Re_L	Net Force (N)	C_D	Absolute Force (N)	Current (mA)
0.6598	1129.	0.1693E-04	0.01660	0.2890E-03	0.1360E-01
0.9331	1596.	0.1188E-04	0.00582	0.2839E-03	0.1258E-01
1.1428	1955.	0.2984E-04	0.00975	0.3019E-03	0.1207E-01
1.3196	2258.	0.1170E-04	0.00287	0.2837E-03	0.1176E-01
1.4754	2524.	0.1344E-04	0.00264	0.2855E-03	0.1196E-01
1.6162	2765.	0.3749E-04	0.00613	0.3095E-03	0.1125E-01
1.7457	2987.	0.2196E-04	0.00308	0.2940E-03	0.1145E-01
1.8662	3193.	0.3568E-04	0.00437	0.3077E-03	0.1156E-01
1.9794	3387.	0.2897E-04	0.00316	0.3010E-03	0.1125E-01
2.0865	3570.	0.3689E-04	0.00362	0.3089E-03	0.1125E-01

Table 4.21: AC Source—reversed orientation: with 14 kV high voltage discharge

Air speed (m/s)	Re_L	Net Force (N)	C_D	Absolute Force (N)	Current (mA)
0.6598	1129.	-0.3593E-04	-0.03523	0.3237E-03	0.5798E-01
0.9331	1596.	-0.2289E-04	-0.01122	0.3368E-03	0.5287E-01
1.1428	1955.	-0.1847E-04	-0.00604	0.3412E-03	0.5624E-01
1.3196	2258.	-0.4078E-04	-0.01000	0.3189E-03	0.5451E-01
1.4754	2524.	-0.3070E-04	-0.00602	0.3290E-03	0.5287E-01
1.6162	2765.	-0.2144E-05	-0.00035	0.3575E-03	0.6647E-01
1.7457	2987.	-0.3471E-04	-0.00486	0.3249E-03	0.7496E-01
1.8662	3193.	-0.2899E-04	-0.00355	0.3307E-03	0.7158E-01
1.9794	3387.	-0.3224E-04	-0.00351	0.3274E-03	0.7670E-01
2.0865	3570.	-0.3334E-04	-0.00327	0.3263E-03	0.7332E-01

Table 4.22: AC Source—reversed orientation: with 16 kV high voltage discharge

Air speed (m/s)	Re_L	Net Force (N)	C_D	Absolute Force (N)	Current (mA)
0.6598	1129.	-0.8078E-04	-0.07920	0.3519E-03	0.1245E+00
0.9331	1596.	-0.7713E-04	-0.03781	0.3555E-03	0.1296E+00
1.1428	1955.	-0.7584E-04	-0.02479	0.3568E-03	0.1227E+00
1.3196	2258.	-0.8772E-04	-0.02150	0.3449E-03	0.1245E+00
1.4754	2524.	-0.8773E-04	-0.01720	0.3449E-03	0.1245E+00
1.6162	2765.	-0.6541E-04	-0.01069	0.3673E-03	0.1278E+00
1.7457	2987.	-0.8129E-04	-0.01139	0.3514E-03	0.1329E+00
1.8662	3193.	-0.7279E-04	-0.00892	0.3599E-03	0.1261E+00
1.9794	3387.	-0.8439E-04	-0.00919	0.3483E-03	0.1278E+00
2.0865	3570.	-0.9104E-04	-0.00893	0.3416E-03	0.1414E+00

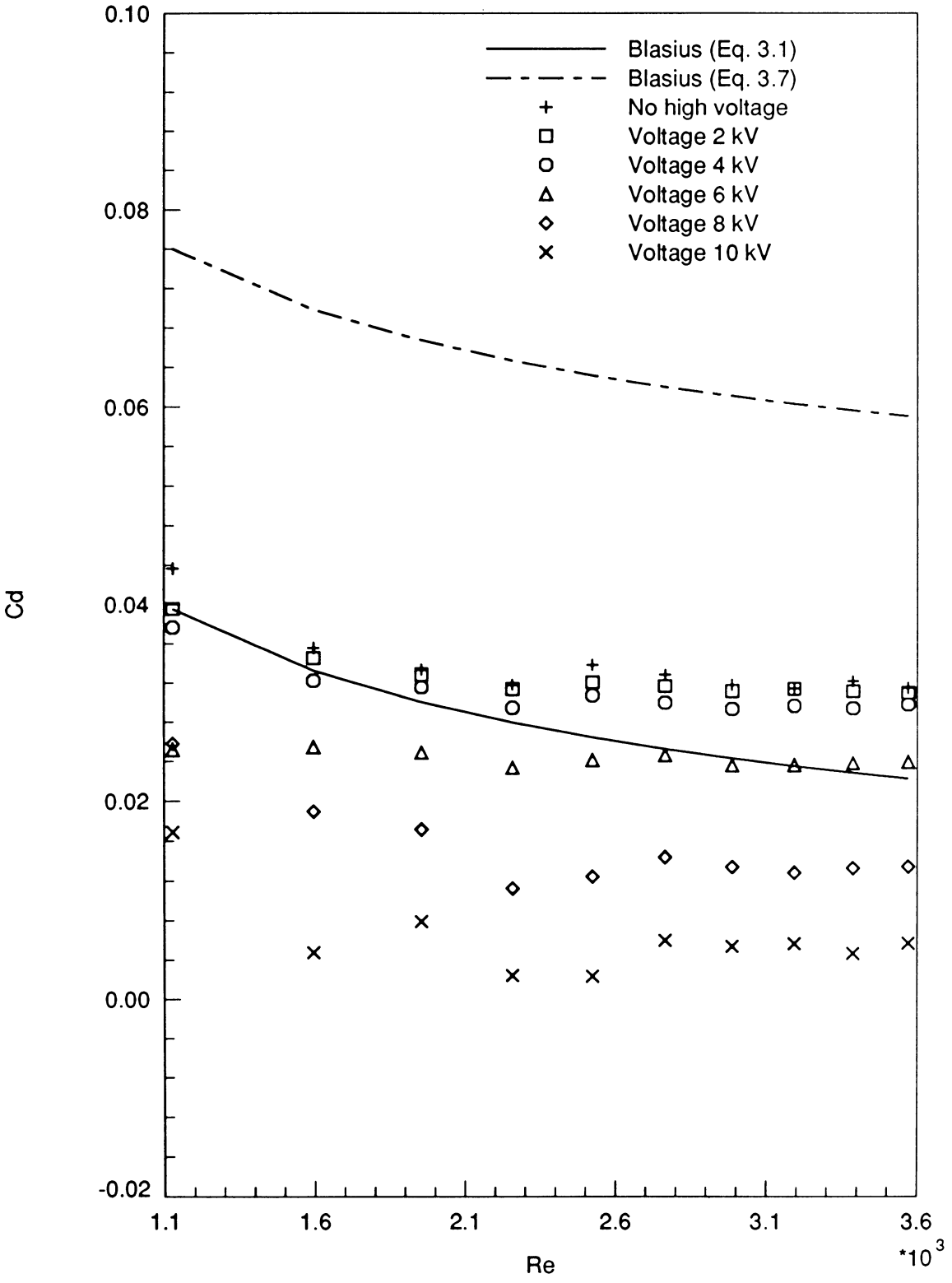

Figure 4.11: AC Source—reversed orientation: Re vs. C_D, with 2 kV–10 kV high voltage discharge

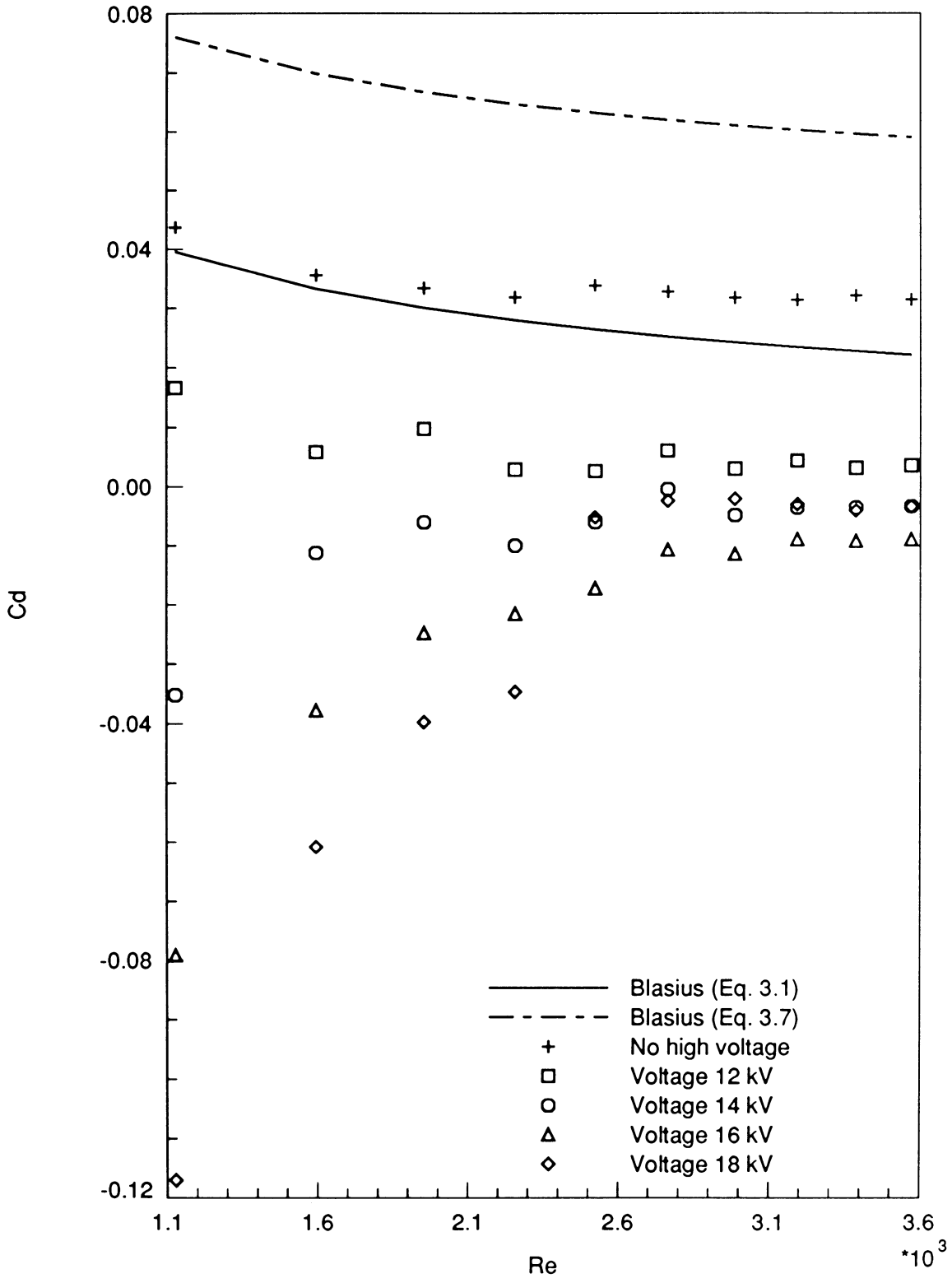

Figure 4.12: AC Source—reversed orientation: Re vs. C_D, with 12 kV–18 kV high voltage discharge

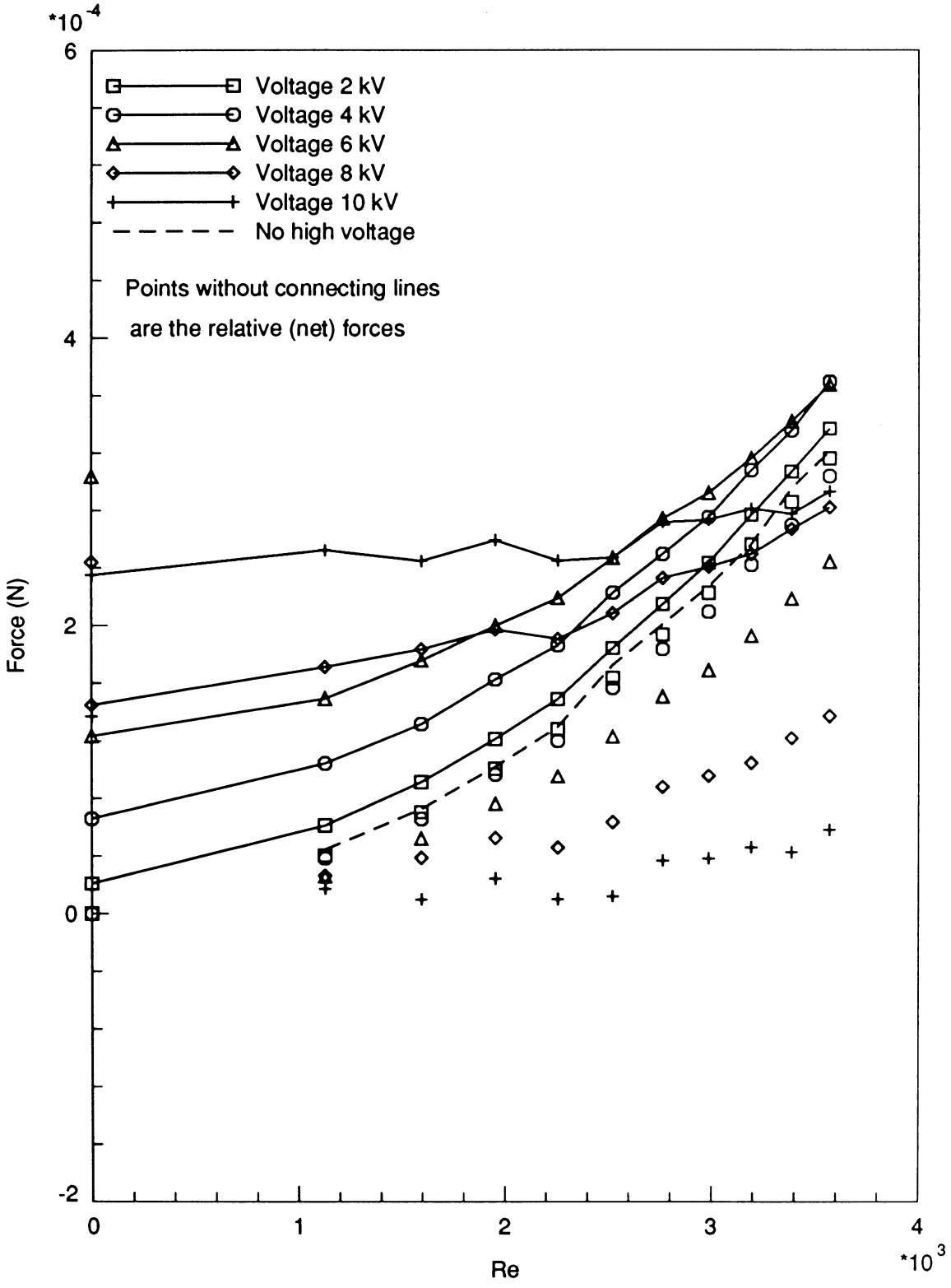

Figure 4.13: AC Source—reversed orientation: Re vs. Force, with 2 kV–10 kV high voltage discharge

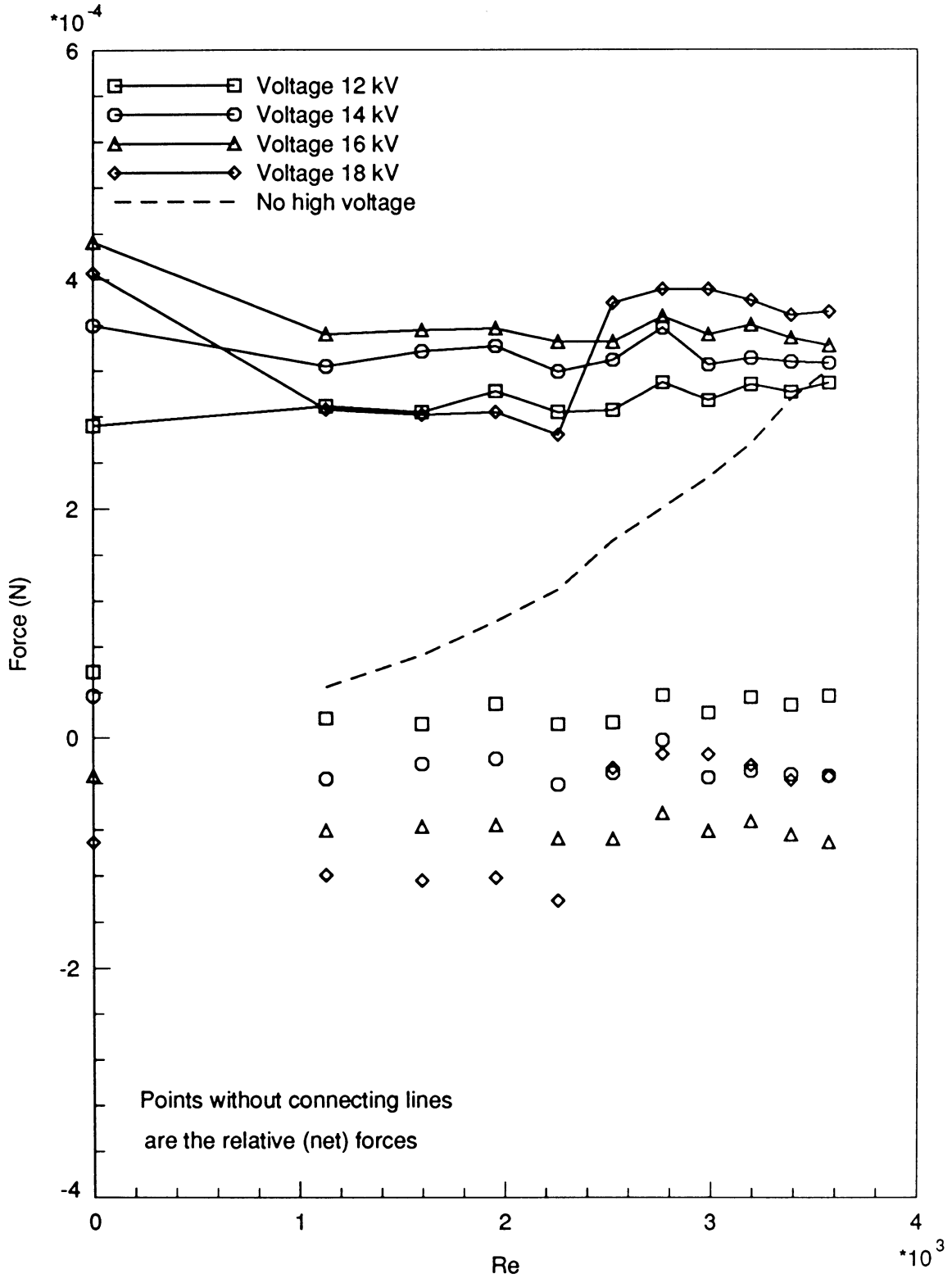

Figure 4.14: AC Source—reversed orientation: Re vs. Force, with 12 kV–18 kV high voltage discharge

Table 4.23: AC Source—reversed orientation: with 18 kV high voltage discharge

Air speed (m/s)	Re_L	Net Force (N)	C_D	Absolute Force (N)	Current (mA)
0.6598	1129.	-0.1194E-03	-0.11700	0.2862E-03	0.1687E+00
0.9331	1596.	-0.1241E-03	-0.06082	0.2815E-03	0.1738E+00
1.1428	1955.	-0.1217E-03	-0.03978	0.2838E-03	0.1772E+00
1.3196	2258.	-0.1416E-03	-0.03471	0.2639E-03	0.1790E+00
1.4754	2524.	-0.2653E-04	-0.00520	0.3790E-03	0.1738E+00
1.6162	2765.	-0.1431E-04	-0.00234	0.3912E-03	0.1705E+00
1.7457	2987.	-0.1454E-04	-0.00204	0.3910E-03	0.1807E+00
1.8662	3193.	-0.2411E-04	-0.00295	0.3814E-03	0.1756E+00
1.9794	3387.	-0.3710E-04	-0.00404	0.3684E-03	0.1790E+00
2.0865	3570.	-0.3403E-04	-0.00334	0.3715E-03	0.1790E+00

DC source—positive polarity

Table 4.24: DC Source—positive polarity: with 2 kV high voltage discharge

Air speed (m/s)	Re	Net Force (N)	C_D	Absolute Force (N)	Current (mA)
0.6598	1129.	0.1989E-04	0.01950	-0.1846E-04	0.0000E+00
0.9331	1596.	0.4935E-04	0.02419	0.1100E-04	0.0000E+00
1.1428	1955.	0.8514E-04	0.02783	0.4679E-04	0.0000E+00
1.3196	2258.	0.1156E-03	0.02834	0.7728E-04	0.0000E+00
1.4754	2524.	0.1551E-03	0.03042	0.1168E-03	0.0000E+00
1.6162	2765.	0.1738E-03	0.02839	0.1354E-03	0.0000E+00
1.7457	2987.	0.2205E-03	0.03089	0.1822E-03	0.0000E+00
1.8662	3193.	0.2629E-03	0.03223	0.2246E-03	0.0000E+00
1.9794	3387.	0.2934E-03	0.03196	0.2550E-03	0.0000E+00
2.0865	3570.	0.3199E-03	0.03136	0.2815E-03	0.0000E+00

Table 4.25: DC Source—positive polarity: with 4 kV high voltage discharge

Air speed (m/s)	Re	Net Force (N)	C_D	Absolute Force (N)	Current (mA)
0.6598	1129.	0.6838E-05	0.00671	-0.7349E-04	0.0000E+00
0.9331	1596.	0.1996E-04	0.00979	-0.6036E-04	0.0000E+00
1.1428	1955.	0.5713E-04	0.01867	-0.2319E-04	0.0000E+00
1.3196	2258.	0.8272E-04	0.02028	0.2401E-05	0.0000E+00
1.4754	2524.	0.1191E-03	0.02336	0.3879E-04	0.0000E+00
1.6162	2765.	0.1342E-03	0.02192	0.5384E-04	0.0000E+00
1.7457	2987.	0.1894E-03	0.02653	0.1091E-03	0.0000E+00
1.8662	3193.	0.2358E-03	0.02890	0.1555E-03	0.0000E+00
1.9794	3387.	0.2671E-03	0.02910	0.1868E-03	0.0000E+00
2.0865	3570.	0.2878E-03	0.02822	0.2075E-03	0.0000E+00

Table 4.26: DC Source—positive polarity: with 6 kV high voltage discharge

Air speed (m/s)	Re	Net Force (N)	C_D	Absolute Force (N)	Current (mA)
0.6598	1129.	-0.5966E-05	-0.00585	-0.1283E-03	0.0000E+00
0.9331	1596.	0.3966E-05	0.00194	-0.1183E-03	0.0000E+00
1.1428	1955.	0.3447E-04	0.01126	-0.8785E-04	0.0000E+00
1.3196	2258.	0.3959E-04	0.00970	-0.8272E-04	0.0000E+00
1.4754	2524.	0.9024E-04	0.01770	-0.3207E-04	0.0000E+00
1.6162	2765.	0.8878E-04	0.01451	-0.3353E-04	0.0000E+00
1.7457	2987.	0.1578E-03	0.02211	0.3553E-04	0.0000E+00
1.8662	3193.	0.2060E-03	0.02525	0.8373E-04	0.0000E+00
1.9794	3387.	0.2405E-03	0.02620	0.1182E-03	0.0000E+00
2.0865	3570.	0.2563E-03	0.02513	0.1340E-03	0.0000E+00

Table 4.27: DC Source—positive polarity: with 8 kV high voltage discharge

Air speed (m/s)	Re	Net Force (N)	C_D	Absolute Force (N)	Current (mA)
0.6598	1129.	-0.2039E-04	-0.01999	-0.1888E-03	0.0000E+00
0.9331	1596.	-0.8858E-05	-0.00434	-0.1773E-03	0.0000E+00
1.1428	1955.	0.2582E-04	0.00844	-0.1426E-03	0.0000E+00
1.3196	2258.	0.2722E-04	0.00667	-0.1412E-03	0.0000E+00
1.4754	2524.	0.5082E-04	0.00996	-0.1176E-03	0.0000E+00
1.6162	2765.	0.4980E-04	0.00814	-0.1187E-03	0.0000E+00
1.7457	2987.	0.1322E-03	0.01852	-0.3622E-04	0.0000E+00
1.8662	3193.	0.1809E-03	0.02217	0.1240E-04	0.0000E+00
1.9794	3387.	0.2144E-03	0.02336	0.4596E-04	0.0000E+00
2.0865	3570.	0.2200E-03	0.02157	0.5152E-04	0.0000E+00

Table 4.28: DC Source—positive polarity: with 10 kV high voltage discharge

Air speed (m/s)	Re	Net Force (N)	C_D	Absolute Force (N)	Current (mA)
0.6598	1129.	-0.3288E-04	-0.03224	-0.2478E-03	0.0000E+00
0.9331	1596.	-0.2457E-04	-0.01204	-0.2395E-03	0.0000E+00
1.1428	1955.	0.1586E-04	0.00518	-0.1990E-03	0.0000E+00
1.3196	2258.	0.1215E-04	0.00298	-0.2028E-03	0.0000E+00
1.4754	2524.	0.3574E-04	0.00701	-0.1792E-03	0.0000E+00
1.6162	2765.	0.2930E-04	0.00479	-0.1856E-03	0.1023E-03
1.7457	2987.	0.9089E-04	0.01273	-0.1240E-03	0.0000E+00
1.8662	3193.	0.1493E-03	0.01830	-0.6558E-04	0.0000E+00
1.9794	3387.	0.1976E-03	0.02152	-0.1734E-04	0.0000E+00
2.0865	3570.	0.1884E-03	0.01847	-0.2649E-04	0.0000E+00

Table 4.29: DC Source—positive polarity: with 12 kV high voltage discharge

Air speed (m/s)	Re	Net Force (N)	C_D	Absolute Force (N)	Current (mA)
0.6598	1129.	-0.4475E-04	-0.04387	-0.3167E-03	0.0000E+00
0.9331	1596.	-0.3610E-04	-0.01770	-0.3080E-03	0.0000E+00
1.1428	1955.	0.9781E-05	0.00320	-0.2622E-03	0.0000E+00
1.3196	2258.	-0.1614E-05	-0.00040	-0.2736E-03	0.0000E+00
1.4754	2524.	0.2423E-04	0.00475	-0.2477E-03	0.0000E+00
1.6162	2765.	0.1392E-04	0.00228	-0.2580E-03	0.1023E-03
1.7457	2987.	0.7548E-04	0.01057	-0.1965E-03	0.0000E+00
1.8662	3193.	0.1243E-03	0.01524	-0.1476E-03	0.0000E+00
1.9794	3387.	0.1619E-03	0.01764	-0.1100E-03	0.0000E+00
2.0865	3570.	0.1523E-03	0.01493	-0.1196E-03	0.0000E+00

Table 4.30: DC Source—positive polarity: with 14 kV high voltage discharge

Air speed (m/s)	Re	Net Force (N)	C_D	Absolute Force (N)	Current (mA)
0.6598	1129.	-0.4378E-04	-0.04293	-0.3907E-03	0.1023E-03
0.9331	1596.	-0.3610E-04	-0.01770	-0.3830E-03	0.0000E+00
1.1428	1955.	-0.5142E-04	-0.01680	-0.3983E-03	0.6136E-03
1.3196	2258.	-0.1775E-03	-0.04352	-0.5245E-03	0.4295E-02
1.4754	2524.	-0.1591E-03	-0.03119	-0.5060E-03	0.4295E-02
1.6162	2765.	-0.1594E-03	-0.02605	-0.5063E-03	0.1432E-02
1.7457	2987.	-0.4916E-04	-0.00689	-0.3961E-03	0.1432E-02
1.8662	3193.	0.1856E-04	0.00228	-0.3284E-03	0.7158E-03
1.9794	3387.	0.8635E-04	0.00941	-0.2606E-03	0.8181E-03
2.0865	3570.	0.8725E-04	0.00855	-0.2597E-03	0.6136E-03

Table 4.31: DC Source—positive polarity: with 16 kV high voltage discharge

Air speed (m/s)	Re	Net Force (N)	C_D	Absolute Force (N)	Current (mA)
0.6598	1129.	-0.1543E-03	-0.15130	-0.6381E-03	0.2577E-01
0.9331	1596.	-0.1572E-03	-0.07708	-0.6410E-03	0.2557E-01
1.1428	1955.	-0.1447E-03	-0.04728	-0.6284E-03	0.3180E-01
1.3196	2258.	-0.2032E-03	-0.04980	-0.6869E-03	0.3099E-01
1.4754	2524.	-0.1379E-03	-0.02704	-0.6217E-03	0.3354E-01
1.6162	2765.	-0.1799E-03	-0.02940	-0.6637E-03	0.3129E-01
1.7457	2987.	-0.5043E-04	-0.00706	-0.5342E-03	0.2250E-01
1.8662	3193.	-0.8366E-04	-0.01025	-0.5674E-03	0.6238E-02
1.9794	3387.	-0.6744E-04	-0.00735	-0.5512E-03	0.4397E-02
2.0865	3570.	-0.6688E-04	-0.00656	-0.5506E-03	0.4704E-02

Table 4.32: DC Source—positive polarity: with 18 kV high voltage discharge

Air speed (m/s)	Re	Net Force (N)	C_D	Absolute Force (N)	Current (mA)
0.6598	1129.	-0.1160E-05	-0.00114	-0.7150E-03	0.9337E-01
0.9331	1596.	-0.2152E-03	-0.10550	-0.9290E-03	0.9531E-01
1.1428	1955.	-0.2286E-03	-0.07472	-0.9424E-03	0.1002E+00
1.3196	2258.	-0.2692E-03	-0.06598	-0.9830E-03	0.1005E+00
1.4754	2524.	-0.1543E-03	-0.03025	-0.8681E-03	0.7690E-01
1.6162	2765.	-0.4376E-04	-0.00715	-0.7576E-03	0.8181E-01
1.7457	2987.	0.3030E-04	0.00424	-0.6835E-03	0.8314E-01
1.8662	3193.	0.1535E-04	0.00188	-0.6985E-03	0.6115E-01
1.9794	3387.	0.1523E-03	0.01660	-0.5615E-03	0.5011E-01
2.0865	3570.	0.2060E-04	0.00202	-0.6932E-03	0.6933E-01

Table 4.33: DC Source—positive polarity: with 20 kV high voltage discharge

Air speed (m/s)	Re	Net Force (N)	C_D	Absolute Force (N)	Current (mA)
0.6598	1129.	0.5748E-04	0.05636	-0.7252E-03	0.1457E+00
0.9331	1596.	-0.1238E-04	-0.00607	-0.7951E-03	0.1362E+00
1.1428	1955.	-0.5205E-04	-0.01701	-0.8348E-03	0.1513E+00
1.3196	2258.	-0.1609E-03	-0.03943	-0.9436E-03	0.1483E+00
1.4754	2524.	-0.2063E-04	-0.00404	-0.8034E-03	0.1419E+00
1.6162	2765.	-0.1027E-03	-0.01678	-0.8854E-03	0.1331E+00
1.7457	2987.	0.7388E-04	0.01035	-0.7088E-03	0.1362E+00
1.8662	3193.	0.1564E-03	0.01916	-0.6264E-03	0.9347E-01
1.9794	3387.	0.5303E-04	0.00578	-0.7297E-03	0.1253E+00
2.0865	3570.	0.1058E-03	0.01038	-0.6769E-03	0.1248E+00

Table 4.34: DC Source—positive polarity: with 22 kV high voltage discharge

Air speed (m/s)	Re	Net Force (N)	C_D	Absolute Force (N)	Current (mA)
0.6598	1129.	-0.1750E-04	-0.01716	-0.7079E-03	0.2012E+00
0.9331	1596.	-0.1252E-03	-0.06137	-0.8156E-03	0.1969E+00
1.1428	1955.	-0.8891E-04	-0.02906	-0.7793E-03	0.2042E+00
1.3196	2258.	-0.3108E-03	-0.07619	-0.1001E-02	0.2074E+00
1.4754	2524.	-0.2068E-03	-0.04055	-0.8973E-03	0.2068E+00
1.6162	2765.	-0.1575E-03	-0.02574	-0.8479E-03	0.1897E+00
1.7457	2987.	-0.1116E-03	-0.01564	-0.8021E-03	0.2112E+00
1.8662	3193.	-0.1764E-04	-0.00216	-0.7081E-03	0.1621E+00
1.9794	3387.	-0.8156E-04	-0.00888	-0.7720E-03	0.2001E+00
2.0865	3570.	-0.1073E-03	-0.01052	-0.7977E-03	0.1974E+00

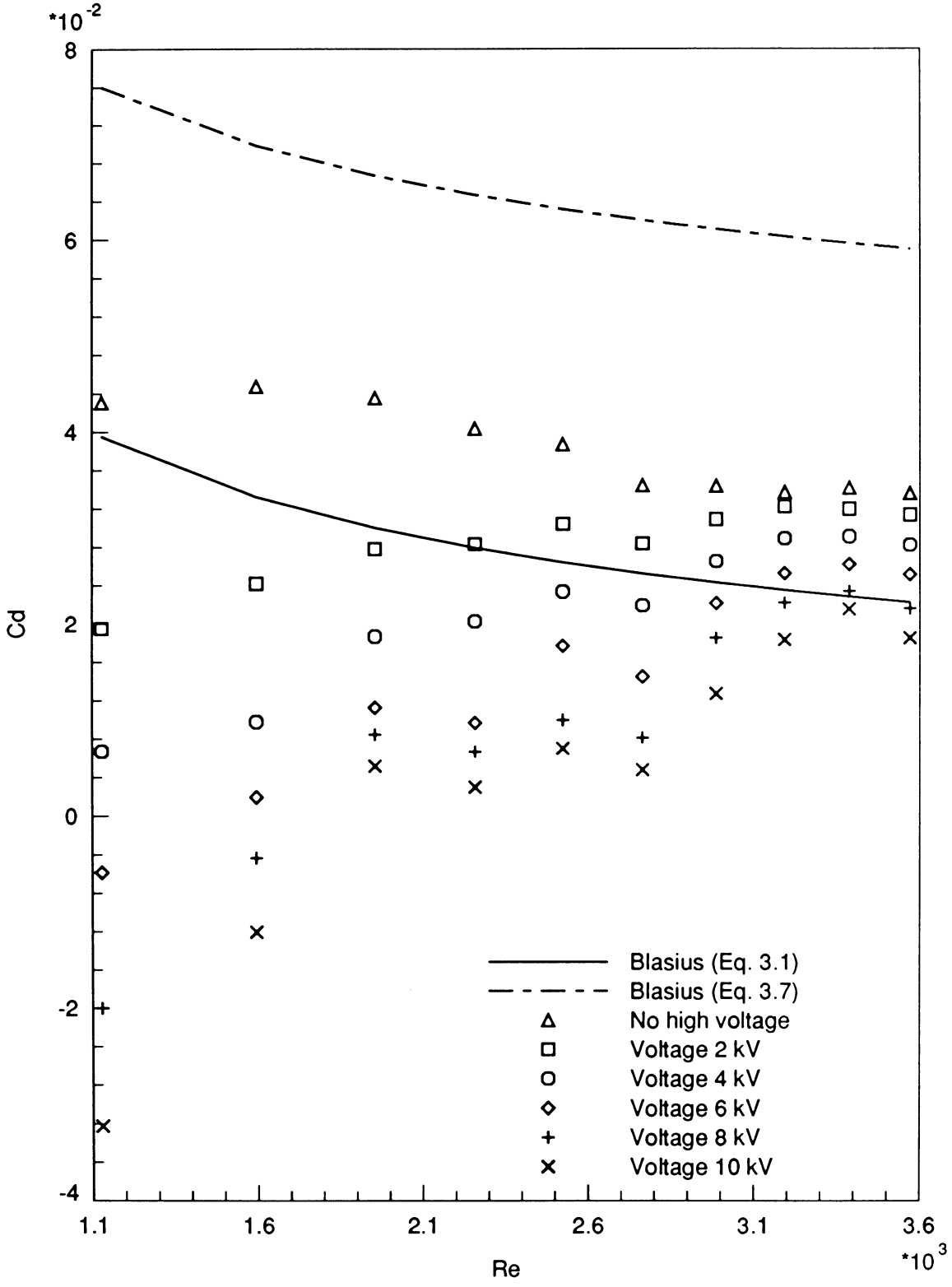

Figure 4.15: DC Source—positive polarity: Re vs. C_D, with 2 kV–10 kV high voltage discharge

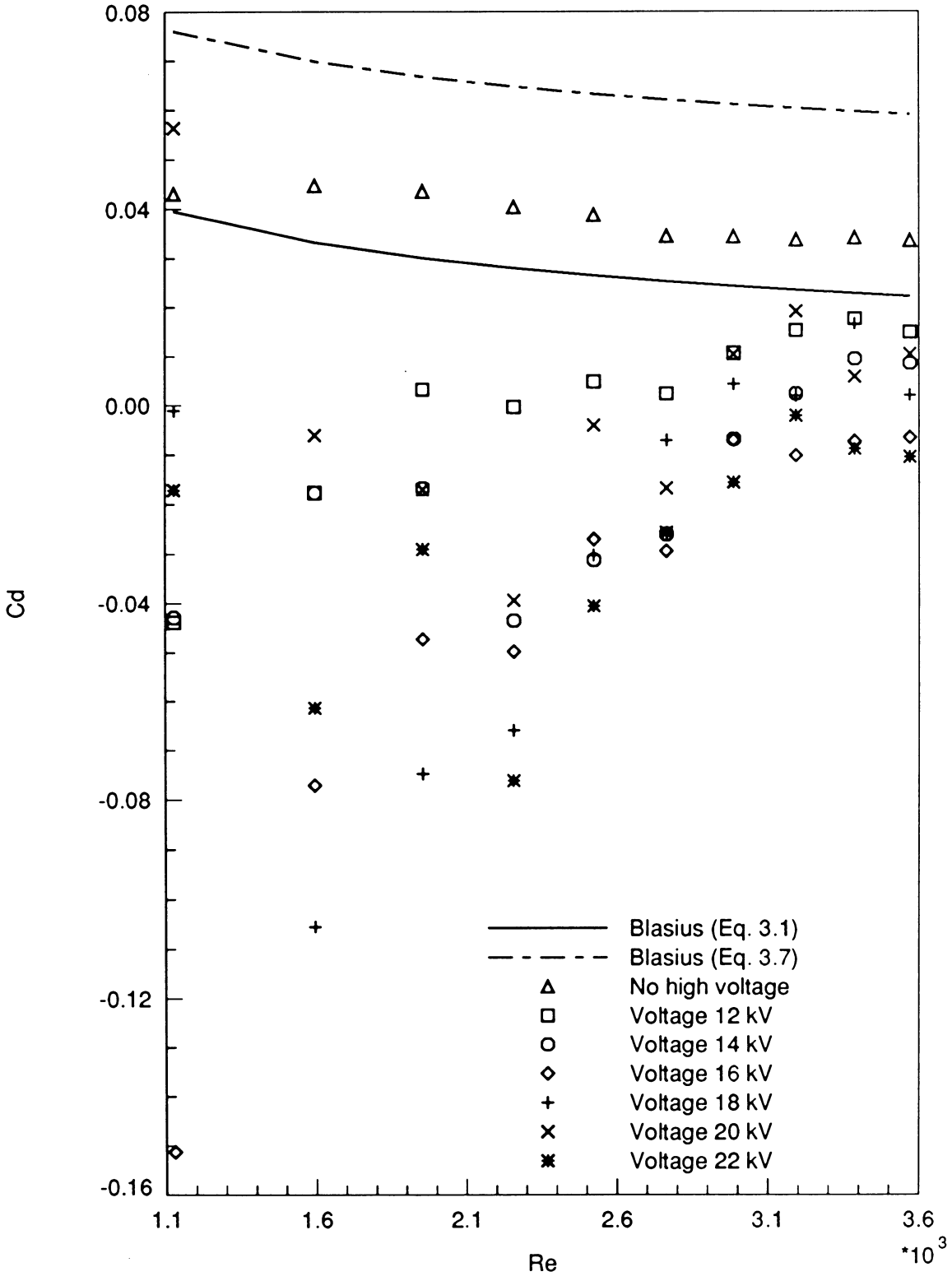

Figure 4.16: DC Source—positive polarity: Re vs. C_D, with 12 kV–22 kV high voltage discharge

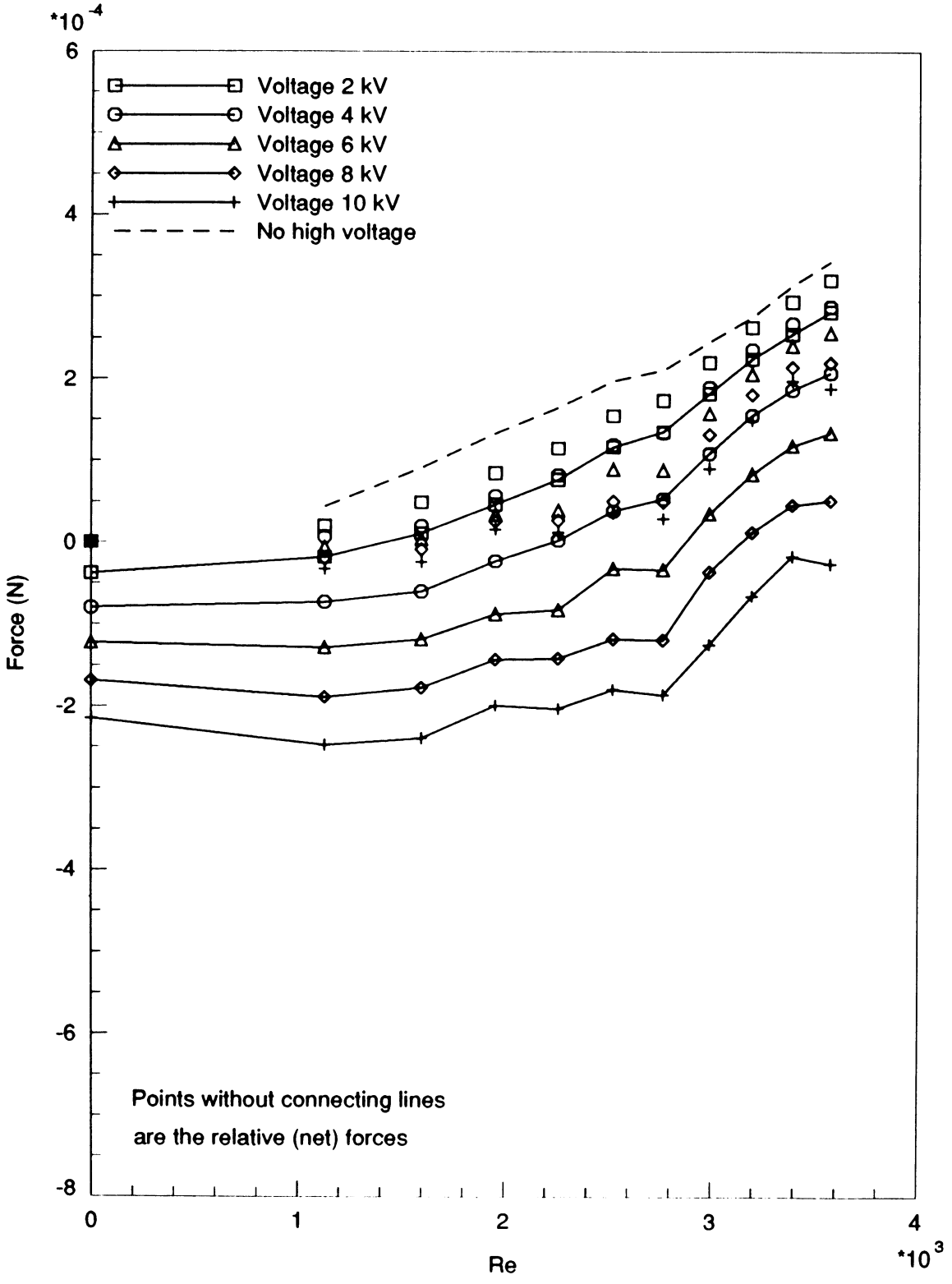

Figure 4.17: DC Source—positive polarity: Re vs. Force, with 2 kV–10 kV high voltage discharge

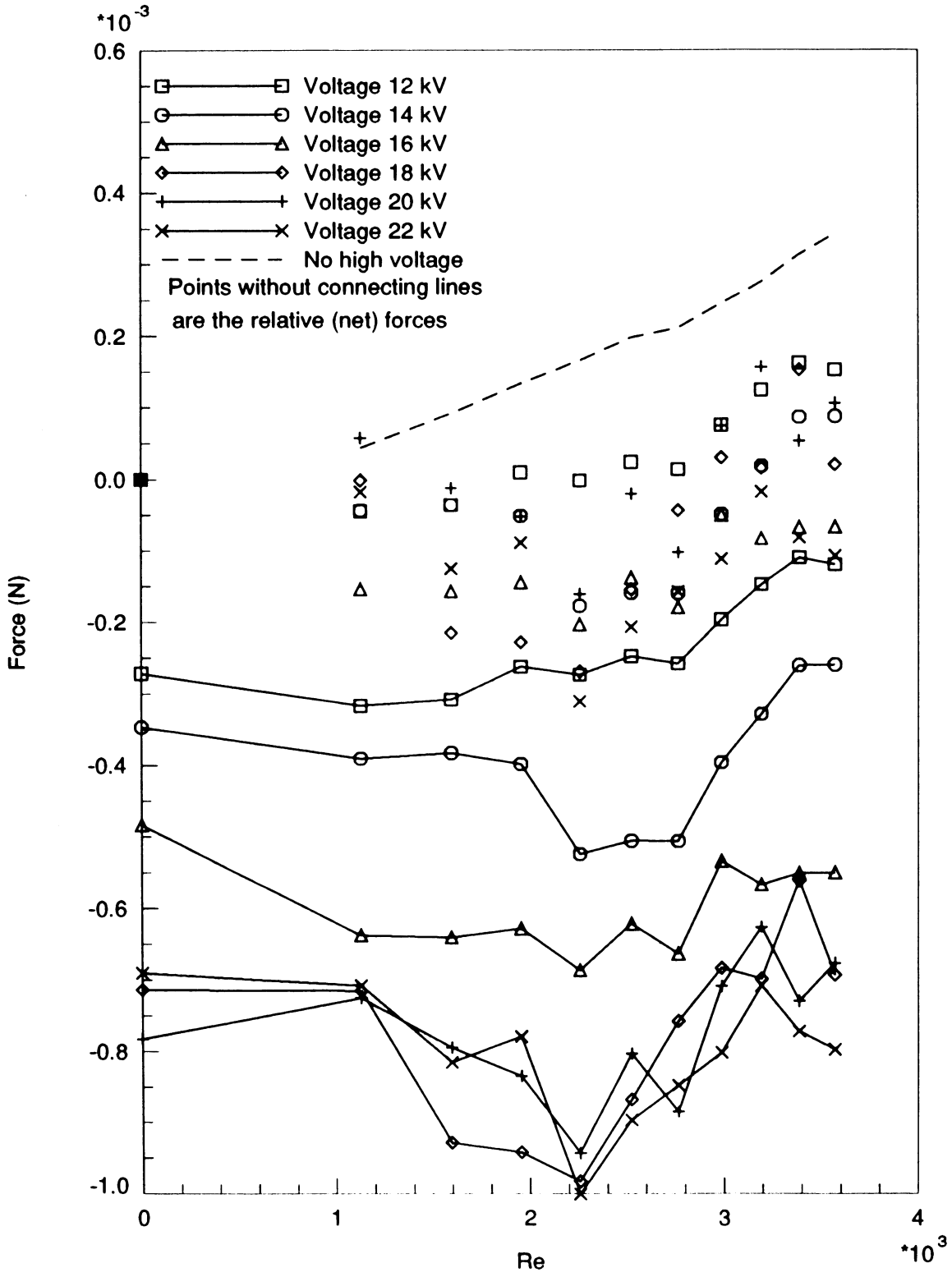

Figure 4.18: DC Source—positive polarity: Re vs. Force, with 12 kV–22 kV high voltage discharge

DC source—negative polarity

Table 4.35: DC Source—negative polarity: with 2 kV high voltage discharge

Air speed (m/s)	Re	Net Force (N)	C_D	Absolute Force (N)	Current (mA)
0.6598	1129.	0.3413E-04	0.03346	0.3101E-04	0.0000E+00
0.9331	1596.	0.7784E-04	0.03816	0.7473E-04	0.0000E+00
1.1428	1955.	0.1061E-03	0.03466	0.1030E-03	0.0000E+00
1.3196	2258.	0.1477E-03	0.03621	0.1446E-03	0.0000E+00
1.4754	2524.	0.1810E-03	0.03549	0.1779E-03	0.0000E+00
1.6162	2765.	0.2040E-03	0.03334	0.2009E-03	0.0000E+00
1.7457	2987.	0.2419E-03	0.03388	0.2388E-03	0.0000E+00
1.8662	3193.	0.2749E-03	0.03369	0.2718E-03	0.0000E+00
1.9794	3387.	0.3134E-03	0.03414	0.3103E-03	0.0000E+00
2.0865	3570.	0.3457E-03	0.03389	0.3426E-03	0.0000E+00

Table 4.36: DC Source—negative polarity: with 4 kV high voltage discharge

Air speed (m/s)	Re	Net Force (N)	C_D	Absolute Force (N)	Current (mA)
0.6598	1129.	0.3218E-04	0.03155	0.1272E-04	0.0000E+00
0.9331	1596.	0.8661E-04	0.04246	0.6716E-04	0.0000E+00
1.1428	1955.	0.1068E-03	0.03490	0.8733E-04	0.0000E+00
1.3196	2258.	0.1582E-03	0.03879	0.1388E-03	0.0000E+00
1.4754	2524.	0.1902E-03	0.03729	0.1707E-03	0.0000E+00
1.6162	2765.	0.2070E-03	0.03383	0.1876E-03	0.0000E+00
1.7457	2987.	0.2515E-03	0.03523	0.2321E-03	0.0000E+00
1.8662	3193.	0.2810E-03	0.03444	0.2616E-03	0.0000E+00
1.9794	3387.	0.3253E-03	0.03544	0.3058E-03	0.0000E+00
2.0865	3570.	0.3571E-03	0.03501	0.3377E-03	0.0000E+00

Table 4.37: DC Source—negative polarity: with 6 kV high voltage discharge

Air speed (m/s)	Re	Net Force (N)	C_D	Absolute Force (N)	Current (mA)
0.6598	1129.	0.2672E-04	0.02619	-0.5543E-05	0.0000E+00
0.9331	1596.	0.8960E-04	0.04393	0.5735E-04	0.0000E+00
1.1428	1955.	0.1022E-03	0.03340	0.6995E-04	0.0000E+00
1.3196	2258.	0.1639E-03	0.04018	0.1317E-03	0.0000E+00
1.4754	2524.	0.1909E-03	0.03744	0.1587E-03	0.0000E+00
1.6162	2765.	0.2047E-03	0.03344	0.1724E-03	0.0000E+00
1.7457	2987.	0.2528E-03	0.03541	0.2205E-03	0.0000E+00
1.8662	3193.	0.2822E-03	0.03459	0.2500E-03	0.0000E+00
1.9794	3387.	0.3318E-03	0.03615	0.2996E-03	0.0000E+00
2.0865	3570.	0.3628E-03	0.03557	0.3305E-03	0.0000E+00

Table 4.38: DC Source—negative polarity: with 8 kV high voltage discharge

Air speed (m/s)	Re	Net Force (N)	C_D	Absolute Force (N)	Current (mA)
0.6598	1129.	0.7819E-05	0.00767	-0.3855E-04	0.0000E+00
0.9331	1596.	0.8946E-04	0.04386	0.4309E-04	0.0000E+00
1.1428	1955.	0.9137E-04	0.02986	0.4500E-04	0.0000E+00
1.3196	2258.	0.1647E-03	0.04037	0.1183E-03	0.0000E+00
1.4754	2524.	0.1872E-03	0.03671	0.1408E-03	0.0000E+00
1.6162	2765.	0.1951E-03	0.03189	0.1488E-03	0.0000E+00
1.7457	2987.	0.2517E-03	0.03526	0.2053E-03	0.0000E+00
1.8662	3193.	0.2816E-03	0.03452	0.2353E-03	0.0000E+00
1.9794	3387.	0.3375E-03	0.03677	0.2911E-03	0.0000E+00
2.0865	3570.	0.3644E-03	0.03573	0.3180E-03	0.0000E+00

Table 4.39: DC Source—negative polarity: with 10 kV high voltage discharge

Air speed (m/s)	Re	Net Force (N)	C_D	Absolute Force (N)	Current (mA)
0.6598	1129.	0.1293E-04	0.01268	-0.5393E-04	0.0000E+00
0.9331	1596.	0.9303E-04	0.04561	0.2616E-04	0.0000E+00
1.1428	1955.	0.8378E-04	0.02738	0.1692E-04	0.0000E+00
1.3196	2258.	0.1722E-03	0.04222	0.1054E-03	0.0000E+00
1.4754	2524.	0.1948E-03	0.03820	0.1279E-03	0.0000E+00
1.6162	2765.	0.1951E-03	0.03189	0.1283E-03	0.0000E+00
1.7457	2987.	0.2481E-03	0.03476	0.1813E-03	0.0000E+00
1.8662	3193.	0.2830E-03	0.03468	0.2161E-03	0.0000E+00
1.9794	3387.	0.3500E-03	0.03813	0.2831E-03	0.0000E+00
2.0865	3570.	0.3680E-03	0.03608	0.3011E-03	0.0000E+00

Table 4.40: DC Source—negative polarity: with 12 kV high voltage discharge

Air speed (m/s)	Re	Net Force (N)	C_D	Absolute Force (N)	Current (mA)
0.6598	1129.	0.3729E-04	0.03656	-0.1042E-03	0.0000E+00
0.9331	1596.	0.1071E-03	0.05249	-0.3446E-04	0.0000E+00
1.1428	1955.	0.9917E-04	0.03241	-0.4237E-04	0.0000E+00
1.3196	2258.	0.2193E-03	0.05375	0.7774E-04	0.0000E+00
1.4754	2524.	0.2084E-03	0.04087	0.6687E-04	0.0000E+00
1.6162	2765.	0.2114E-03	0.03455	0.6989E-04	0.0000E+00
1.7457	2987.	0.2359E-03	0.03304	0.9437E-04	0.0000E+00
1.8662	3193.	0.3028E-03	0.03711	0.1613E-03	0.0000E+00
1.9794	3387.	0.3524E-03	0.03839	0.2109E-03	0.0000E+00
2.0865	3570.	0.3865E-03	0.03789	0.2449E-03	0.0000E+00

Table 4.41: DC Source—negative polarity: with 14 kV high voltage discharge

Air speed (m/s)	Re	Net Force (N)	C_D	Absolute Force (N)	Current (mA)
0.6598	1129.	0.3087E-04	0.03027	-0.2158E-03	0.0000E+00
0.9331	1596.	0.3984E-04	0.01953	-0.2068E-03	0.3681E-02
1.1428	1955.	0.6777E-04	0.02215	-0.1789E-03	0.0000E+00
1.3196	2258.	0.1661E-03	0.04072	-0.8050E-04	0.0000E+00
1.4754	2524.	0.1735E-03	0.03403	-0.7310E-04	0.0000E+00
1.6162	2765.	0.1690E-03	0.02761	-0.7765E-04	0.0000E+00
1.7457	2987.	0.1707E-03	0.02392	-0.7588E-04	0.0000E+00
1.8662	3193.	0.2483E-03	0.03044	0.1706E-05	0.0000E+00
1.9794	3387.	0.2806E-03	0.03056	0.3393E-04	0.9817E-02
2.0865	3570.	0.3378E-03	0.03312	0.9118E-04	0.5522E-02

Table 4.42: DC Source—negative polarity: with 16 kV high voltage discharge

Air speed (m/s)	Re	Net Force (N)	C_D	Absolute Force (N)	Current (mA)
0.6598	1129.	0.1103E-04	0.01081	-0.1978E-03	0.4776E-01
0.9331	1596.	0.8791E-04	0.04310	-0.1209E-03	0.3303E-01
1.1428	1955.	0.1008E-03	0.03294	-0.1080E-03	0.2996E-01
1.3196	2258.	0.8746E-04	0.02144	-0.1214E-03	0.2966E-01
1.4754	2524.	0.9215E-04	0.01807	-0.1167E-03	0.2055E-01
1.6162	2765.	0.8438E-04	0.01379	-0.1245E-03	0.3099E-01
1.7457	2987.	0.6385E-04	0.00894	-0.1450E-03	0.3753E-01
1.8662	3193.	0.3300E-03	0.04044	0.1212E-03	0.3099E-01
1.9794	3387.	0.2539E-03	0.02766	0.4508E-04	0.4827E-01
2.0865	3570.	0.2216E-03	0.02172	0.1274E-04	0.4039E-01

Table 4.43: DC Source—negative polarity: with 18 kV high voltage discharge

Air speed (m/s)	Re	Net Force (N)	C_D	Absolute Force (N)	Current (mA)
0.6598	1129.	0.7703E-04	0.07553	-0.1558E-03	0.7567E-01
0.9331	1596.	0.9144E-04	0.04483	-0.1414E-03	0.7077E-01
1.1428	1955.	0.1050E-03	0.03430	-0.1279E-03	0.6310E-01
1.3196	2258.	0.8394E-04	0.02058	-0.1489E-03	0.6391E-01
1.4754	2524.	0.7677E-04	0.01505	-0.1561E-03	0.6136E-01
1.6162	2765.	0.1517E-03	0.02478	-0.8121E-04	0.6780E-01
1.7457	2987.	0.1204E-03	0.01687	-0.1124E-03	0.7619E-01
1.8662	3193.	0.2689E-03	0.03296	0.3604E-04	0.6770E-01
1.9794	3387.	0.2311E-03	0.02518	-0.1720E-05	0.8641E-01
2.0865	3570.	0.2037E-03	0.01997	-0.2917E-04	0.8692E-01

Table 4.44: DC Source—negative polarity: with 20 kV high voltage discharge

Air speed (m/s)	Re	Net Force (N)	C_D	Absolute Force (N)	Current (mA)
0.6598	1129.	0.1687E-03	0.16540	-0.1946E-03	0.1026E+00
0.9331	1596.	0.1882E-03	0.09227	-0.1751E-03	0.1084E+00
1.1428	1955.	0.2610E-03	0.08530	-0.1023E-03	0.1005E+00
1.3196	2258.	0.2935E-03	0.07193	-0.6981E-04	0.9797E-01
1.4754	2524.	0.2911E-03	0.05708	-0.7219E-04	0.9562E-01
1.6162	2765.	0.3195E-03	0.05221	-0.4377E-04	0.1025E+00
1.7457	2987.	0.3204E-03	0.04487	-0.4291E-04	0.1030E+00
1.8662	3193.	0.3338E-03	0.04091	-0.2948E-04	0.9889E-01
1.9794	3387.	0.3660E-03	0.03987	0.2719E-05	0.1224E+00
2.0865	3570.	0.2156E-03	0.02113	-0.1477E-03	0.1411E+00

Table 4.45: DC Source—negative polarity: with 22 kV high voltage discharge

Air speed (m/s)	Re	Net Force (N)	C_D	Absolute Force (N)	Current (mA)
0.6598	1129.	0.4850E-04	0.04755	-0.4509E-03	0.2007E+00
0.9331	1596.	0.2459E-03	0.12050	-0.2536E-03	0.1652E+00
1.1428	1955.	0.2158E-03	0.07053	-0.2836E-03	0.1879E+00
1.3196	2258.	0.4127E-03	0.10120	-0.8673E-04	0.1444E+00
1.4754	2524.	0.3947E-03	0.07740	-0.1047E-03	0.1498E+00
1.6162	2765.	0.4414E-03	0.07213	-0.5803E-04	0.1363E+00
1.7457	2987.	0.4708E-03	0.06594	-0.2865E-04	0.1546E+00
1.8662	3193.	0.3434E-03	0.04208	-0.1561E-03	0.1633E+00
1.9794	3387.	0.3604E-03	0.03927	-0.1390E-03	0.2096E+00
2.0865	3570.	0.3767E-03	0.03693	-0.1228E-03	0.1931E+00

Table 4.46: DC Source—negative polarity: with 24 kV high voltage discharge

Air speed (m/s)	Re	Net Force (N)	C_D	Absolute Force (N)	Current (mA)
0.6598	1129.	0.1168E-03	0.11450	-0.4247E-03	0.2562E+00
0.9331	1596.	0.7958E-04	0.03901	-0.4619E-03	0.2528E+00
1.1428	1955.	0.2107E-03	0.06886	-0.3307E-03	0.2456E+00
1.3196	2258.	0.3281E-03	0.08043	-0.2133E-03	0.2564E+00
1.4754	2524.	0.3178E-03	0.06231	-0.2237E-03	0.2272E+00
1.6162	2765.	0.2722E-03	0.04448	-0.2692E-03	0.2457E+00
1.7457	2987.	0.4183E-03	0.05859	-0.1231E-03	0.2018E+00
1.8662	3193.	0.3961E-03	0.04854	-0.1454E-03	0.2093E+00
1.9794	3387.	0.4885E-03	0.05321	-0.5299E-04	0.2620E+00
2.0865	3570.	0.4900E-03	0.04804	-0.5144E-04	0.2456E+00

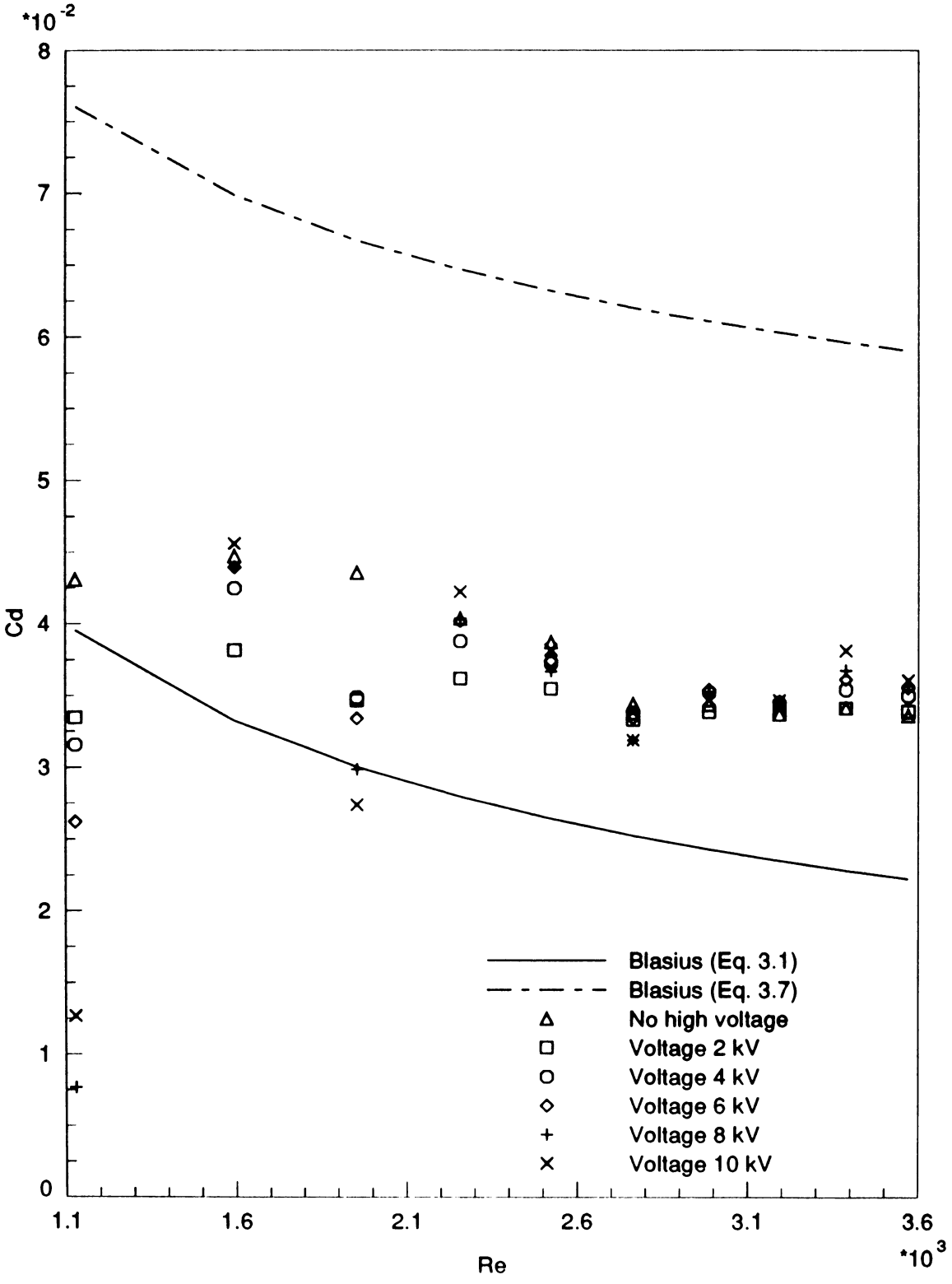

Figure 4.19: DC Source—negative polarity: Re vs. C_D, with 2 kV–10 kV high voltage discharge

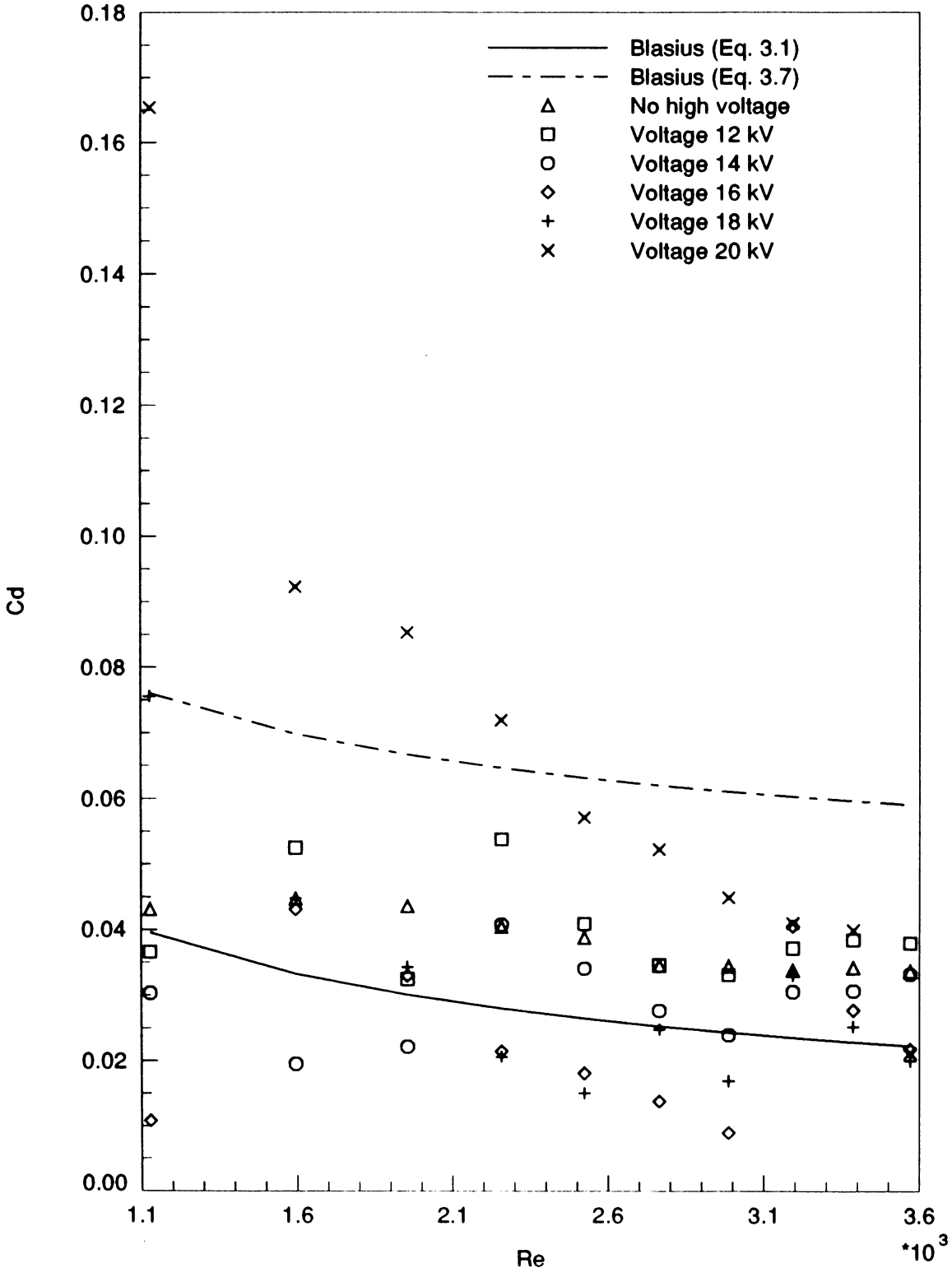

Figure 4.20: DC Source—negative polarity: Re vs. C_D, with 12 kV–20 kV high voltage discharge

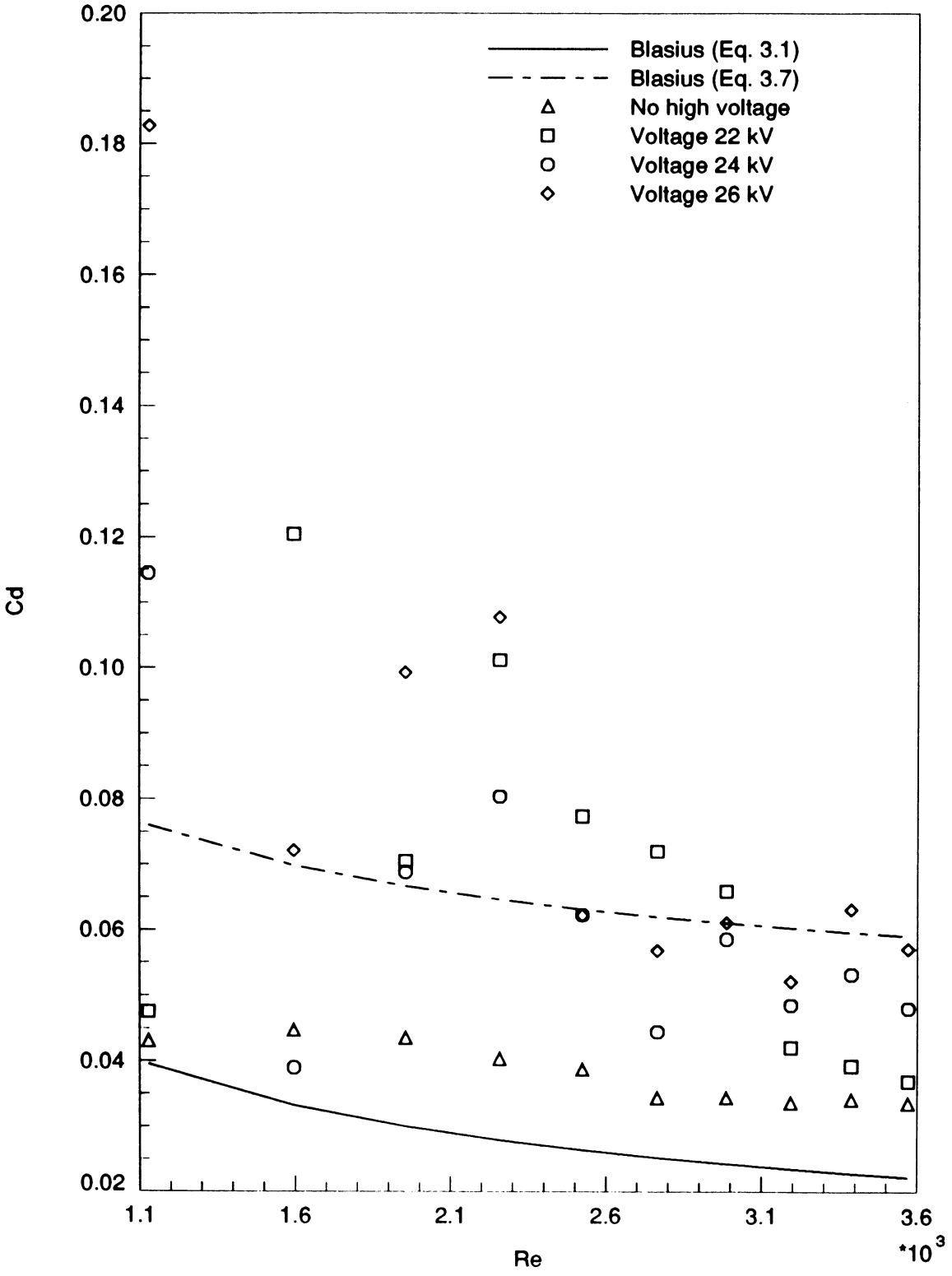

Figure 4.21: DC Source—negative polarity: Re vs. C_D, with 22 kV–26 kV high voltage discharge

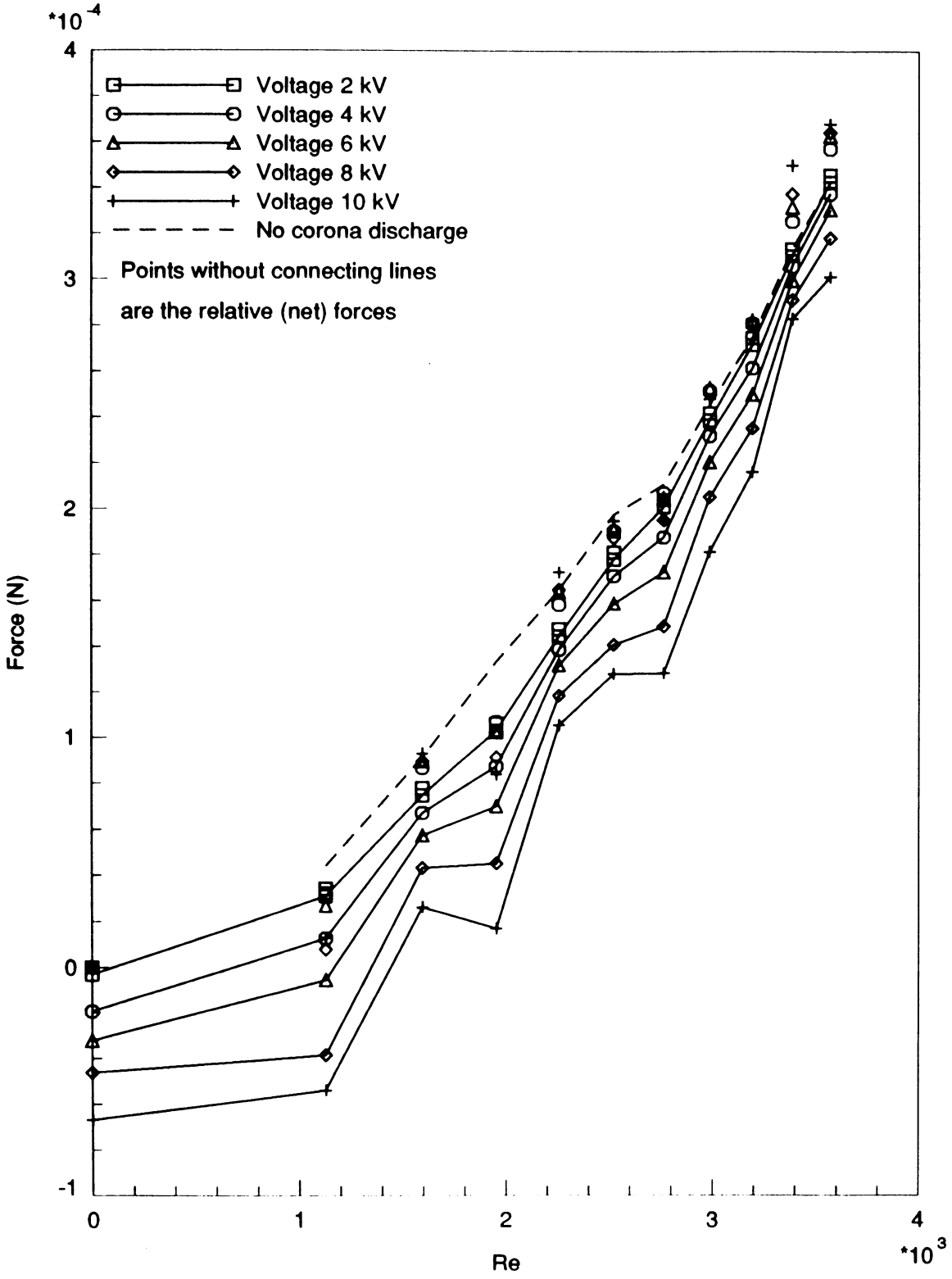

Figure 4.22: DC Source—negative polarity: Re vs. Force, with 2 kV–10 kV high voltage discharge

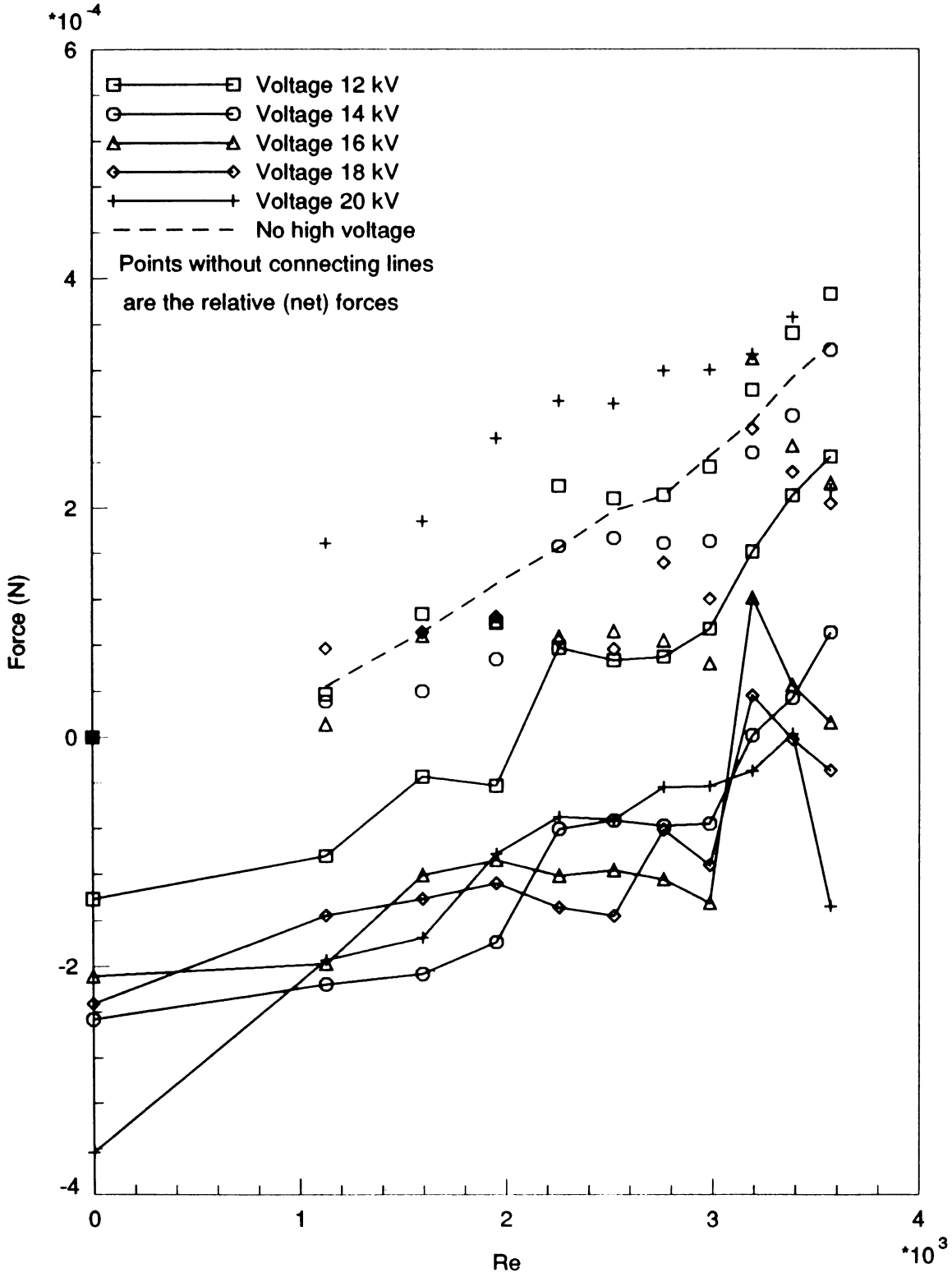

Figure 4.23: DC Source—negative polarity: Re vs. Force, with 12 kV–20 kV high voltage discharge

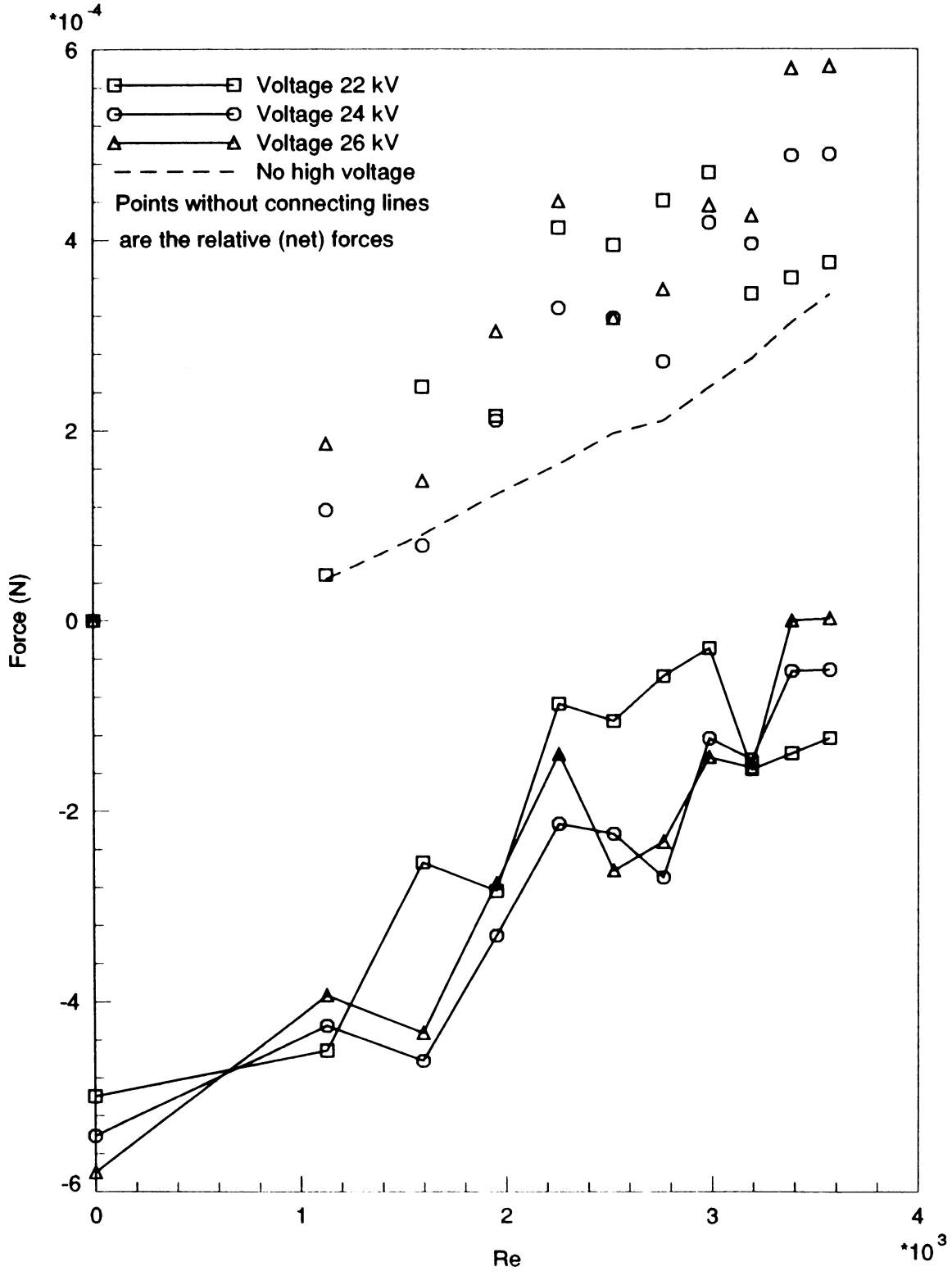

Figure 4.24: DC Source—negative polarity: Re vs. Force, with 22 kV–26 kV high voltage discharge

Table 4.47: DC Source—negative polarity: with 26 kV high voltage discharge

Air speed (m/s)	Re	Net Force (N)	C_D	Absolute Force (N)	Current (mA)
0.6598	1129.	0.1863E-03	0.18270	-0.3933E-03	0.3242E+00
0.9331	1596.	0.1472E-03	0.07215	-0.4324E-03	0.3336E+00
1.1428	1955.	0.3039E-03	0.09933	-0.2756E-03	0.3259E+00
1.3196	2258.	0.4399E-03	0.10780	-0.1396E-03	0.3224E+00
1.4754	2524.	0.3174E-03	0.06225	-0.2621E-03	0.3134E+00
1.6162	2765.	0.3478E-03	0.05684	-0.2317E-03	0.3165E+00
1.7457	2987.	0.4364E-03	0.06112	-0.1432E-03	0.3004E+00
1.8662	3193.	0.4253E-03	0.05212	-0.1543E-03	0.3071E+00
1.9794	3387.	0.5796E-03	0.06314	0.4481E-07	0.3234E+00
2.0865	3570.	0.5820E-03	0.05707	0.2469E-05	0.3116E+00

Photographs of actual discharge on the plate

As noted above, these photographs were taken with the glass plate outside the wind tunnel. The left blade is the charged electrode, and in the actual experiment the air was flowing was from the left to right.

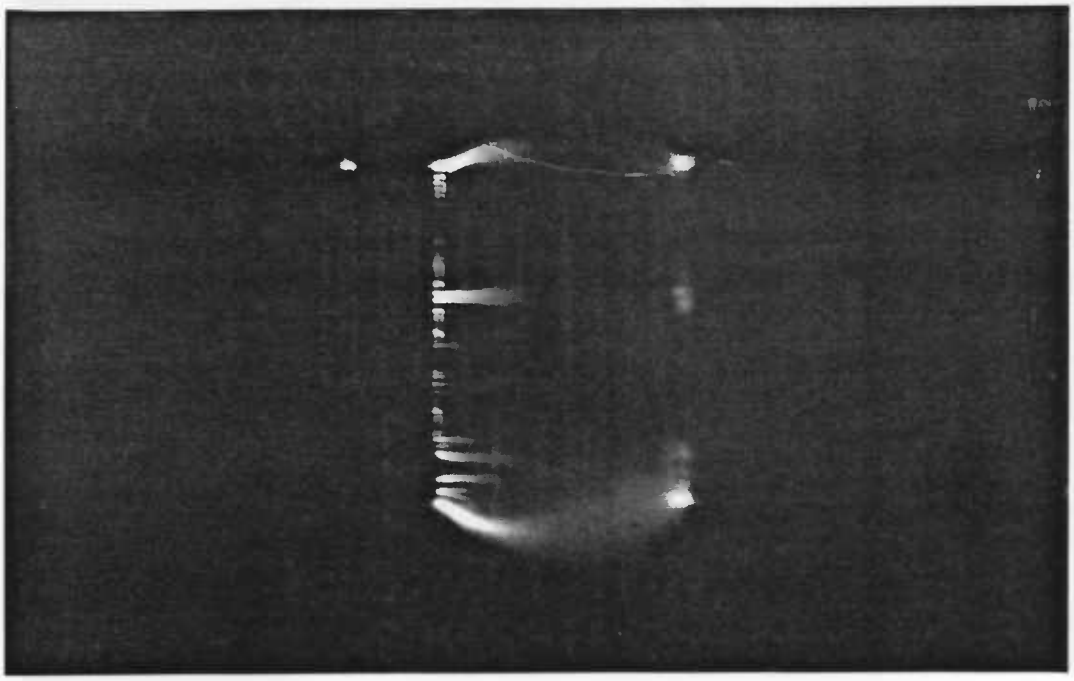

Figure 4.25: AC Source, 20 kV high voltage discharge: top view

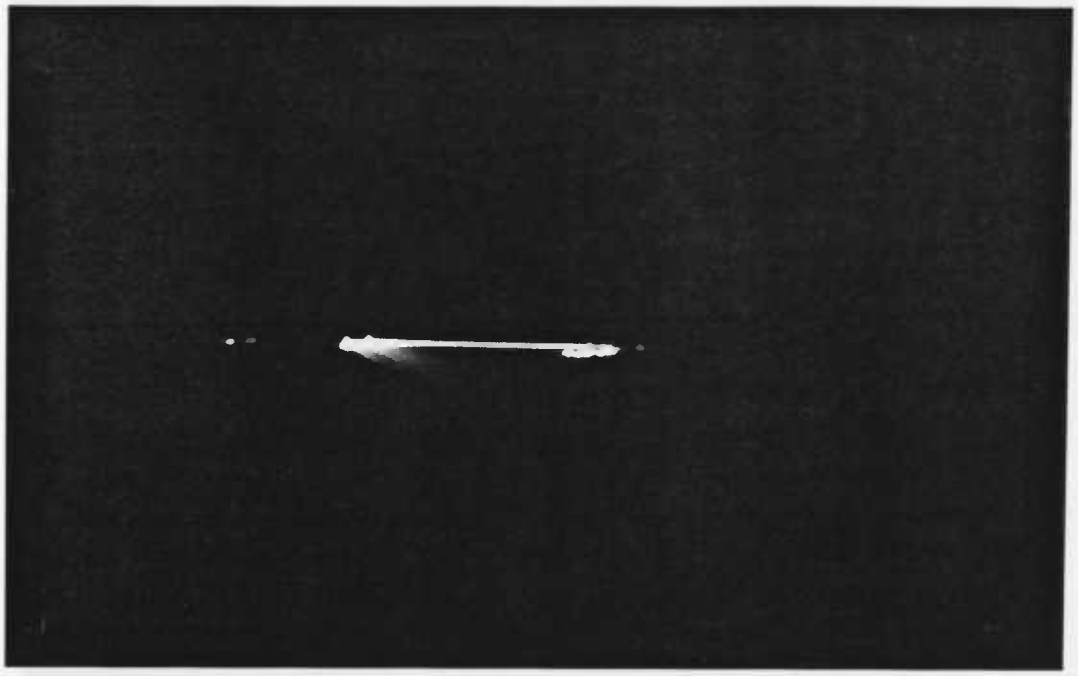

Figure 4.26: AC Source, 20 kV high voltage discharge: side view

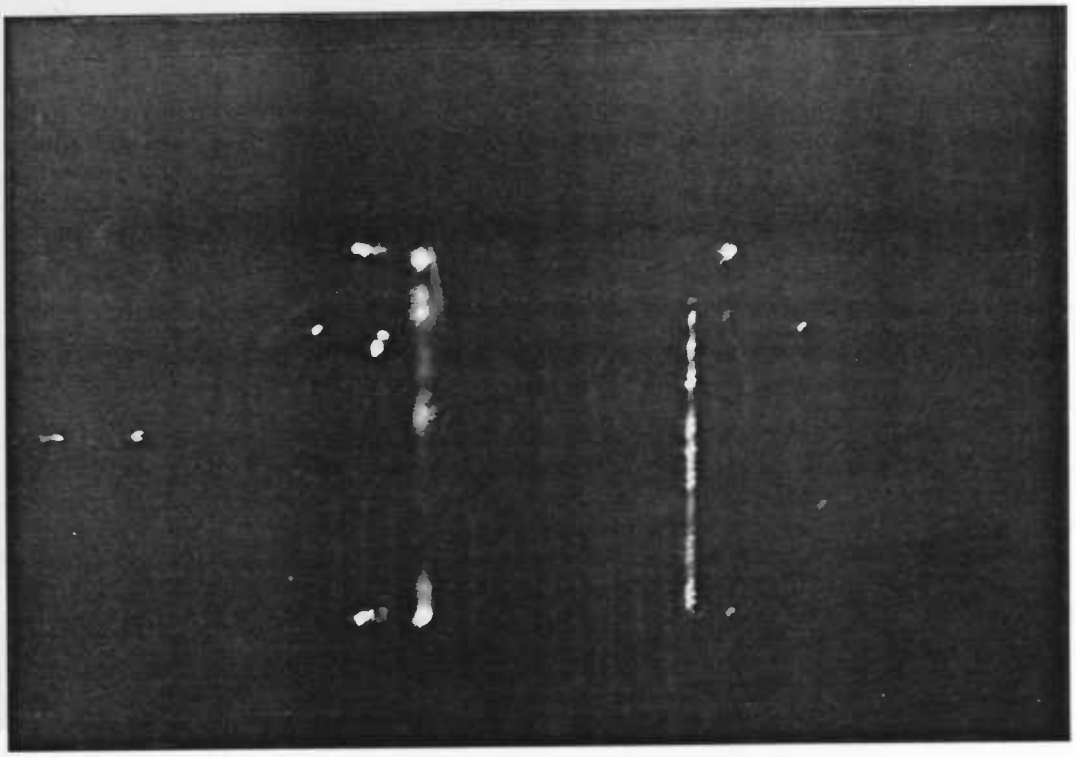

Figure 4.27: DC Source—positive polarity, 22 kV high voltage discharge: top view

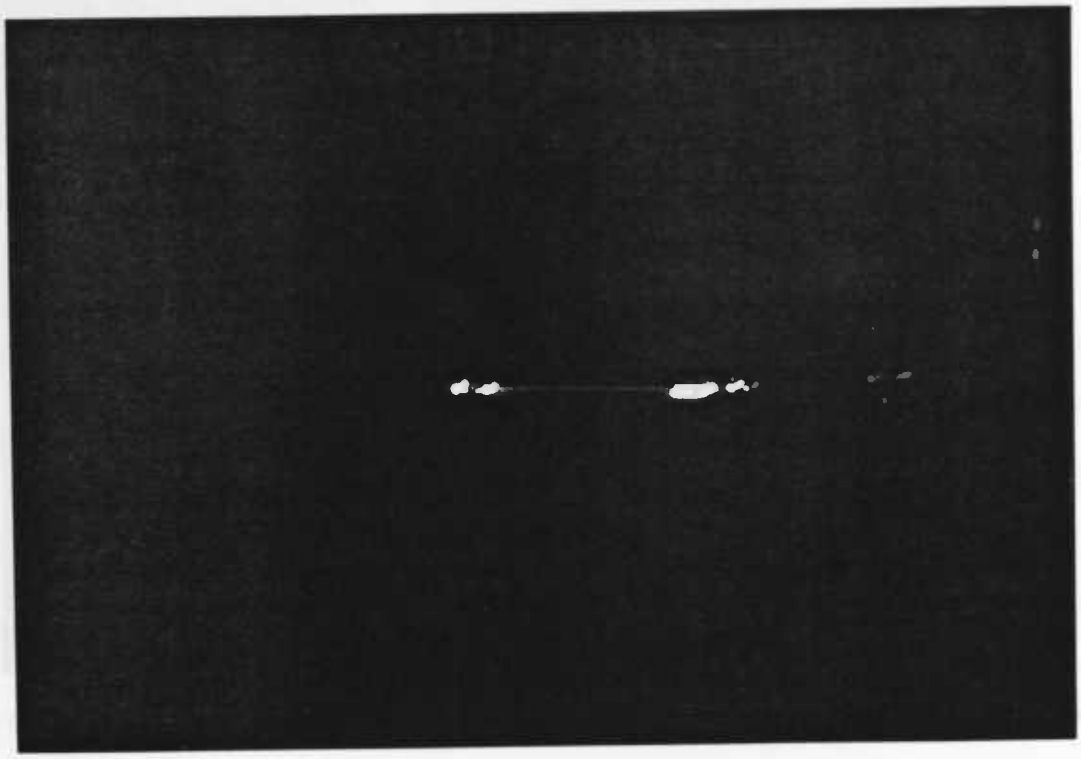

Figure 4.28: DC Source—positive polarity, 22 kV high voltage discharge: side view

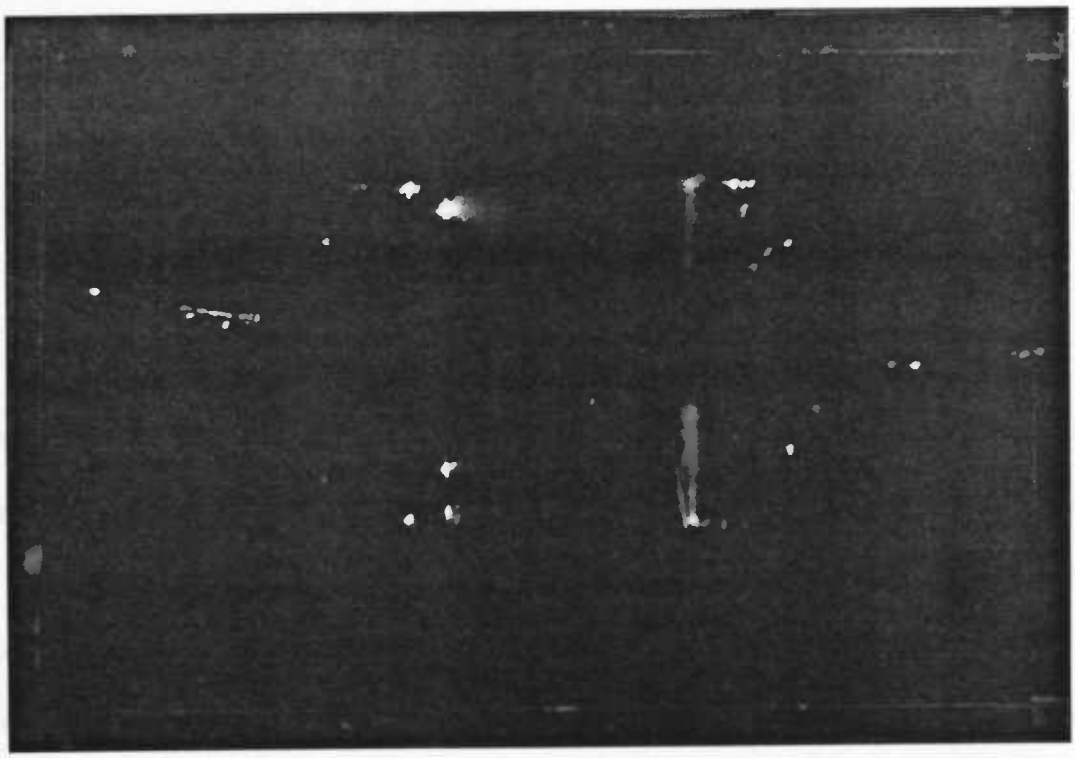

Figure 4.29: DC Source—negative polarity, 26 kV high voltage discharge: top view

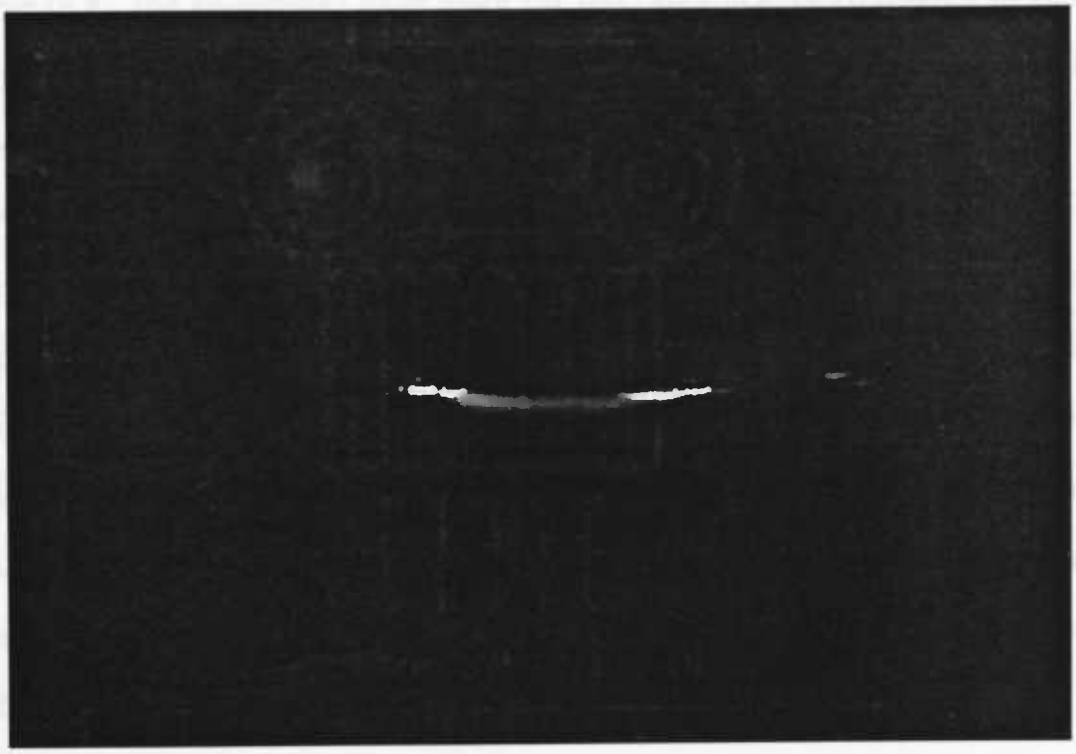

Figure 4.30: DC Source—negative polarity, 26 kV high voltage discharge: side view

CHAPTER 5. STATISTICAL ANALYSIS

There are two major factors affecting the drag coefficient of the flat plate: air speed and corona discharge. It is known that both factors *are* important; however, just as the case of any experiment involving physical measurements, there are other possible factors causing experimental errors which, in turn, cause some uncertainties in the experimental results [14]. Some obvious questions are: *How important is the high voltage discharge (or the air speed) to the plate drag? Does one particular type of discharge (e.g., the ac-corona) have more (or less) significance compared to the other (dc) types of corona? Do the variations in corona discharge (or the air speed) have a uniform effect on the plate drag? And how reproducible are the experimental data?* To answer these questions the experimental data has to be analyzed statistically.

Several statistical methods to analyze different types of experiments have been developed [21]; however, not all of them are applicable to this particular study. An analysis which is widely used in experiments involving several independent sources of variation is the *analysis of variance.* Moreover, the fact that the plate drag was calculated from the average value of several data makes it necessary to evaluate the uniformity of these data, thus a *comparison of the uniformities of two experiments* is needed. This chapter will present the results of such analyses.

Analysis of Variance

In this analysis air speed and high voltage discharge are the *independent variables.* One variable (i.e., the corona discharge) was varied while the other (i.e., the air speed) was held constant. For each condition the strain and the voltage drop across a resistor on the ground line (representing drag force and current, respectively) were recorded. These data are the *dependent variables* of this experiment.

Four different experiments were conducted: AC-normal and reversed strain gages orientation and DC-positive and negative polarity. All raw-data files[1] for each experiments were processed with the computer program of Appendix E. The *mean-square ratio* are tabulated below, and are compared to the tabulated F distribution value found in Reference [21]. The difference between these two values (calculated and tabulated) is the indicator of whether a significant difference exists between the tested factors (in this case: air speed and voltage), or whether the observed difference is due to chance or the experimental error alone.

Strain data

Table 5.1 is the analysis of variance of the *strain* where the air speed is held constant, and Table 5.2 is for high voltage discharge constant.

As can be seen in these tables, the air speed, high voltage discharge, and the interaction between these two factors significantly affect the plate's drag since the mean-square ratio was greater than the minimum value required for the factor(s) to be significant at 99.9% confidence level (e.g., from Table 5.1, for AC-normal orientation,

[1]The term *file* here denotes a set of experimental data for a given air speed or high voltage discharge. Tables F.1 and F.2 of Appendix F are examples of such files.

Table 5.1: Analysis of Variance—Overall: Strain table—constant air speed files

Source	Mean-square ratio					
	Voltage	DF[a]	Air speed	DF	Interaction	DF
AC-normal	34.235 (2.96)[b]	10	22.405 (2.96)	10	26.553 (1.49)	100
AC-reversed	3.326 (3.10)	9	34.486 (2.96)	10	22.742 (1.54)	90
DC-positive	3.553 (2.87)	11	1.700 (2.96)	10	6.229 (1.48)	110
DC-negative	6.412 (2.69)	13	18.260 (2.96)	10	7.221 (1.45)	130

Table 5.2: Analysis of Variance—Overall: Strain table—constant voltage files

Source	Mean-square ratio					
	Voltage	DF	Air speed	DF	Interaction	DF
AC-normal	3286.690 (2.96)	10	19296.590 (2.96)	10	133.367 (1.49)	100
AC-reversed	5613.124 (2.96)	10	3112.941 (3.10)	9	147.278 (1.54)	90
DC-positive	159.532 (2.96)	10	1214.184 (2.87)	11	2.626 (1.48)	110
DC-negative	597.790 (2.96)	10	377.862 (2.69)	13	4.932 (1.45)	130

[a]Degrees of freedom

[b]The number in parentheses is the table value indicating minimum MSR required for factors to be significant at 99.9% confidence

the MSR value is 34.235, which is greater than tabulated value, 2.96, for the same degrees of freedom)—except for DC source with negative polarity, where the air speed does not have any significance over the plate's drag[2]. Interestingly, these significances are not uniform, indicating there are differences among different electric sources. To further investigate this phenomenon, the data-files were processed individually. Table 5.3 shows the analysis of variance of the individual files where the air speed was held constant, thus in these files the high voltage was the factor being tested, and similarly in Table 5.4 the air speed was the factor being tested.

[2]It does, if the confidence level is lowered to 90%, where the tabulated value is 1.60

ıble 5.3: Analysis of Variance—Individual: Strain table—constant air speed files

onstant ir speed (torr)	Mean-square ratio			
	AC-normal[a] Table value 3.61	AC-reversed Table value 3.82	DC-positive Table value 3.45	DC-negative Table value 3.19
0.000	683.193	735.168	36.241	53.586
0.002	522.405	2388.367	78.961	68.733
0.004	843.190	598.285	227.766	48.917
0.006	4116.951	415.914	112.678	39.884
0.008	1593.026	259.654	381.695	36.285
0.010	613.251	241.704	526.750	26.818
0.012	2112.365	201.354	221.357	32.835
0.014	5114.475	165.449	80.248	17.482
0.016	5913.098	256.473	49.410	35.450
0.018	8450.662	106.487	113.330	26.128
0.020	6955.070	75.147	143.122	54.094

[a]For values of Degrees of freedom, see Tables 5.1 and 5.2. Also in Tables 5.4 rough 5.8.

Table 5.4: Analysis of Variance—Individual: Strain table—constant voltage files

onstant Voltage (kV)	Mean-square ratio			
	AC-normal Table value 3.61	AC-reversed Table value 3.61	DC-positive Table value 3.61	DC-negative Table value 3.61
2	32651.107	35709.242	708.946	10476.470
4	15822.842	20828.395	183.501	4209.810
6	9573.164	5927.448	79.787	1745.816
8	2669.721	909.258	44.848	1066.169
10	1229.718	515.859	26.058	790.444
12	377.207	159.884	17.003	84.357
14	92.828	100.714	14.771	45.634
16	4.345	52.779	6.687	18.751
18	7.177	118.084	12.460	19.900
20	3.449		6.914	31.826
22			3.857	53.656
24				36.740
26				24.368

On average, the numbers in the first two columns are greater than the other two columns for both factors, indicating the AC-discharge was more affected by these factors. Another observation from these tables shows that the numbers in Table 5.3 have a relatively uniform order of magnitude regardless of the air speed, while in Table 5.4 the numbers are decreasing in value with increasing voltage. A conclusion that can be drawn is that the high voltage discharge has the same effect on the strain, regardless of the air speed, while for higher voltage the air speed has less effect on the plate's drag, or in other words, at higher voltage, the strain becomes less dependent on the air speed[3].

Current data

For each experiment the voltage drop across a resistor on the ground-line of the power source was also recorded. This voltage was converted to current by dividing it by the resistance[4]. The raw-data files were also analyzed and the results are shown in Table 5.5 through Table 5.8.

Comparing the mean-square ratio value of voltage, air speed and the interaction between the two in Table 5.5 and 5.6, we can immediately see that voltage is the only factor that has a significant effect on the current. Furthermore, Table 5.7 and 5.8 do not show any trend as in the strain tables. Table 5.7 shows the voltage has (almost) uniform effects on the current regardless of the air speed. The mean-square ratio values of Table 5.8 are much less than those of Table 5.7, indicating a decreased dependency of current on the air speed.

---

[3]See Chapter 6 for further discussion on this phenomenon.

[4]For details of this procedure see Appendix C.

Table 5.5: Analysis of Variance—Overall: Current table—constant air speed files

Source	Mean-square ratio		
	Voltage	Air speed	Interaction
AC-normal	126.787 (2.96)	0.000 (2.96)	0.000 (1.49)
AC-reversed	217.365 (3.10)	0.672 (2.96)	0.491 (1.54)
DC-positive	96.935 (2.87)	0.936 (2.96)	1.727 (1.48)
DC-negative	80.369 (2.69)	0.883 (2.96)	0.816 (1.45)

Table 5.6: Analysis of Variance—Overall: Current table—constant voltage files

Source	Mean-square ratio		
	Voltage	Air speed	Interaction
AC-normal	0.000 (2.96)	2371.722 (2.96)	0.000 (1.49)
AC-reversed	7.417 (2.96)	15060.177 (3.10)	5.524 (1.54)
DC-positive	13.584 (2.96)	3109.532 (2.87)	3.645 (1.48)
DC-negative	16.663 (2.96)	5058.361 (2.69)	4.086 (1.45)

Table 5.7: Analysis of Variance—Individual: Current table—constant air speed files

Constant Air speed (torr)	Mean-square ratio			
	AC-normal Table value 3.61	AC-reversed Table value 3.82	DC-positive Table value 3.45	DC-negative Table value 3.19
0.000	215.588	339.257	165.826	1025.814
0.002	215.588	884.446	3778.976	2946.011
0.004	215.588	1790.850	1571.195	484.447
0.006	215.588	2269.582	1002.729	1042.174
0.008	215.588	1983.052	677.592	847.512
0.010	215.588	1895.060	426.025	358.379
0.012	215.588	1306.616	189.563	1410.193
0.014	215.588	2613.366	245.433	140.951
0.016	215.588	2707.864	61.070	146.687
0.018	215.588	2626.000	411.737	623.233
0.020	215.588	3965.108	220.412	813.403

Table 5.8: Analysis of Variance—Individual: Current table—constant voltage files

Constant Voltage (kV)	Mean-square ratio			
	AC-normal Table value 3.61	AC-reversed Table value 3.61	DC-positive Table value 3.61	DC-negative Table value 3.61
2	0.001	2.445	$\star$[a]	$\star$
4	0.001	9.435	$\star$	$\star$
6	0.013	6.661	$\star$	$\star$
8	0.004	8.977	$\star$	$\star$
10	0.036	22.125	5.000	$\star$
12	0.036	9.444	10.000	$\star$
14	0.000[b]	14.302	2.154	6.771
16	0.000	3.907	6.718	5.762
18	0.000	2.856	4.620	3.357
20	0.001		3.527	4.263
22			4.954	7.174
24				4.240
26				3.293

[a] Uniform data, uncalculable.

[b] The 0.000 value in this table means the mean-square ratio is less than 5.0×10^{-4}

Comparison of The Uniformities of The Experiments

The comparison of the uniformities can be made by means of the F distribution. The method is described as follows:

Consider two normally distributed independent random samples

$$x_1, x_2, \ldots, x_{n_x}$$

with mean μ_x, variance ${\sigma_x}^2$, and a sample variance ${s_x}^2$, for n_x samples; and

$$y_1, y_2, \ldots, y_{n_x}$$

with mean μ_y, variance ${\sigma_y}^2$, and a sample variance ${s_y}^2$, for n_y samples. Then,

$$ {\chi_x}^2 = \frac{(n_x - 1){s_x}^2}{{\sigma_x}^2} $$

and

$$ {\chi_y}^2 = \frac{(n_y - 1){s_y}^2}{{\sigma_y}^2} $$

where ${\chi_x}^2$ and ${\chi_y}^2$ are random variables which have χ^2 distribution with degrees of freedom $\nu_x = (n_x - 1)$ and $\nu_y = (n_y - 1)$, respectively.

By the definition of an F variable,

$$ F = \frac{{\chi_x}^2/\nu_x}{{\chi_y}^2/\nu_y} = \frac{\frac{(n_x-1){s_x}^2}{{\sigma_x}^2}\frac{1}{n_x-1}}{\frac{(n_y-1){s_y}^2}{{\sigma_y}^2}\frac{1}{n_y-1}} = \frac{{s_x}^2/{\sigma_x}^2}{{s_y}^2/{\sigma_y}^2} \tag{5.1} $$

has an F distribution with $\nu_x = (n_x - 1)$ and $\nu_y = (n_y - 1)$ degrees of freedom.

The probability of F having a greater value than $F_{\alpha;\nu_x;\nu_y}$:

$$ P(F > F_{\alpha;\nu_x;\nu_y}) = \alpha $$

and consequently,

$$ P(F \leq F_{\alpha;\nu_x;\nu_y}) = 1 - \alpha $$

From Equation 5.1,

$$ \begin{aligned} P\left(\frac{{s_x}^2/{\sigma_x}^2}{{s_y}^2/{\sigma_y}^2} \leq F_{\alpha;\nu_x;\nu_y}\right) &= 1 - \alpha \\ P\left(\frac{{s_x}^2{\sigma_y}^2}{{s_y}^2{\sigma_x}^2} \leq F_{\alpha;\nu_x;\nu_y}\right) &= 1 - \alpha \end{aligned} \tag{5.2} $$

Therefore, with $(1 - \alpha)$ confidence,

$$ \frac{{s_x}^2{\sigma_y}^2}{{s_y}^2{\sigma_x}^2} \leq F_{\alpha;\nu_x;\nu_y} $$

or

$$\frac{{\sigma_y}^2}{{\sigma_x}^2} \leq F_{\alpha;\nu_x;\nu_y} \frac{{s_y}^2}{{s_x}^2} \tag{5.3}$$

From Equation 5.3, the comparison of uniformities test is defined:

At $(1-\alpha)$ *confidence level, if* $\frac{{s_x}^2}{{s_y}^2} > F_{\alpha;\nu_x;\nu_y}$, *then the ratio of the true variances* $\frac{{\sigma_x}^2}{{\sigma_y}^2}$ *is greater than 1; or in other words, the x-experiment is more variable than the y-experiment* [21].

To apply this test to the raw-data files, we need to calculate the variance of each file and compare these values with a reference variance. Since we are interested in knowing the uniformities of these high voltage discharge files, the reference variance has to be determined in such a way that it is independent of the high voltage discharge. Therefore, it was decided to use the raw-data of plate drag without high voltage discharge (both normal and reversed orientation) as the reference variances. The variances of each air speed variation were calculated independently, then they are averaged to get two reference variances for normal and reversed orientation, respectively.

The raw-data files used were of constant high voltage. The variance of each air speed variation was calculated from six measurements, hence the degree of freedom is $(n-1) = 5$. If, for every air speed variation, the value of

$$\frac{Variance}{Reference\ Variance}$$

is greater than the tabulated value, then it can be concluded that the variation of the distribution of that particular experiment is less uniform than the variation of the plate-drag-without-corona-discharge experiment. The results are presented in Table 5.9 through 5.12.

Table 5.9: Comparison of uniformities: AC Source--Normal orientation

Air Speed (torr)	Variance/Reference Variance Corona discharge									
	2 kV	4 kV	6 kV	8 kV	10 kV	12 kV	14 kV	16 kV	18 kV	20 kV
0.002	0.09	0.11	0.19	1.25	1.86	4.60	1.72	4.56	19.37	4.50
0.004	0.04	0.13	0.06	0.38	0.37	1.74	12.38	2.57	5.76	10.55
0.006	0.08	0.06	0.26	0.21	1.33	1.86	2.39	0.18	0.71	0.63
0.008	0.03	0.08	0.16	0.27	1.75	6.06	1.38	10.59	0.90	1.06
0.010	0.02	0.06	0.16	0.30	1.11	2.37	2.47	35.59	9.66	17.07
0.012	0.04	0.14	0.08	0.43	0.35	5.26	1.13	1.13	7.45	6.35
0.014	0.06	0.18	0.09	0.06	0.40	0.77	3.12	1.28	1.45	3.33
0.016	0.06	0.10	0.37	0.65	0.08	2.10	1.50	2.45	1.98	1.06
0.018	0.04	0.05	0.06	0.19	1.12	0.19	0.90	1.35	0.75	3.76
0.020	0.02	0.04	0.13	0.41	0.16	2.91	1.46	0.43	2.86	2.44

Reference Variance (no corona) = 0.16473
Degree of freedom: (n-1) = 5
Table value, F(0.10,5,5) = 3.45
Table value, F(0.01,5,5) = 11.0

Table 5.10: Comparison of uniformities: AC Source - Reversed strain gages

Air Speed (torr)	Variance/Reference Variance Corona discharge								
	2 kV	4 kV	6 kV	8 kV	10 kV	12 kV	14 kV	16 kV	18 kV
0.002	0.06	0.10	0.26	0.05	0.21	1.09	0.81	1.37	1.12
0.004	0.02	0.06	0.06	0.40	0.23	1.02	0.49	8.75	4.96
0.006	0.05	0.03	0.07	0.05	0.16	4.24	4.47	4.02	5.26
0.008	0.02	0.05	0.15	2.67	2.50	3.33	2.97	0.52	6.09
0.010	0.12	0.09	0.07	0.29	0.40	1.57	5.81	7.53	4.16
0.012	0.08	0.04	0.64	1.34	0.37	0.52	0.41	1.04	16.86
0.014	0.13	0.27	0.63	1.55	1.54	2.39	1.07	5.81	2.08
0.016	0.13	0.35	0.43	1.37	0.63	0.79	0.49	0.68	1.73
0.018	0.04	0.05	0.18	0.79	0.70	3.16	1.64	1.56	1.48
0.020	0.05	0.00	0.47	1.08	1.12	1.57	0.43	3.39	4.53

Reference Variance (no corona) = 0.14480
Degree of freedom: (n-1) = 5
Table value, F(0.10,5,5) = 3.45
Table value, F(0.01,5,5) = 11.0

Table 5.11: Comparison of uniformities: DC Source - Positive polarity

Air Speed	Variance/Reference Variance Corona discharge										
(torr)	2 kV	4 kV	6 kV	8 kV	10 kV	12 kV	14 kV	16 kV	18 kV	20 kV	22 kV
0.002	0.62	2.17	3.51	5.13	7.85	11.31	11.98	17.25	12.90	284.28	864.27
0.004	0.26	1.39	3.05	4.47	7.81	9.13	11.34	9.02	121.89	61.96	376.37
0.006	4.31	6.02	13.95	27.76	45.08	78.19	74.82	276.59	229.11	63.87	508.58
0.008	1.37	8.46	17.65	24.16	42.59	59.62	62.91	75.33	136.89	45.33	53.22
0.010	1.32	4.46	10.40	17.64	24.93	39.84	74.08	27.86	65.37	35.49	12.39
0.012	1.12	2.59	6.03	8.28	9.76	12.79	3.73	20.70	412.27	178.96	73.91
0.014	3.15	12.89	30.44	51.40	105.13	165.91	239.87	290.42	438.28	317.98	17.04
0.016	3.29	15.72	37.39	68.05	121.10	169.97	408.19	193.64	166.32	1054.08	372.98
0.018	2.54	13.06	27.73	56.96	102.41	178.92	188.46	170.13	362.44	95.80	31.21
0.020	2.88	10.53	27.54	49.28	87.15	149.05	13.17	130.16	303.32	242.39	41.34

Reference Variance (no corona) = 0.16473
Degree of freedom: (n-1) = 5
Table value, F(0.10,5,5) = 3.45
Table value, F(0.01,5,5) = 11.0

Table 5.12: Comparison of uniformities: DC Source - Negative polarity

Air Speed	Variance/Reference Variance Corona discharge												
(torr)	2 kV	4 kV	6 kV	8 kV	10 kV	12 kV	14 kV	16 kV	18 kV	20 kV	22 kV	24 kV	26 kV
0.002	0.45	1.93	5.32	9.23	11.29	54.81	26.91	59.43	9.86	16.76	1.01	120.91	229.89
0.004	0.06	0.16	0.64	0.94	1.78	40.81	76.92	19.64	17.62	85.97	146.22	20.01	414.31
0.006	0.30	1.06	1.76	2.74	4.71	21.57	46.83	22.96	41.39	58.65	64.60	98.38	257.56
0.008	0.00	0.01	0.03	0.40	0.50	0.58	8.87	88.04	39.58	19.87	12.91	207.75	28.18
0.010	0.02	0.07	0.09	0.03	0.10	21.96	12.86	198.39	131.91	29.39	144.72	84.73	193.54
0.012	0.19	0.33	0.96	1.17	1.23	8.66	30.98	29.63	149.89	75.35	42.27	28.99	305.22
0.014	0.11	0.09	0.05	0.21	0.89	15.55	31.94	38.14	52.59	16.00	136.06	412.27	370.05
0.016	0.23	0.12	0.57	1.23	1.14	2.89	28.04	8.67	32.67	25.71	72.30	226.83	168.76
0.018	0.03	0.01	0.11	0.16	0.55	22.89	123.85	89.93	104.03	195.45	110.86	85.08	12.08
0.020	0.15	0.30	0.31	0.98	1.23	27.80	35.01	62.25	49.22	38.04	103.68	87.43	83.17

Reference Variance (no corona) = 0.16473
Degree of freedom: (n-1) = 5
Table value, F(0.10,5,5) = 3.45
Table value, F(0.01,5,5) = 11.0

In general the table values show good uniformity for lower voltages, i.e., for voltages where the corona was still invisible, and become less uniform for a visible-corona voltage range. Another interesting result is that the DC source has less uniformity compared to the AC source. This is shown in Figure 5.1, where the raw-data values of four different experiments: AC source, normal and reversed orientation, and DC source, positive and negative polarity, at 12 kV corona discharge[5] are plotted together in one graph.

[5] 12 kV is the *critical* voltage for AC where the hissing sound begins to be audible and the corona becomes visible.

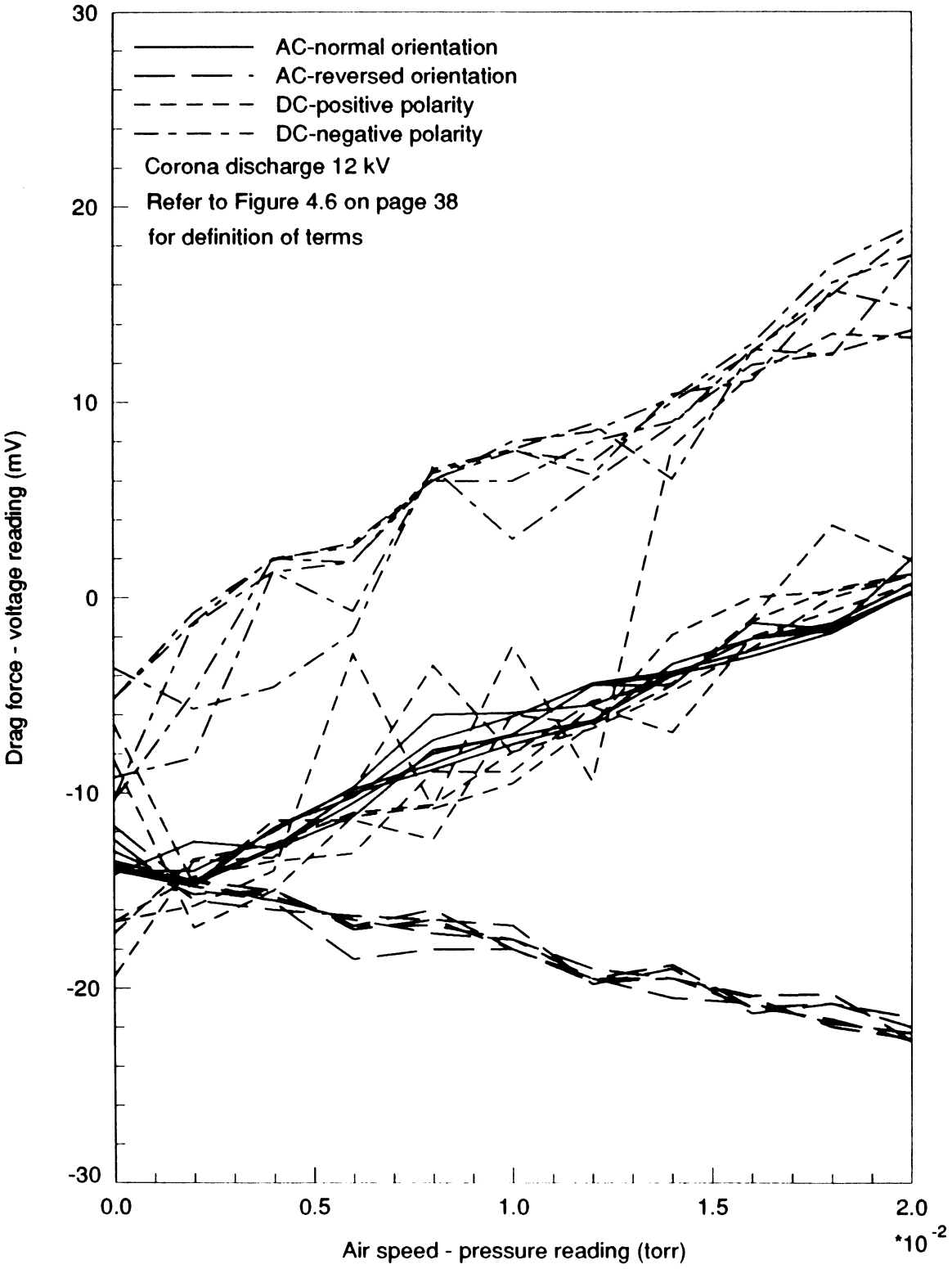

Figure 5.1: Comparison of raw data of four different experiments at 12 kV corona discharge

CHAPTER 6. DISCUSSION AND CONCLUSION

The theoretical solutions for flow over a flat plate includes solutions for an infinite flat plate given by Blasius [27][34][9], the leading-edge solution (Imai) [30][17], and the trailing-edge (triple-deck theory) [35] solution. In addition, numerous experiments have also been conducted for a flow normal to a plate [4][16]. However, no specific discussion was found for a plate both finite in length and width.

It is observed that flat-plate drag measurements depend on testing conditions such as the presence of turbulence and free stream disturbances. The following is brief discussions of the experiment's results.

Wire drag

The method of support plays an important role in drag measurement. In this study a pair of wires was used to hang the plate being measured. The drag measured was the integrated effect of the plate-wire suspension system. The plate drag was found by measuring the drag of a single wire and subtracting it from the total drag. To simulate real testing conditions, the wire being measured was placed in the wake of another wire with the same distance of separation as in the plate-wire system.

The diameter of the wire was 0.0184 inch. *TV Corona Dope* coatings were applied to prevent corona discharge along the wire. This coatings made the diameter of the

wire to be $\approx$ 0.02164 inch. The length of wire subjected to flow was 82 mm.

Standard drag curves for a smooth circular cylinder can be found in literatures [27], which were used to approximate the wire drag. Since the corona dope coatings made the wires slightly irregular, the wire drag would be expected to differ from the standard drag curve, as can be seen in Figure 6.1.

Wall effect

The width of the inner section of the working section is 3.875 in. which is wider than the plate's width, 75 mm ($\approx$ 2.953 in.). This means there is the possibility that the plate's ends fall within the boundary layer region of the wall. A simple theoretical calculation can be performed to check this possibility:

The entrance length was $\approx$ 21 in. (535 mm), where for the simplicity in calculating the boundary-layer thickness in the test section it was assumed that the whole region of this entrance was aligned with the test section of the wind tunnel. The air speed was tested from 0.6598 $m/sec.$ to 2.0865 $m/sec.$ With kinematic viscosity, $\nu = 1.46 \times 10^{-5}\ m^2/sec.$:

$$For\ V = 0.6598\ m/sec \Rightarrow Re_x = \frac{Vx}{\nu} = 24177.6$$

$$For\ V = 2.0865\ m/sec \Rightarrow Re_x = \frac{Vx}{\nu} = 76457.4$$

The boundary layer thickness can then be calculated using the relation:

$$\frac{\delta}{x} = \frac{5}{\sqrt{Re_x}}$$

or

$$\delta = \frac{5x}{\sqrt{Re_x}}$$

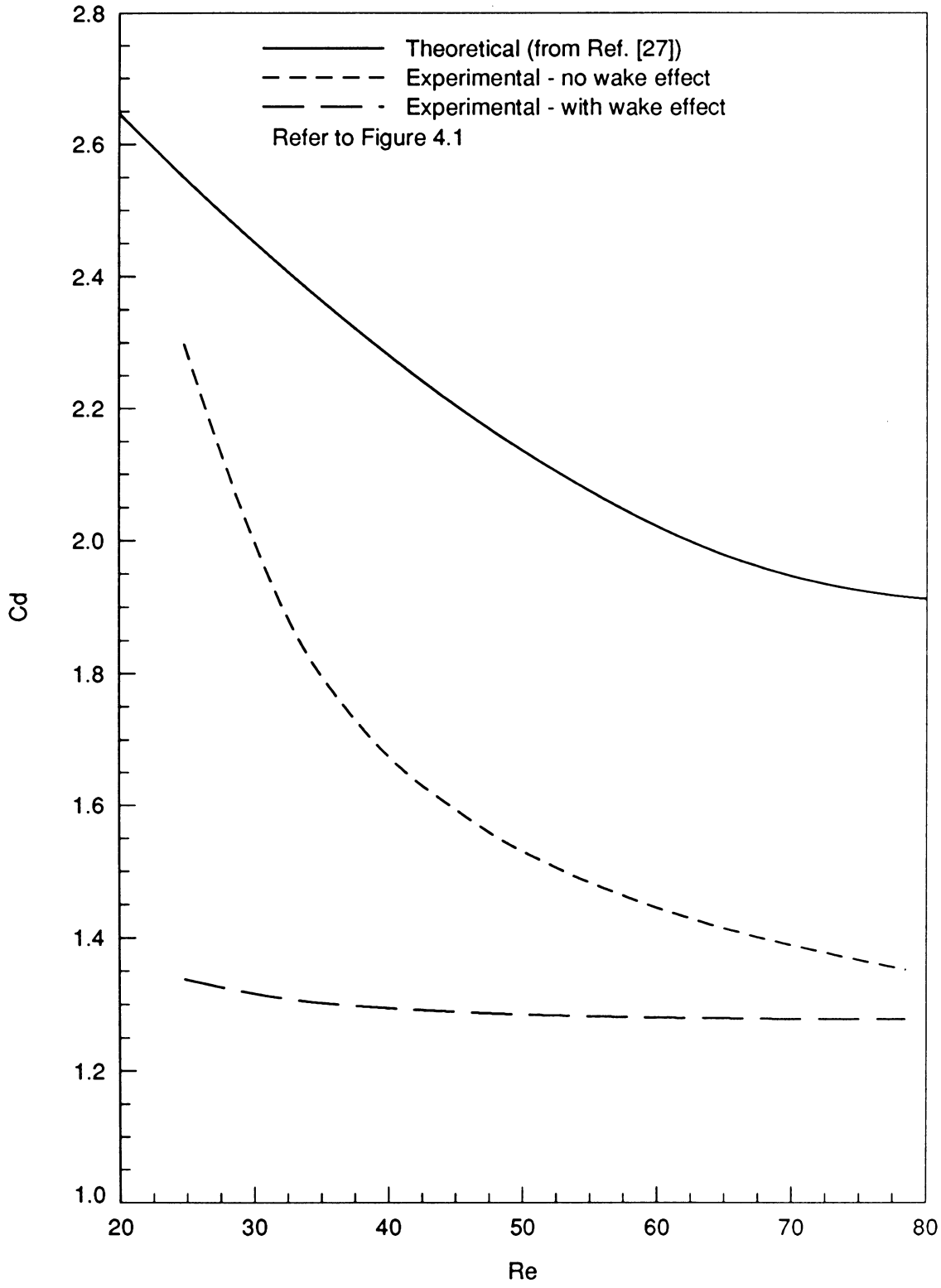

Figure 6.1: Wire drag compared to standard drag curve for smooth circular cylinder within the same range of Reynolds number

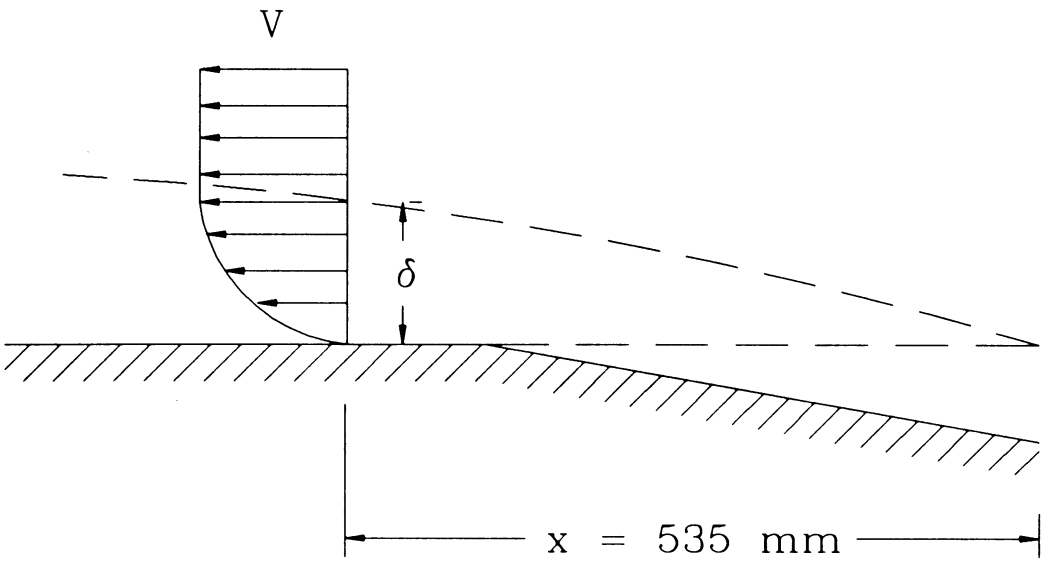

Figure 6.2: Wall effect on the plate

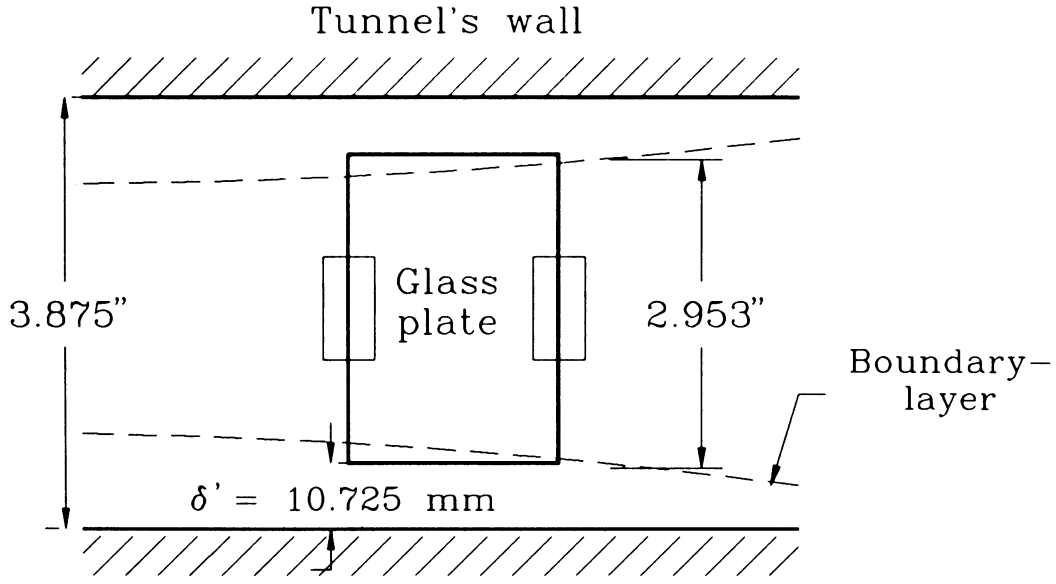

Figure 6.3: Top view of the working section of wind tunnel

For $V = 0.6598\ m/sec \Rightarrow \delta = 17.2\ mm$ and

for $V = 2.0865\ m/sec \Rightarrow \delta = 9.7\ mm$

The closest distance between the glass plate and the tunnel wall was 10.725 mm; therefore, a portion of the glass plate was within the boundary layer region.

Another way to check the possibility of the glass plate within the boundary layer region was by calculating the necessary pressure drop in the pitot tube such that the boundary layer just reaches the edge of the glass plate (δ' = the closest distance between the glass plate and the tunnel).

The *limiting* Re_x is

$$Re_x = \left[\frac{5x}{\delta'}\right]^2 = 62208.96 = \frac{Vx}{\nu}$$

and the air speed is

$$V = \frac{Re_x \nu}{x} = 1.6976 m/sec = \sqrt{\frac{2\Delta p}{\rho}}$$

which corresponds to a pressure difference of

$$\Delta p = 1.765266 Pa = 0.01324 torr$$

This value is within the range of pressure reading of the air speed which was measured to be 0.002–0.020 *torr*. Therefore, a portion of the glass plate was within the boundary layer region.

Plate drag

Figure 4.5 on page 36 shows the result of plate drag measurement together with the theoretical drag curves obtained from the theoretical solutions. It was speculated

earlier that the theoretical calculation would overpredict the actual drag due to the higher drag coefficient of a flat plate normal to the flow compared to the actual plate. This was found to be true. However, the actual curves possess slightly different trends from the theoretical curves. This phenomenon was perhaps due to the disturbances of the flow due to acoustical and mechanical vibrations of the fan [12], which created a non-uniform flow.

A computer program was written to re-construct the experimental result based on the theoretical solution. Drag coefficient approximated based on Van Dyke's formula was used to estimate the drag force and, in turn, estimate the voltage reading of the strain gages. The result is shown in Figure 6.4 and Table 6.1. It can be seen that the data agrees in low air speed, but it diverges for higher air speeds.

Table 6.1: Comparison of experimental - estimation data based on theoretical calculation

Air speed (Pressure reading) torr	Strain (Voltage reading) Experimental mV	Theoretical mV
0.002	2.850	2.894
0.004	5.350	4.727
0.006	7.650	6.414
0.008	9.550	8.015
0.010	11.500	9.557
0.012	12.717	11.054
0.014	14.733	12.515
0.016	16.550	13.946
0.018	18.700	15.351
0.020	20.500	16.734

Another possible explanation is that the *flat plate normal to the flow* approximation overpredicts the overall drag, since a *flat plate normal to the flow* will have greater wake behind the plate, thus giving a greater drag; whereas in a *finite flat*

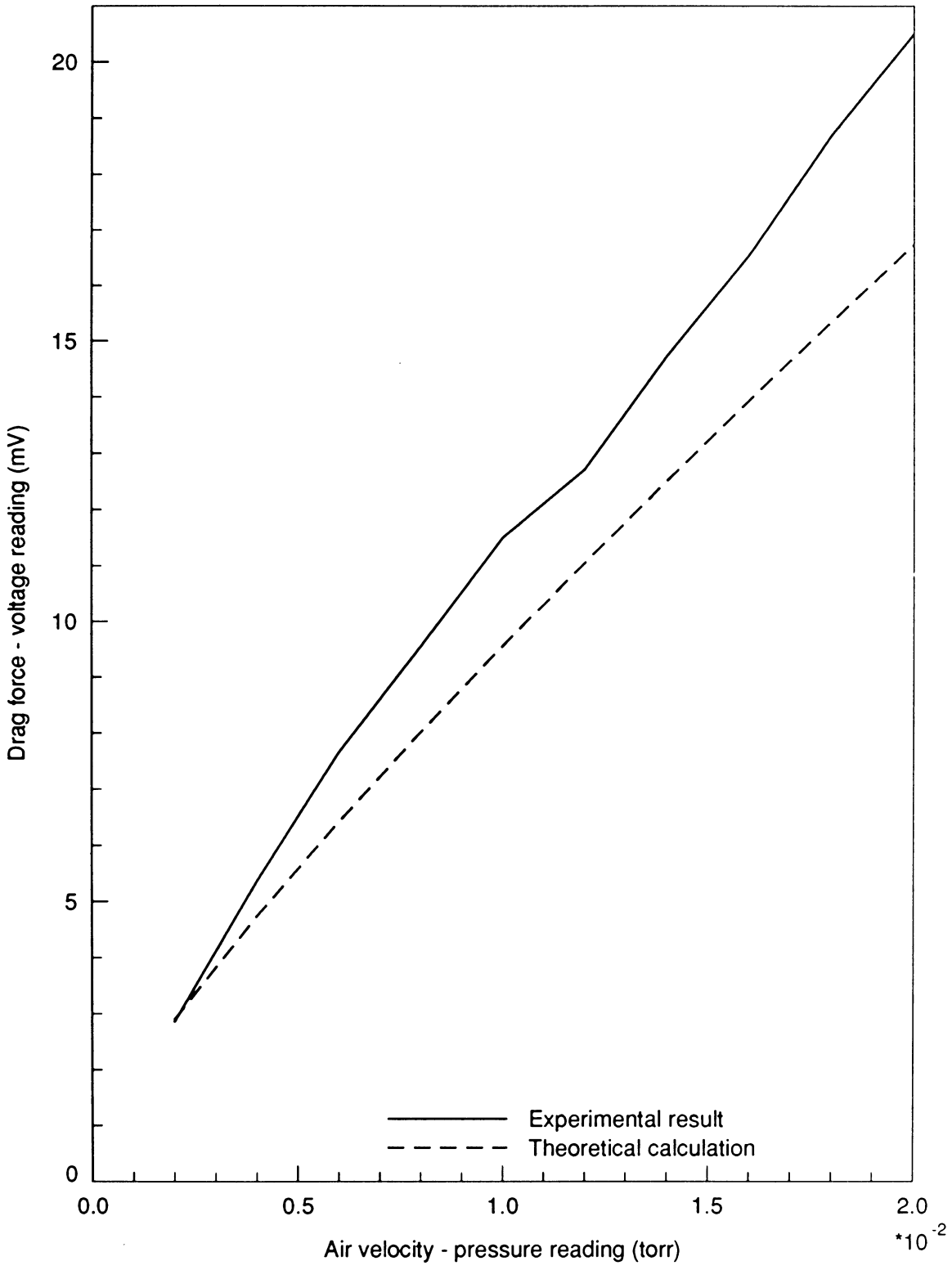

Figure 6.4: Comparison experimental - estimation data based on theoretical calculation

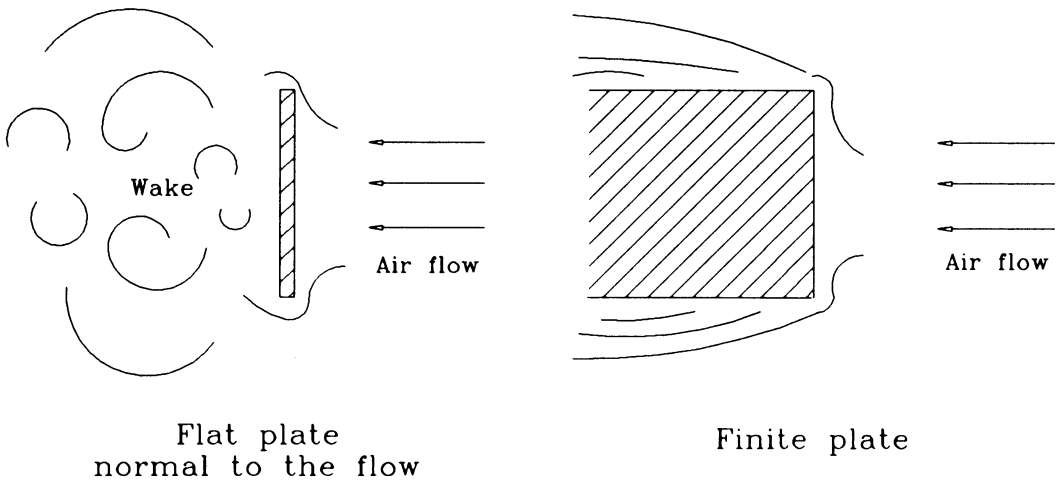

Figure 6.5: Flat plate normal to the flow vs. finite plate

plate case this wake does not exist.

Plate drag with corona discharge

It was mentioned earlier that the beam was deflected whenever the high voltage source was turned on even without air flow. There are two possible causes for this deflection: thrust force due to the ionic wind[1] and electrostatic attraction to the surroundings. To further examine the effect of these forces another test was conducted, where the whole force-sensor system was reversed, i.e., the strain gages were located *upstream* of the airflow direction in the wind tunnel[2].

Since the blade-electrode that produces corona also generates wind that blows

[1] See Chapter 1.

[2] See also Figure 4.6 on page 38.

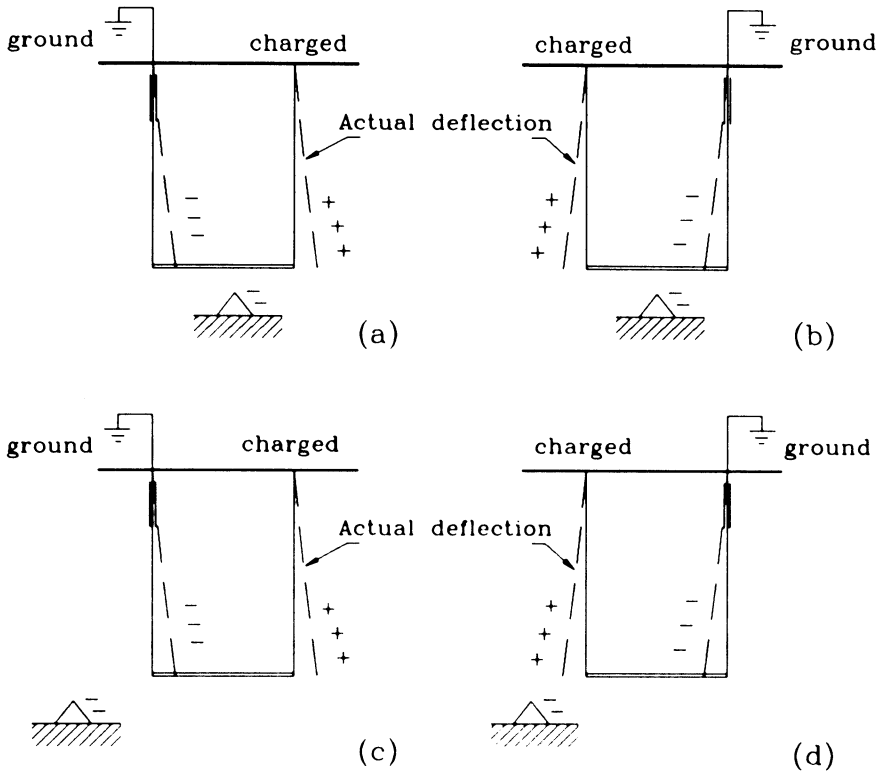

Figure 6.6: Deflection on normal- and reversed-strain gages orientation

parallel to it, theoretically, the plate-wire suspension system would be deflected toward the charged-side due to the reaction on the thrust force. This is exactly what happened in the experiments. On both condition, normal and reversed orientation, the plate-wire was deflected toward the charged-side, as shown with dashed-line in Figure 6.6. This phenomenon was observed in all experiments, i.e., AC with normal and reversed strain gages orientation, and DC with positive and negative polarity[3].

[3]See also Chapter 4, Figure 4.9–4.10, 4.13–4.14, 4.17–4.18, 4.22–4.24, Reynolds

Therefore, it was concluded that thrust force caused the deflection.

Electrostatic effect occur between two charged-bodies. Bodies with different charge will attract while bodies with the same charge will repel. This fact raised the possibility that electrostatic effect occurs between the beam-wire and an arbitrary object of the surrounding. To simulate this, suppose the object was located between the beam-wire as shown in Figure 6.6(a) and (b). Furthermore, for the sake of argument, suppose that the beam-wire was positively charged, while the other beam-wire was grounded and negatively charged. Since the object was a part of the surroundings, it was also negatively charged. Theoretically, because of different charge the *ground*-electrode would be repelled from the object and the *charged*-electrode would be attracted to it. In the case of normal orientation strain gages (Figure 6.6(a)), the plate-wire system should be deflected to the left, while in the reversed strain gages orientation (Figure 6.6(b)) it should be deflected to the right. However, as shown in those figure the actual deflection was to the right for normal orientation and to the left for reversed orientation, contrary to theory. It follows if the arbitrary object was located as described, then the electrostatic effect would not occur.

Now, suppose the object was located either to the left or to the right of the plate-wire suspension system as shown in Figure 6.6(c) and (d). Theoretically, the *ground*-electrode would be repelled from the object (or the *charged*-electrode would be attracted to the object), in other words: the plate-wire system would be deflected to the right for the normal orientation experiment (Figure 6.6(c)); and similarly, it

---

number vs. drag force. Notice that the absolute force at the no-air-flow condition was negative for normal strain gages orientation (AC and DC), and was positive for reversed strain gages orientation; means that the plate-wire was deflected toward the charged-side.

would be deflected to the left for the reversed orientation experiment (Figure 6.6(d)). This condition was consistent with the experimental results. Therefore, if the arbitrary object was located as described, an electrostatic effect did occur. However, the location of this arbitrary object was uncertain; therefore, it is still uncertain if this test would confirm whether an electrostatic effect caused the deflection.

It was thought earlier that the AC-corona would not have an electrostatic effect, since the positive and negative charges alternate between the two electrodes; however, this was not the case, since the deflection was also recorded in the AC experiments. Moreover, if there is a *disturbance* in the AC circuits, e.g., current flow from metal to glass to another metal like the blade-electrode and glass plate configuration used in this experiment, then there is a possibility of a *diode effect.* This would cause a net positive or negative charge to built up which could give a net force to the glass plate.

The method of testing was to charge the electrodes to a fixed voltage, record the data, and then turn the charge off. This procedure insured that the arbitrary zero of the strain gage reading was not drifting. It was noticed that the time needed for the DC source charging to relax to zero was more than that of the AC source[4]. This was probably due to the fact that DC source build up charges between the wire and the surrounding; therefore, the plate-wire system was affected by the electrostatic forces which were still existed until the charges was neutralized. In the AC case the charge built up (if they occurred) was very small; hence the zero was reached faster.

In the experiments one of the beam-wire support system was charged while the

[4]In an experiment on a point-to-plane corona discharge [29], Shaughnessy and Solomon also observed that DC-corona required an excessively long averaging time to obtain stable mean.

other beam-wire and the rest of the wind tunnel was grounded. This raised another possibility of *unbalanced charge*, where the electric field around the *charged*-electrode was stronger then that of the *ground*-one. This unbalance would produce a *net force* between the electrodes, hence causing the plate-wire to deflect.

From the possibilities discussed above it is still uncertain which effect was the real cause of the deflection. There is still a possibility that there are more than one factors involved. Therefore, it is safe to say that the cause of the deflection remains uncertain.

Statistical analysis[5], as well as the plots in Chapter 4 show greater uncertainties and more scatters for DC-corona. This may be the result of greater electrostatic effects on DC experiments. Futhermore, while in the lower voltage range the curves of Chapter 4 showed less scatter, the higher voltage range the curves showed increase scatter. The result of analysis of variance of Chapter 5 also shows that in the higher voltage region, there is less dependency of the drag force to the air speed. One possible explanation of these phenomena is that at higher voltage thrust and electrostatic force dominates the deflection sensed by the strain gages[6].

Current

The statistical analysis of Chapter 5 confirms the experimental results that there is no dependence of current with the air speed. However, the current is found to be dependent on the input voltage. Figure 6.7 shows the current-voltage characteristic

[5]See Chapter 5.

[6]See plots Reynolds number vs. force of Chapter 4; the absolute force acting on the plate-wire without air flow of higher voltage was relatively higher than that of the lower voltage.

of this experiment. The data was the average of all constant-voltage files[7].

There is an abrupt increased in current at critical voltage for all experiments. In AC experiments this jump occurred at a voltage $\approx$ 12 kV, while in DC tests it occurred at a voltage $\approx$ 14 kV. Interestingly, these are the voltages where hissing sound was first audible and the corona became visible. The term *visible* here does not mean that the corona can be seen in an ordinary room condition, since *corona* is only a weak glow which can be seen if the surrounding is dark. Therefore, this phenomenon suggests that current is a better indicator of corona than is the voltage[8].

Conclusion

- Although the plate drag experimental results for both normal and reversed strain gages orientation (see Figure 4.5) show a slight trend-deviation, it can be concluded that the results are in general agreement with the theoretical calculation. The difference is probably due to the fact that a finite flat plate possesses a different property from the *flat plate plus plate normal to the flow* approximation (see Figure 3.1 and 6.5). While the actual plate drag is higher than the calculated flat-plate drag because of its thickness, it was mentioned earlier that the approximation would over-estimate the actual drag, and indeed the actual curves lie in between the flat-plate and *total* drag curves.

- In general the AC high voltage discharge gives more uniform drag character-

[7] For an example of these files, refer to Appendix F.

[8] The phenomenon is in agreement with the definition of corona given by Leob and cited by Malik et al. [22] Shaughnessy and Solomon [29] also observed the same phenomenon on the point-to-plane corona discharge experiments.

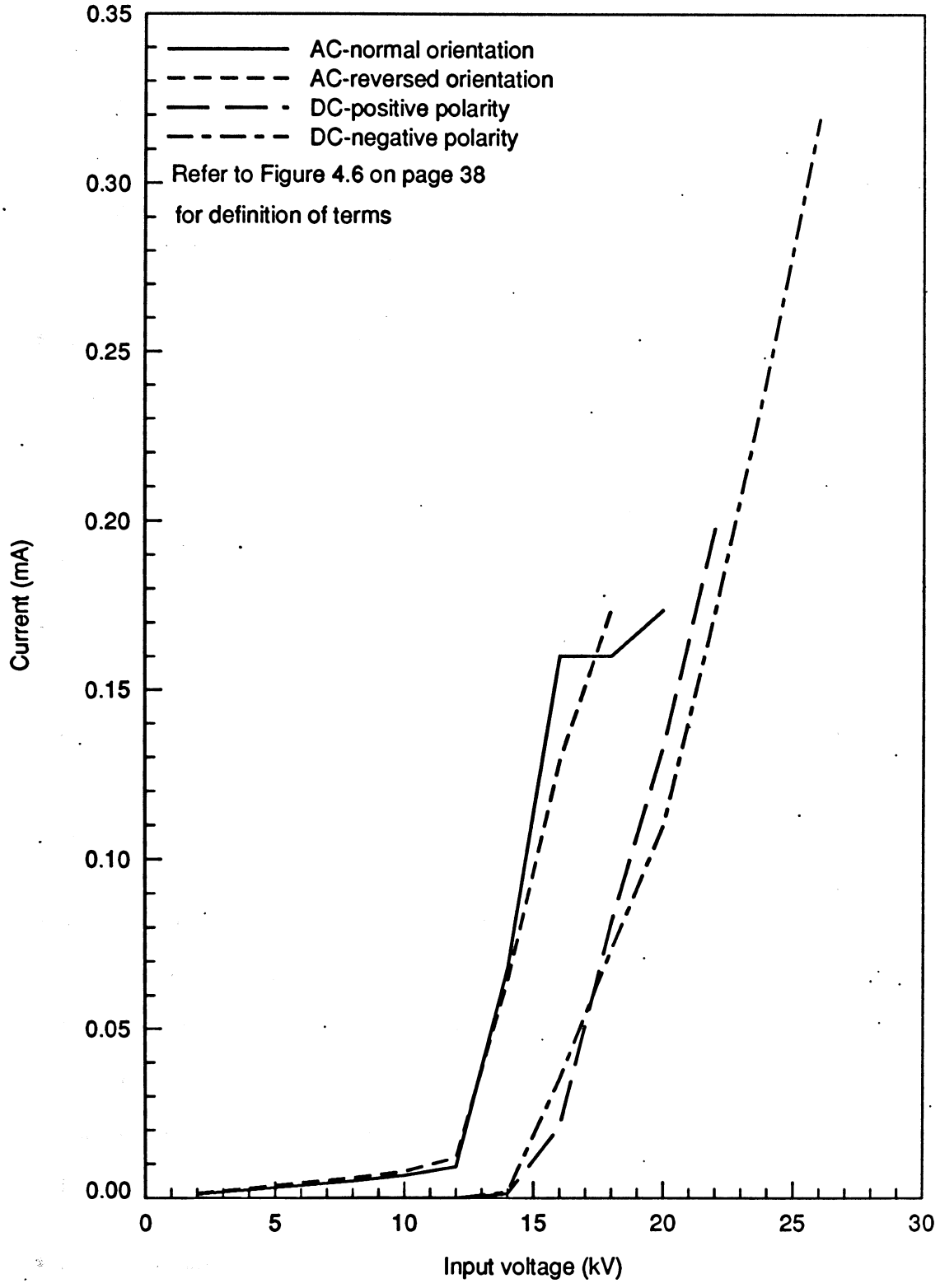

Figure 6.7: Current-voltage characteristic of different power sources

istic and well behaved data (Figure 4.7, 4.8, 4.11 and 4.12, also Table 5.9 and 5.10), while the DC shows erratic data with increased scatter (Figure 4.15, 4.16, and 4.19 through 4.21, also Table 5.11 and 5.12). This result is probably due to the fact that the DC high voltage discharge is more susceptible to electrostatic effects than is AC voltage.

- On comparing the DC-positive polarity *(positive corona)* and DC-negative polarity *(negative corona)* shown in Chapter 4, it can be seen that the positive corona has relatively more uniform discharge than the negative corona. This phenomenon was also reported by Shaughnessy and Solomon [29] on an experiment involving point-to-plane corona discharge.

- The data for higher voltage region show more uncertainties and obvious deviation from the theory. The reason is probably due to thrust and electrostatic effect dominating the drag effect. This is supported by the analysis of variance in Chapter 5 which shows less dependency of strain gages voltage reading on the air speed (see Table 5.4) in the higher voltage regions.

- The comparison of plate drag with and without the high voltage discharge in Chapter 4 shows a reduction in drag coefficient, which signifies the fact that high voltage discharge does play an important role in drag reduction. In the light of previous conclusions, shown in Table 6.2 is percent reduction in drag coefficient of the plate with AC high voltage discharge in the range of 2 to 10 kV.

- Statistical analysis played an important role in analyzing the experimental results and helped improve confidence in the data while indicating phenomenon

Table 6.2: Percent reduction in drag coefficient on the plate with AC high voltage discharge

High voltage discharge (kV)	Percent reduction normal orientation (%)	Percent reduction reversed orientation (%)
2.0	2.69	2.84
4.0	12.80	7.33
6.0	27.05	24.87
8.0	19.63	49.32
10.0	72.40	73.20

Calculated as

$$\frac{C_{D\,without\ high\ voltage\ discharge} - C_{D\,with\ high\ voltage\ discharge}}{C_{D\,without\ high\ voltage\ discharge}} \times 100\%$$

and averaged from ten-Reynolds number data.

which otherwise might be overlooked, e.g., the effect of high voltage discharge at low and high air speeds on page 87.

BIBLIOGRAPHY

[1] Bartnikas, R., and E.J. McMahon. *Corona Measurement and Interpretation.* Vol. 1, *Engineering Dielectrics.* Philadelphia, PA: American Society for Testing and Materials, 1979.

[2] Bassin, M.G., S.M. Brodsky, and H. Wolkoff. *Statics and Strength of Materials.* New York, NY: McGraw-Hill Book Co., 1979.

[3] Beckwith, T.G., N.L. Buck, and R.D. Marangoni. *Mechanical Measurements.* Reading, MA: Addison-Wesley Publishing Company, 1982.

[4] Blevins, R.D. *Applied Fluid Dynamics Handbook.* New York, NY: Van Nostrand Reinhold Company, 1984.

[5] Bushnell, D.M., and J.N. Hefner (editors). *Viscous Drag Reduction in Boundary Layers.* Vol. 123, *Progress in Astronautics and Aeronautics.* Washington, DC: American Institute of Aeronautics and Astronautics, Inc., 1990.

[6] Cobine, J.D. *Gaseous Conductors.* New York, NY: Dover Publications, Inc., 1958.

[7] Colver, G.M., and Y. Nakai. "Flame stabilization by an electrical discharge and flame visualization of the influence of a semi-insulating wall on the ionic-wind." In *Proceedings of the* 13^{th} *annual meeting of the IEEE Industry Applications Society held in Toronto 1-5 October 1978,* 95-104. IEEE-IAS, 1978.

[8] Cook, R.D., and W.C. Young. *Advanced Mechanics of Materials.* New York, NY: Macmillan Publishing Co., 1985.

[9] Currie, I.G. *Fundamental Mechanics of Fluids.* New York, NY: McGraw-Hill Book Co., 1974.

[10] Dally, J.W., and W.F. Riley. *Experimental Stress Analysis.* New York, NY: McGraw-Hill Book Company, 1991.

[11] Dally, J.W., W.F. Riley, and K.G. McConnell. *Instrumentation for Engineering Measurements.* New York, NY: John Wiley & Sons, Inc., 1984.

[12] Forouraghi, K. "Measurement of sphere-resistance at low velocities of air in a subsonic wind tunnel." M.S. thesis, Iowa State University, 1987.

[13] Fox, R.W., and A.T. McDonald. *Introduction to Fluid Mechanics.* New York, NY: John Wiley & Sons, Inc., 1985.

[14] Hall, J.L. "Using statistics in experimental test programs." Lecture notes, Iowa State University, 1989.

[15] Happel, J., and H. Brenner. *Low Reynolds Number Hydrodynamics.* Englewood Cliffs, NJ: Prentice-Hall, Inc., 1965.

[16] Hughes, W.F., and J.A. Brighton. *Fluid Dynamics.* Schaum's Outline Series, New York, NY: McGraw-Hill Book Company, 1967.

[17] Imai, I. "Second approximation to the laminar boundary-layer flow over a flat plate." *Journal of The Aeronautical Sciences,* 24 (1957): 155-156.

[18] Kays, W.M., and M.E. Crawford. *Convective Heat and Mass Transfer.* New York, NY: McGraw-Hill Book Co., 1980.

[19] Kuo, Y.H. "On the flow of an incompressible viscous fluid past a flat plate at moderate reynolds numbers." *Journal of Mathematics and Physics,* 32 (1953): 83-101.

[20] Lawton, J., and F.J. Weinberg. *Electrical Aspects of Combustion.* Oxford, UK: Clarendon Press, 1969.

[21] Lipson, C., and N.J. Sheth. *Statistical Design and Analysis of Engineering Experiments.* New York, NY: McGraw-Hill Book Co., 1973.

[22] Malik, M.R., L.M. Weinstein, and M.Y. Hussaini. "Ion wind drag reduction." In *Proceedings of the* 21^{st} *AIAA Aerospace Sciences Meeting held in Reno 10-13 January 1983,* New York: American Institute of Aeronautics and Astronautics, 1983.

[23] Medvedev, V.F., and M.S. Krakov. "Flow separation control by means of magnetic fluid." *Journal of Magnetism and Magnetic Materials,* 39 (1983): 119-122.

[24] Munson, B.R., D.F. Young, and T.H. Okiishi. *Fundamentals of Fluid Mechanics.* New York, NY: John Wiley & Sons, Inc., 1990.

[25] Oberg, E., F.D. Jones, and H.L. Horton. *Machinery's Handbook*, 23^{rd} Edition. New York, NY: Industrial Press, Inc., 1988.

[26] Roark, R.J. *Formulas for Stress and Strain.* New York, NY: McGraw-Hill Book Co., 1965.

[27] Schlichting, H. *Boundary Layer Theory.* New York, NY: McGraw-Hill Book Co., 1979.

[28] Scibor-rylski, A.J. *Road Vehicle Aerodynamics.* London, UK: John Wiley & Sons, Inc., 1975.

[29] Shaughnessy, E.J., and G.S. Solomon. "Electrohydrodynamic pressure of the point-to-plane corona discharge." *The Journal of the American Association for Aerosol Research,* 24, no. 2 (1991):193-200.

[30] Van Dyke, M. *Perturbation Methods in Fluid Mechanics.* Annotated Edition, Stanford, CA: The Parabolic Press, 1975.

[31] Veldman, A.E.P. "Boundary layer flow past a finite flat plate." Dissertation, Rijksuniversiteit Groningen, 1976.

[32] Weinberg, F.J. (editor). *Advanced Combustion Methods.* London, UK: Academic Press Inc. Ltd., 1986.

[33] Weinstein, L.M., and R. Balasubramanian. "An electrostatically driven surface for flexible wall drag reduction studies." Paper presented at the 2^{nd} International Conference on Drag Reduction, Cambridge, England, August-September, 1977.

[34] White, F.M. *Fluid Mechanics.* New York, NY: McGraw-Hill Book Co., 1986.

[35] White, F.M. *Viscous Fluid Flow.* New York, NY: McGraw-Hill Book Company, 1991.

[36] Young, W.C. *Roark's Formulas for Stress & Strain.* New York, NY: McGraw-Hill Book Co., 1989.

APPENDIX A. STRAIN GAGE CALIBRATION

Calibration on One Wire

The calibration of the sensor was done using precision weights ranging from 1 mg to 150 mg. These weights were put on the tip of the support wire 3.9375 inch long and 0.0184 inch in diameter which was soldered to the tip of a cantilever beam of 2.875 inches long, 0.5 inch wide and 0.005 inch thick,[1] after the threaded rod-support frame was tipped 90 degrees sideways. Two strain gages were used to double the sensitivity. The gages were placed at 75 mm distance from the tip of the beam. Two voltmeters were used simultaneously, *Keithley Digital Multimeter* and *Tektronix Oscilloscope*[2].

To verify the readings, it was considered necessary to put the weights on the tip of the beam and compare the moments from these two forces on the strain gages. Later it was noticed that in some experiments involving high voltage discharge, the strain-voltage readings were negative. To determine whether these negative readings resulted from electrostatic force or thrust force,[3] another experiment was conducted in which the whole plate-wire suspension system was flipped 180° from the position

[1] See Chapter 2 for details on experimental apparatus.

[2] See Appendix C for further study on different measuring instruments used on this study.

[3] See Chapter 6

shown in Figure A.1, i.e., the calibrated beam was on the top.

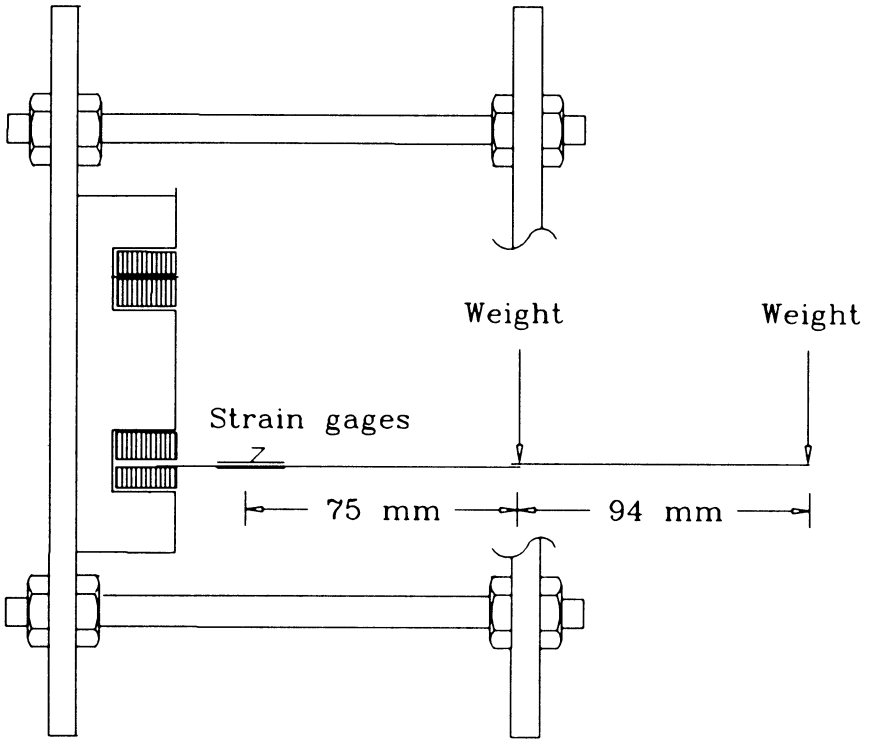

Figure A.1: Calibration on one wire

Table A.1 shows the data, which was plotted as seen in Figure A.2.

The line equations are:

$$Force = 6.6313 \times 10^{-6} Voltage - 5.0823 \times 10^{-6} \tag{A.1}$$

for positive direction, weights on tip of the wire, and

$$Force = 1.5887 \times 10^{-5} Voltage - 2.0243 \times 10^{-6} \tag{A.2}$$

for positive direction, weights on tip of the beam, and

$$Force = 4.7252 \times 10^{-6} Voltage - 4.7348 \times 10^{-6} \tag{A.3}$$

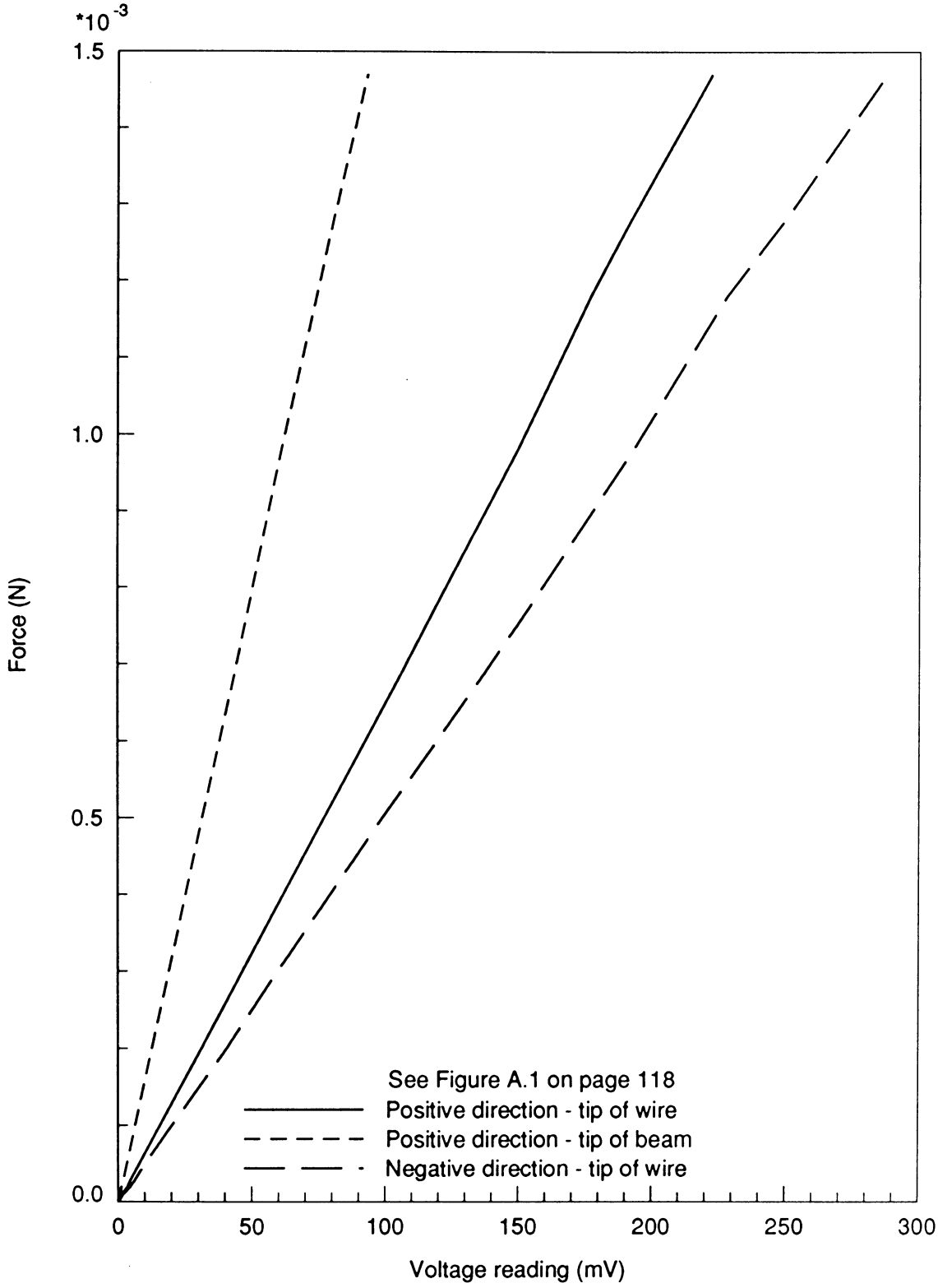

Figure A.2: Calibration Curve - beam-wire system, positive and negative direction

Table A.1: Calibration on tip of wire and tip of beam

Mass	Force[a]	Voltage readings		
		Positive direction		Negative direction
		On tip of the wire	On tip of the beam	
mg	N	mV	mV	mV
0.0	0.000E+00	0.000	0.000	0.000
1.0	0.981E-05	1.550	0.817	2.200
2.0	0.196E-04	3.517	1.300	4.983
3.0	0.294E-04	4.750	2.183	7.050
5.0	0.491E-04	7.817	3.300	10.750
10.0	0.981E-04	15.400	6.267	21.467
20.0	0.196E-03	30.650	12.467	43.333
30.0	0.294E-03	45.650	18.767	63.483
50.0	0.491E-03	75.717	30.933	105.450
70.0	0.687E-03	105.917	43.650	148.667
80.0	0.785E-03	120.533	49.483	169.533
100.0	0.981E-03	149.800	61.117	209.517
120.0	0.118E-02	177.133	74.300	247.500
130.0	0.128E-02	192.217	80.600	271.067
150.0	0.147E-02	222.400	93.217	312.083

[a] with gravity, $g = 9.81 \frac{m}{sec^2}$

for negative direction, weights on tip of the wire.

A simple moment calculation can be performed to verify that there is no additional moment acting on the beam-wire system other than the moment from the weights. For example, from Equation A.1:

For voltage reading 100 mV, the corresponding force acting on the tip of the wire is $6.580477 \times 10^{-4} N$, and from Equation A.2 this force is resulted from voltage reading of 41.54793227 mV. Therefore, the proportion of moment acting on the tip of the wire and moment acting on the tip of the beam must be approximately the

same as their corresponding voltage readings:

$$\frac{6.580477 \times 10^{-4}(2.875 + 3.9375)}{6.580477 \times 10^{-4}(2.875)} \approx \frac{100}{41.54793227}$$

or

$$2.367565217 \approx 2.406858646$$

The difference is only 1.6 %.

Calibration on Two Wires

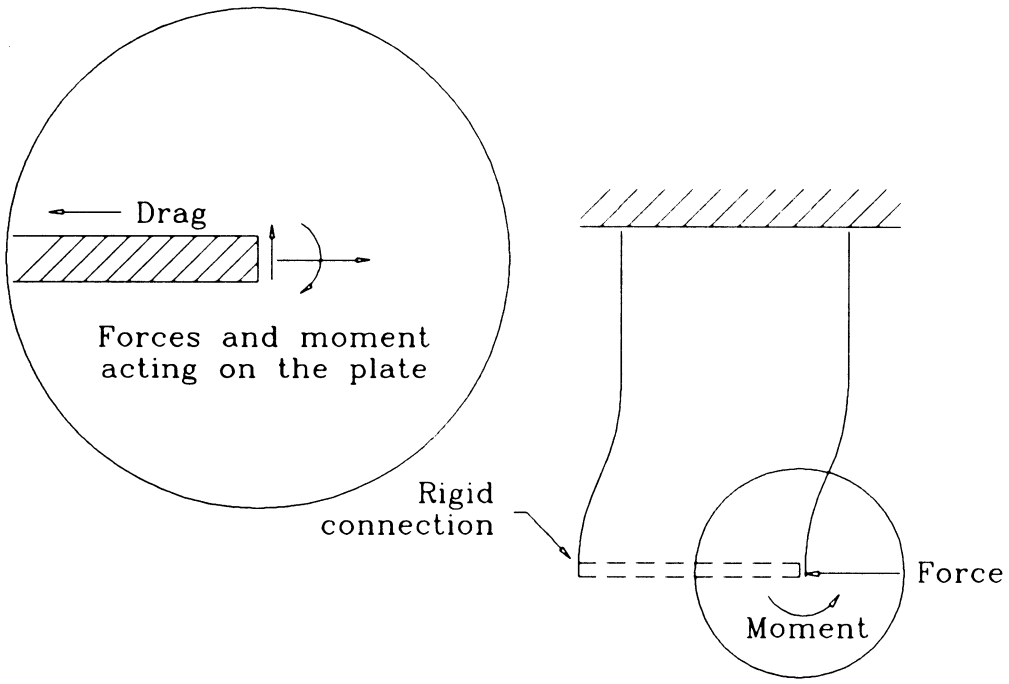

Figure A.3: Wire bending due to the rigid connection wire-plate

It was suspected that the wires might experience a bending moment due to the rigid connection between the wire and the plate (see Figure A.3). The moment on the wire will affect the voltage reading greatly, since it counteracts the actual force sensed

by the strain gages. Therefore, another calibration curve was needed. The experiment was carried out with the frame tipped sideways as in the above experiment. This time two wires were used instead of one. The wires were connected to each other by a rigid 36 mm match-stick to simulate the wire-plate suspension system. The match-stick was used for its light weight, since the weight of the actual plate was too heavy that it dominated the voltage reading.

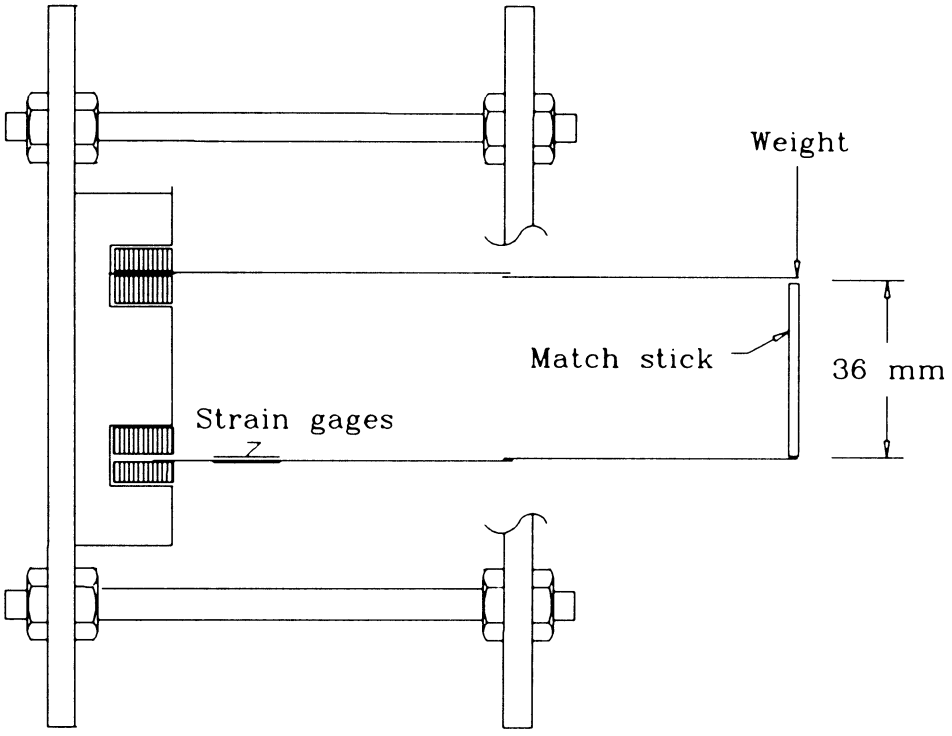

Figure A.4: Calibration on the tip of two wires

As in the case of one-wire system, this two-wire system was also calibrated in the negative direction. The results were shown on Table A.2 and Figure A.5.

Table A.2: Calibration on tip of two wires

Mass	Force[a]	Voltage readings	
		Positive direction	Negative direction
mg	N	mV	mV
0.0	0.000E+00	0.000	0.000
1.0	0.981E-05	0.367	0.533
2.0	0.196E-04	0.683	1.050
3.0	0.294E-04	1.200	1.633
5.0	0.491E-04	1.783	2.383
10.0	0.981E-04	3.733	5.067
20.0	0.196E-03	7.300	10.000
30.0	0.294E-03	11.067	15.267
50.0	0.491E-03	18.350	25.300
70.0	0.687E-03	25.733	35.750
80.0	0.785E-03	29.400	40.717
100.0	0.981E-03	36.750	51.067
120.0	0.118E-02	44.100	61.350
130.0	0.128E-02	47.750	66.467
150.0	0.147E-02	55.050	76.483

[a] with gravity, $g = 9.81 \frac{m}{sec^2}$

The regression equation is

$$Force = 2.6743 \times 10^{-5} Voltage - 3.6444 \times 10^{-7} \tag{A.4}$$

for positive direction, and

$$Force = 1.9226 \times 10^{-5} Voltage + 8.6235 \times 10^{-7} \tag{A.5}$$

for negative direction.

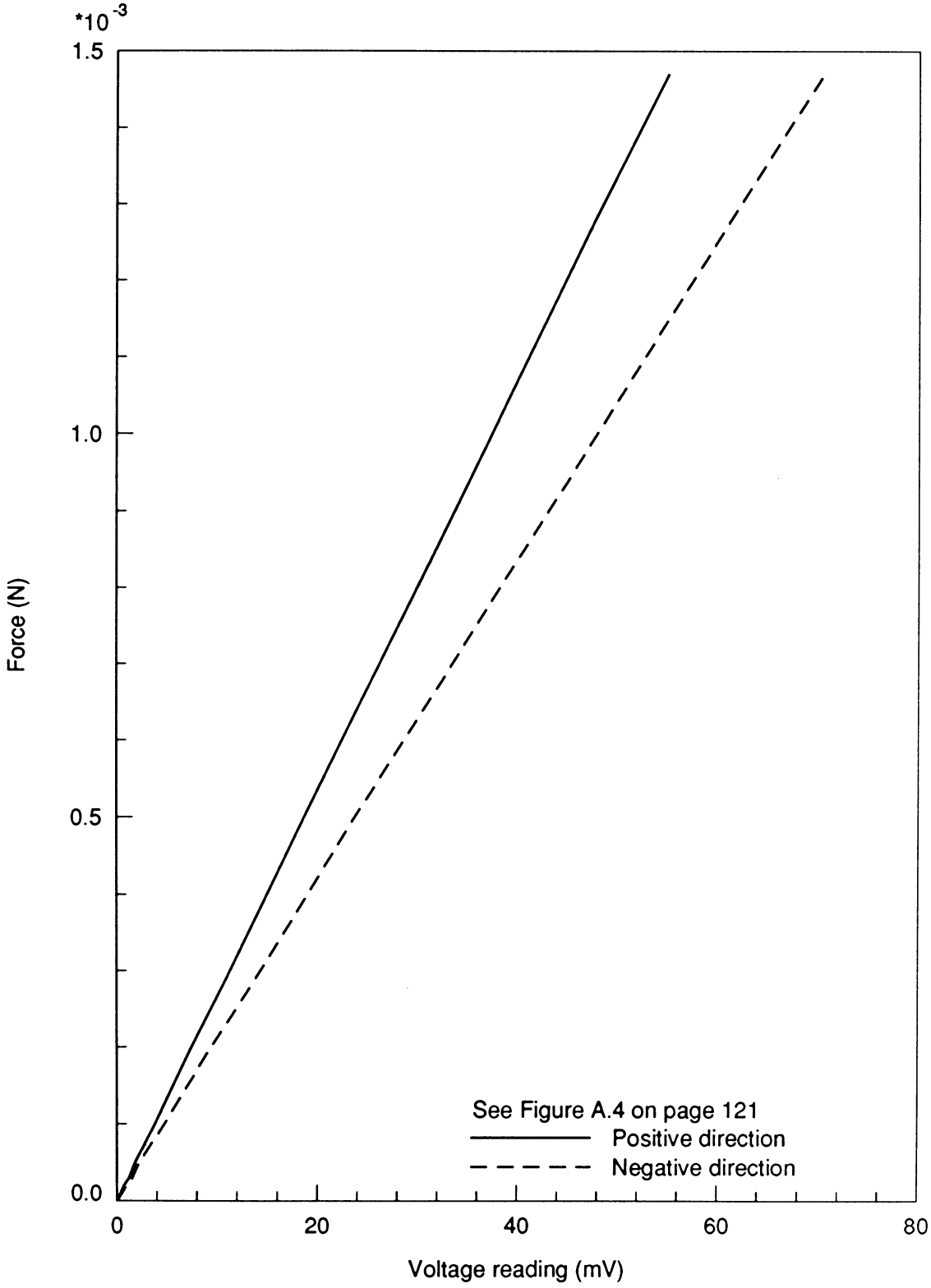

Figure A.5: Calibration Curve - weight on the tip of two wires, positive and negative direction

Theoretical Analysis

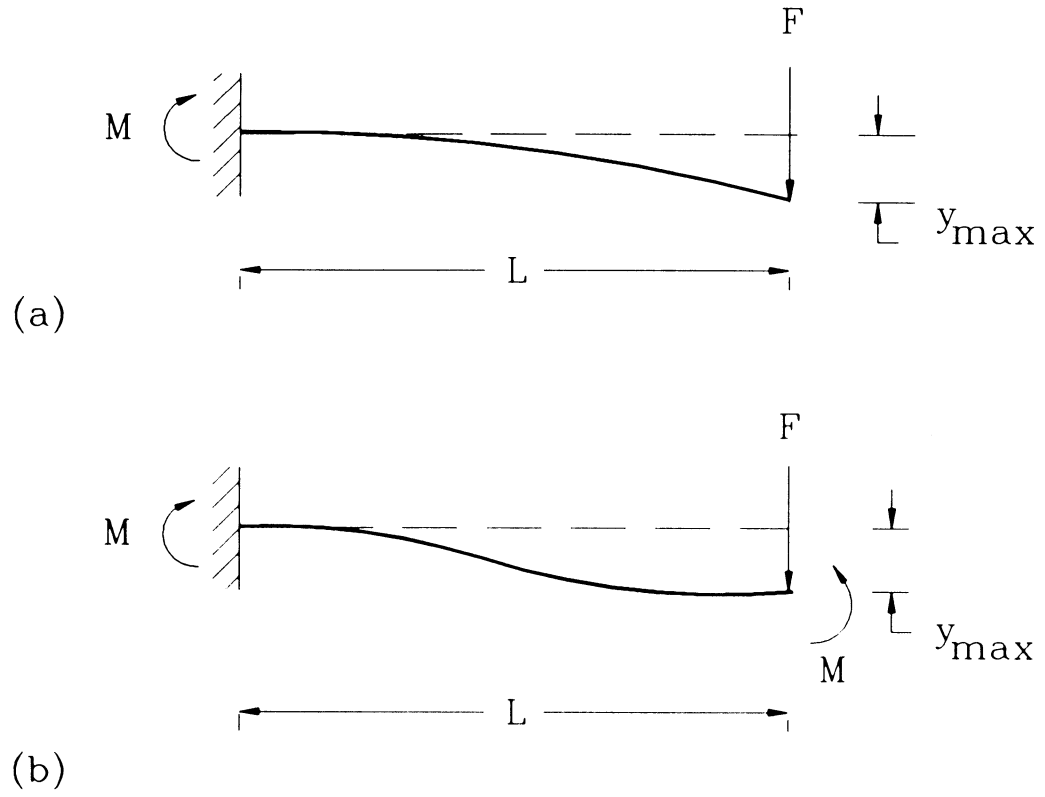

Figure A.6: Cantilever beam: (a) with free end, (b) with guided end

The experimental results in the previous sections were also analyzed theoretically utilizing beam theory. As an approximation, the whole beam and wire suspension system were regarded as a single beam; therefore, all beam theorems can be applied.

Stress sensed by the strain gages is

$$\sigma = \frac{Mc}{I}$$

where M is the bending moment, c is the distance from the neutral axis to the surface,

and I is the moment of inertia of the section of the beam with respect to the neutral axis[36].

For case(a) of Figure A.6, the moment acting on the strain gages is

$$M_{(a)} = FL$$

where F is the load acting on the beam tip and L is the distance from beam tip to the strain gages.

For case(b) of Figure A.6, the moment acting on the strain gages is

$$M_{(b)} = \frac{FL}{2}$$

Therefore, for the same load, F,

$$\frac{M_{(a)}}{M_{(b)}} = 2$$

or,

$$\frac{I\sigma_{(a)}/c}{I\sigma_{(b)}/c} = 2$$

and with the same I and c,

$$\sigma_{(a)} = 2\sigma_{(b)}$$

which indicates that for the same load, the beam in case (b) will produce only half of the strain in case (a), or in other words, the slope of case (b) is two times greater than that of case (a).

The actual experimental result shown in Figure A.7 shows the slope ratio to be $\approx$ 4, which probably resulted because the actual beam-wire system is more complicated than just a simple beam.

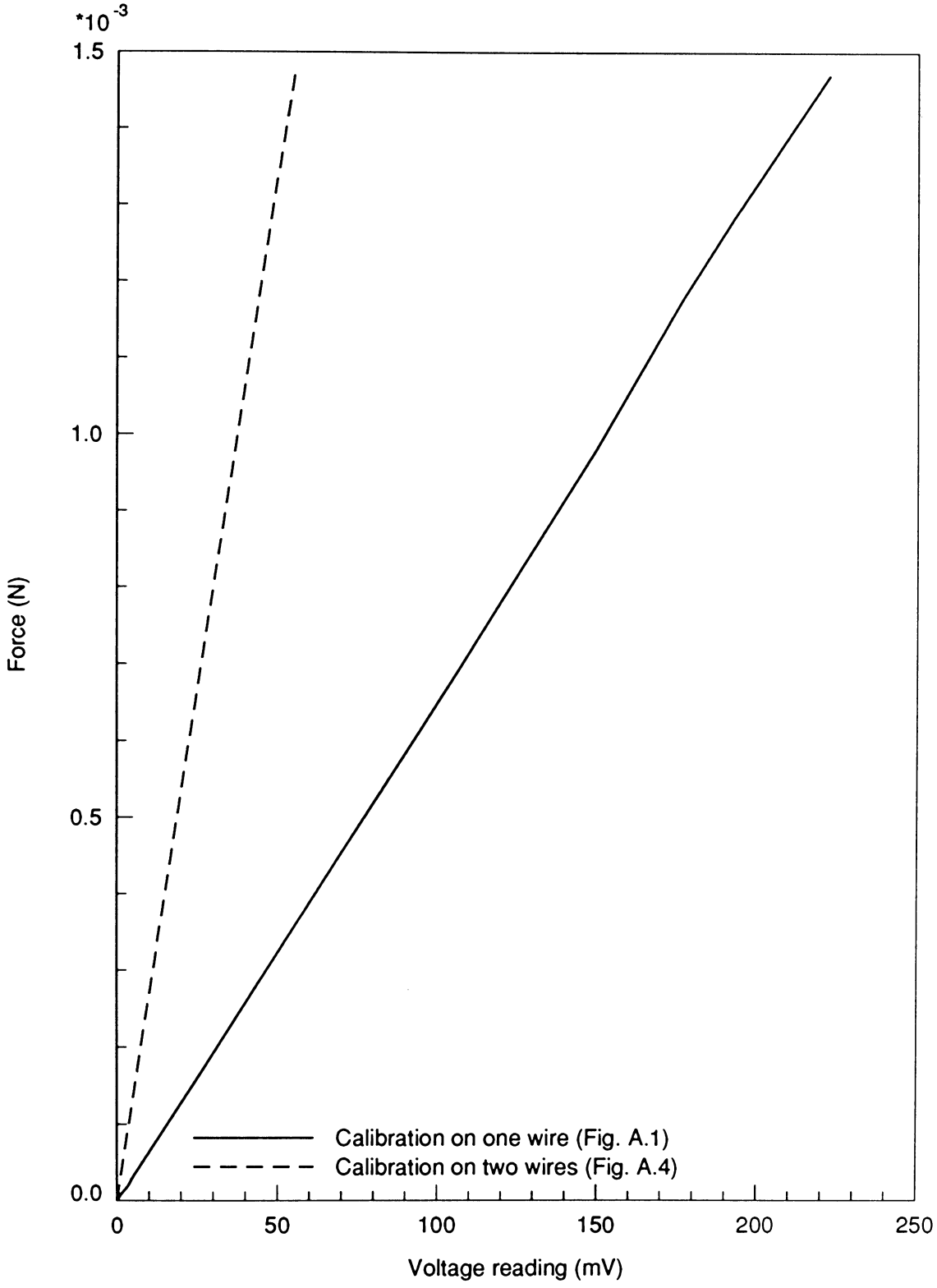

Figure A.7: Calibration curves on one and two wires

Beam Deflection Verification

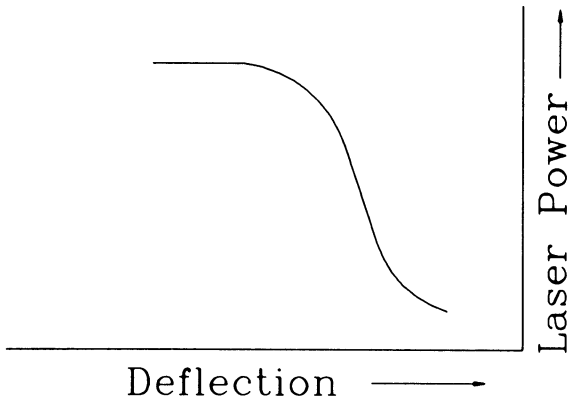

Figure A.8: Wire deflection vs. Laser Power

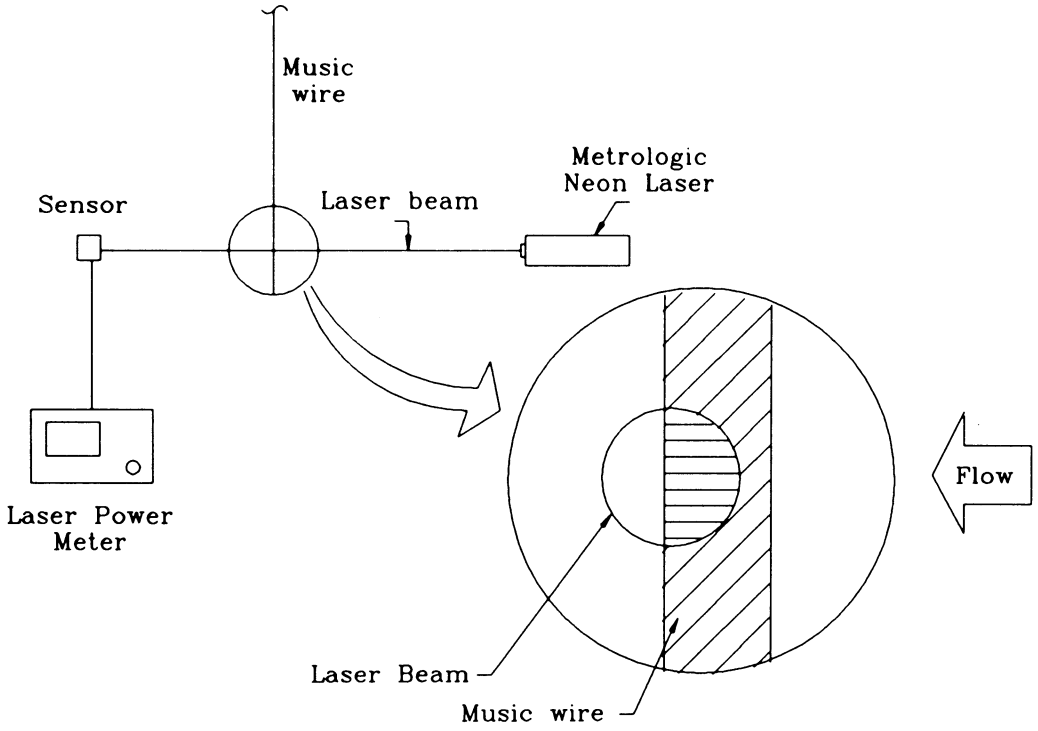

Figure A.9: Beam deflection verification using laser beam

Another important aspect in the strain gage measurement is the verification of the wire (and the beam) deflection, especially since the drag force exerted on the beam is very small. It is virtually impossible to *see* the deflection with the naked eyes.

One way to verify deflection of the wires is to utilize a laser beam and a laser power meter as shown in Figure A.9. The music wire was placed off-center in between laser source and laser power meter. In this way, the light being read by the meter was partially blocked. The wind tunnel was turned on and the wire was deflected due to drag. Meanwhile, the power read by the meter is recorded. A decrease in power shows that the wire was covering the laser beam; and vice versa, an increased power indicated the wire was deflected away from the laser beam.

By choosing the flow direction as a positive deflection, it was demonstrated that the strain gages indeed recorded the drag force in a positive direction, i.e. the air flow direction.

APPENDIX B. AIR SPEED MEASUREMENT

Air speed measurements were carried out by the pressure-difference readings of a pitot-static tube, which were converted to velocity by the relation

$$V = \sqrt{\frac{2\Delta p}{\rho}}$$

where the pressure difference, Δp was read with the aid of *Barocel Electronic Manometer*. This device is capable of reading a pressure difference of 0.002 torr.

To gain confidence in the readings, the electronic manometer was compared to the *Microtector*, a U-tube manometer with a micrometer as the height indicator. The set-up is shown in Figure B.1.

The Microtector is a battery-operated manometer. It has two indicators, a needle-point micrometer and an ammeter. The needle and the manometer liquid act as the conductor. Upon contact, electric current from the battery flows and is read on the ammeter. When the liquid surface inside the manometer changes as a result of pressure changes, the micrometer can be adjusted to get the current reading, thus obtaining the height difference between the surfaces.

There are two possible ways to adjust the micrometer. The first is by maintaining the current reading at a fixed value, say 20 μA, as the *null* indicator; then, with the liquid surface changed, the micrometer was adjusted upward to compensate the change and produce the same current, 20 μA. The adjustment was the pressure

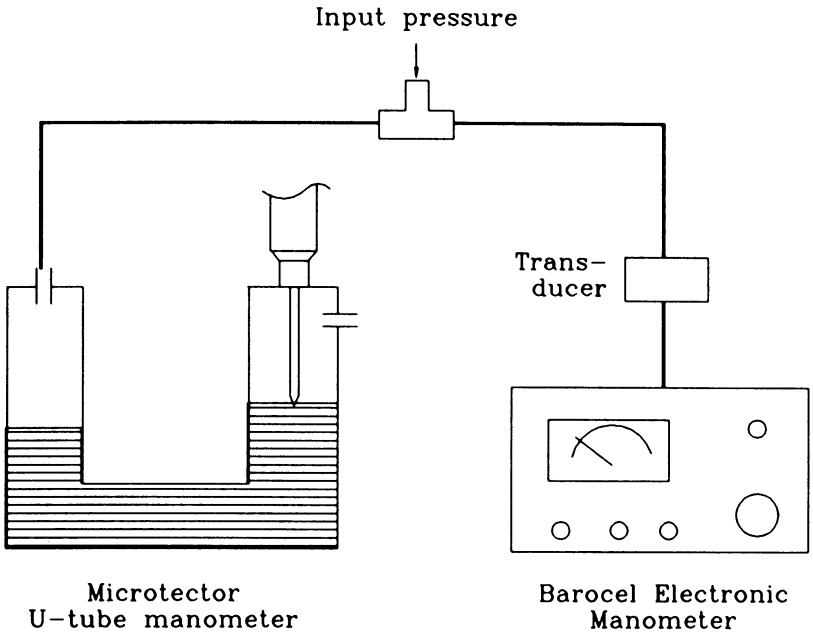

Figure B.1: Comparison of two different manometers

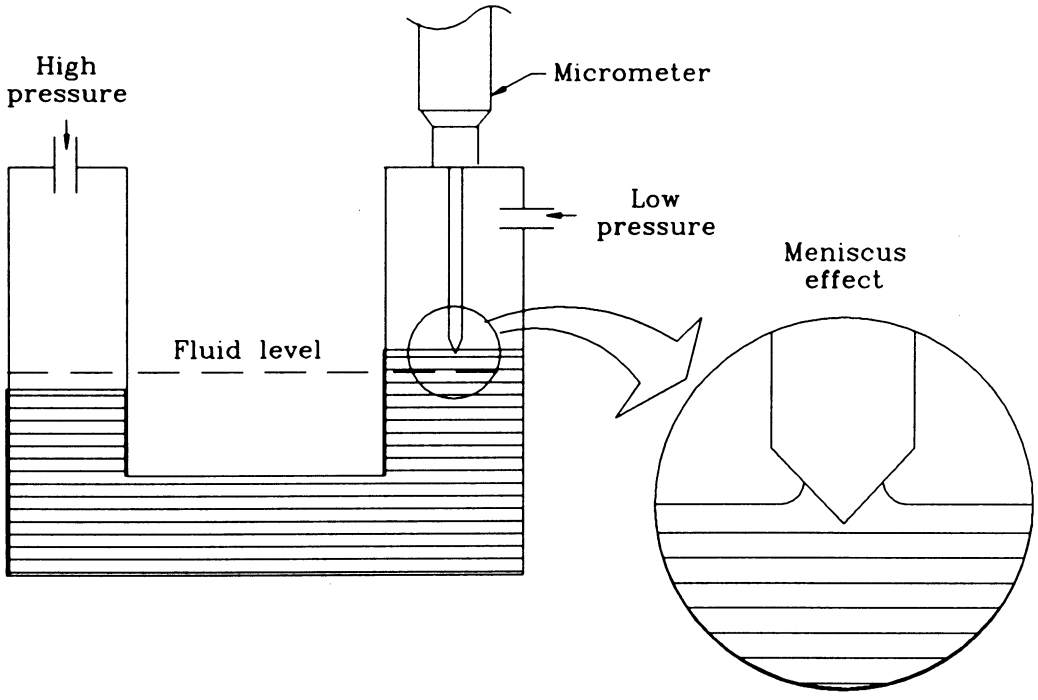

Figure B.2: Microtector manometer

difference in $inch H_2O$. It was called Method A. The second method was to record the micrometer readings of the initial needle-liquid contact as the *zero* height. Then the needle was moved above the surface. As the liquid surface changes, the micrometer was adjusted downward until the needle made contact with the liquid surface. This was called Method B, and was intended to eliminate the *meniscus effect* of Method A(see Fig. B.2).

Table B.1: Pressure reading comparison: Method A

From Microtector		From Barocel	
in. H_2O	corresponding torr	torr	corresponding in. H_2O
0.0560	0.1045	0.0985	0.0528
0.0520	0.0971	0.0915	0.0490
0.0480	0.0896	0.0860	0.0461
0.0440	0.0821	0.0775	0.0415
0.0400	0.0747	0.0710	0.0380
0.0360	0.0672	0.0640	0.0343
0.0320	0.0597	0.0570	0.0305
0.0280	0.0523	0.0495	0.0265
0.0240	0.0448	0.0425	0.0228
0.0200	0.0373	0.0345	0.0185
0.0160	0.0299	0.0270	0.0145
0.0120	0.0224	0.0200	0.0107
0.0080	0.0149	0.0125	0.0067
0.0040	0.0075	0.0060	0.0032

As can be observed from Figure B.3 that the two methods did not differ significantly from each other, showing that the meniscus effect is negligible.

The expected slope for this experiment was one, which means the Microtector and the Barocel Electronic Manometer give very nearly the same pressure reading. However, close examination shows that the Microtector gave a slightly higher pressure difference. This result suggested that a calibration curve should be used. However,

considering the difference is small ($\approx 7\%$) and the fact that a small reading error in the Microtector will be doubled in the resulting data (see Figure B.2), it was decided to use the *Barocel Electronic Manometer* without calibration curve.

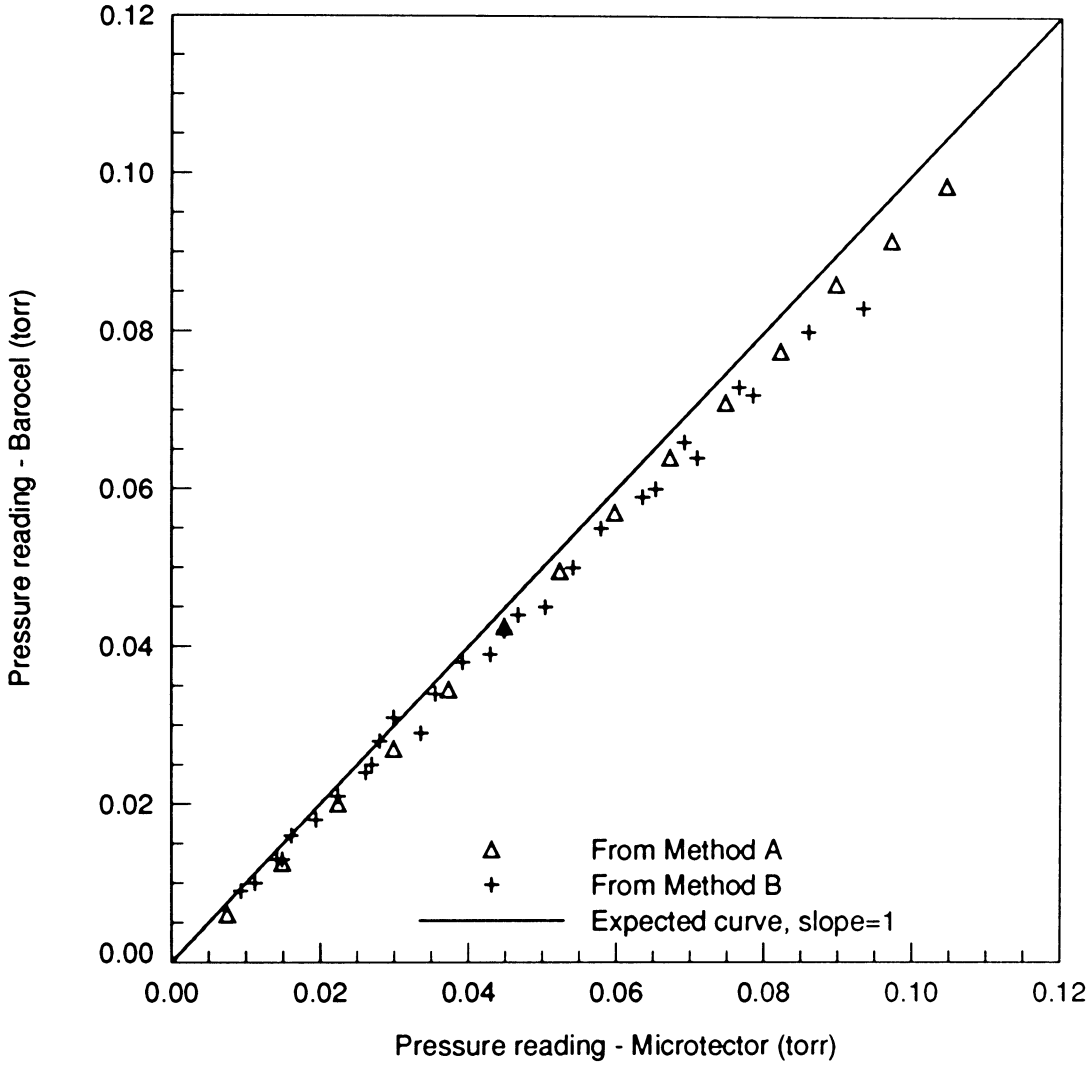

Figure B.3: Pressure comparison

Table B.2: Pressure reading comparison: Method B

From Microtector		From Barocel	
in. H_2O	corresponding torr	torr	corresponding in. H_2O
0.0500	0.0933	0.0830	0.0445
0.0460	0.0859	0.0800	0.0429
0.0420	0.0784	0.0720	0.0386
0.0410	0.0765	0.0730	0.0391
0.0380	0.0709	0.0640	0.0343
0.0370	0.0691	0.0660	0.0354
0.0350	0.0653	0.0600	0.0321
0.0340	0.0635	0.0590	0.0316
0.0310	0.0579	0.0550	0.0295
0.0290	0.0541	0.0500	0.0268
0.0270	0.0504	0.0450	0.0241
0.0250	0.0467	0.0440	0.0236
0.0240	0.0448	0.0420	0.0225
0.0230	0.0429	0.0390	0.0209
0.0210	0.0392	0.0380	0.0204
0.0190	0.0355	0.0340	0.0182
0.0180	0.0336	0.0290	0.0155
0.0160	0.0299	0.0310	0.0166
0.0150	0.0280	0.0280	0.0150
0.0144	0.0269	0.0250	0.0134
0.0140	0.0261	0.0240	0.0129
0.0120	0.0224	0.0210	0.0113
0.0104	0.0194	0.0180	0.0096
0.0086	0.0161	0.0160	0.0086
0.0080	0.0149	0.0130	0.0070
0.0076	0.0142	0.0130	0.0070
0.0060	0.0112	0.0100	0.0054
0.0050	0.0093	0.0090	0.0048

APPENDIX C. CURRENT MEASUREMENT

The power source was equipped with a voltmeter and an ammeter. However, due to the fact that the currents were very small (in the order of 1×10^{-4} *Amp.*), this ammeter was not used. An alternative way to measure the current was to measure the voltage drop across a resistor, and calculate the current with the relation

$$I = \frac{V}{R}$$

There were four different types of voltmeter available, *Keithley 175 Autoranging Multimeter, Tektronix 434 Storage Oscilloscope, Micronta FET-VOM,* and *Simpson 260 VOM.* As a preliminary check, these four voltmeter were compared to each other using a step-down transformer, from 120 V to 2 V (nominal). The result is as follows:

Keithley (input impedance 10 $M\Omega/V_{AC}$)	2.423	V
Tektronix (input impedance 1 $M\Omega/V_{AC}$)	2.298	V
Micronta (input impedance 10 $k\Omega/V_{AC}$)	2.47	V
Simpson (input impedance 5 $k\Omega/V_{AC}$)	1.18	V

From these results it is apparent that the *Simpson* voltmeter was not operating properly; therefore, it was not used for the next experiments.

The next step would be to determine which line could be used to measure the current since there are two ground-lines available[29]. The first was the ground line

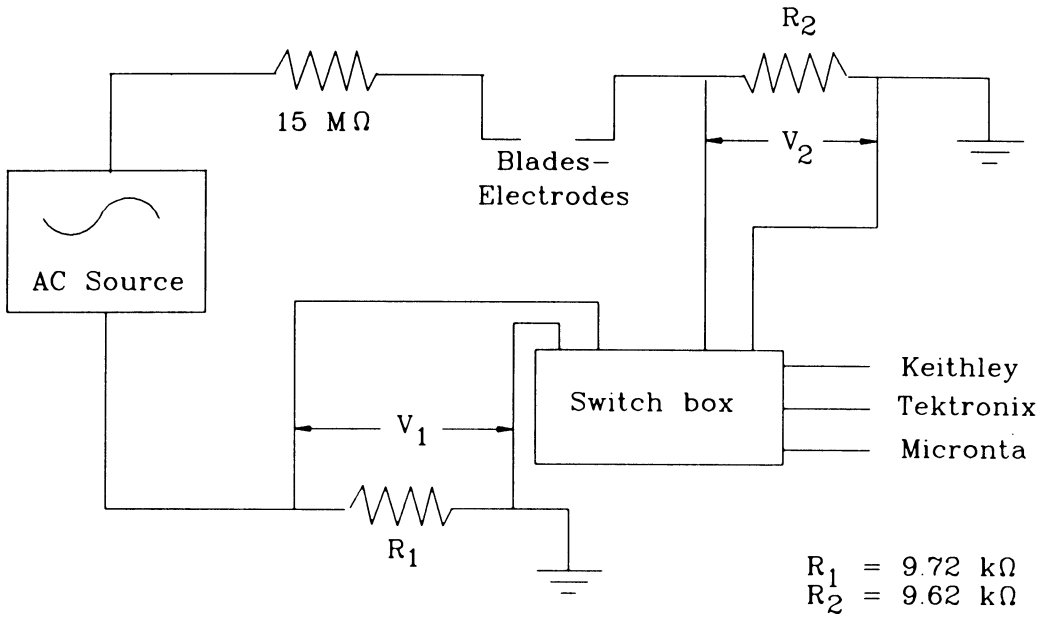

Figure C.1: Current measurement configuration

from the power source *(total current)*, and the second was of the electrode ground line *(net current received by the electrode)*. To gain confidence, these two lines were compared by measuring currents through R_1 and R_2. Both lines had a 10 $k\Omega$ resistor (nominal); however, the values read by the Keithley multimeter were 9.72 $k\Omega$ (R_1) and 9.62 $k\Omega$ (R_2).

The readings from the oscilloscope were peak-to-peak voltage; therefore, they had to be converted to rms value by formula:

$$V_{rms} = \frac{V_{peak-to-peak}}{2\sqrt{2}} \tag{C.1}$$

The Micronta Voltmeter has an input impedance of 10 $k\Omega/V_{AC}$ and the readings were taken on 3-V scale, gives the total impedance to be 30 $k\Omega$. The actual voltage

is:

$$V = V_{reading}\left(\frac{R + R_i}{R_i}\right)$$

where R is the outside resistor and R_i is the total impedance.

Table C.1: Current measured to the razor-blade-electrodes: Raw Data

Voltage	Keithley		Tektronix		Micronta	
kV	V_1[a]	V_2	V_1	V_2	V_1	V_2
0.0	0.333	0.014	0.980	0.540	0.120	0.000
2.5	0.688	0.041	1.950	1.100	0.380	0.000
5.0	1.033	0.081	2.900	1.600	0.650	0.000
7.5	1.375	0.115	3.950	2.150	0.920	0.030
10.0	1.697	0.155	4.800	2.600	1.120	0.040
12.5	1.996	0.240	5.700	3.200	1.430	0.070
15.0	2.365	0.650	6.600	3.700	1.720	0.290
17.5	2.690	1.250	7.600	4.300	2.080	0.400

[a]Subscripts 1 and 2 denote data from voltage reading across R_1 and R_2 respectively. Also in Tables C.2 thru C.6

Table C.2: Current measured to the razor-blade-electrodes: Current

Voltage	Keithley		Tektronix		Micronta	
kV	mA_1	mA_2	mA_1	mA_2	mA_1	mA_2
0.0	0.03426	0.00146	0.03565	0.01985	0.01635	0.00000
2.5	0.07078	0.00426	0.07093	0.04043	0.05176	0.00000
5.0	0.10628	0.00842	0.10548	0.05880	0.08854	0.00000
7.5	0.14146	0.01195	0.14368	0.07902	0.12532	0.00412
10.0	0.17459	0.01611	0.17459	0.09555	0.15256	0.00549
12.5	0.20535	0.02495	0.20733	0.11761	0.19479	0.00961
15.0	0.24331	0.06757	0.24007	0.13598	0.23429	0.03981
17.5	0.27675	0.12994	0.27644	0.15803	0.28333	0.05491

Moreover, this measurement was also compared to a needle-and-flat-plate configuration to see the tunnel's wall effect on the electrical discharge.

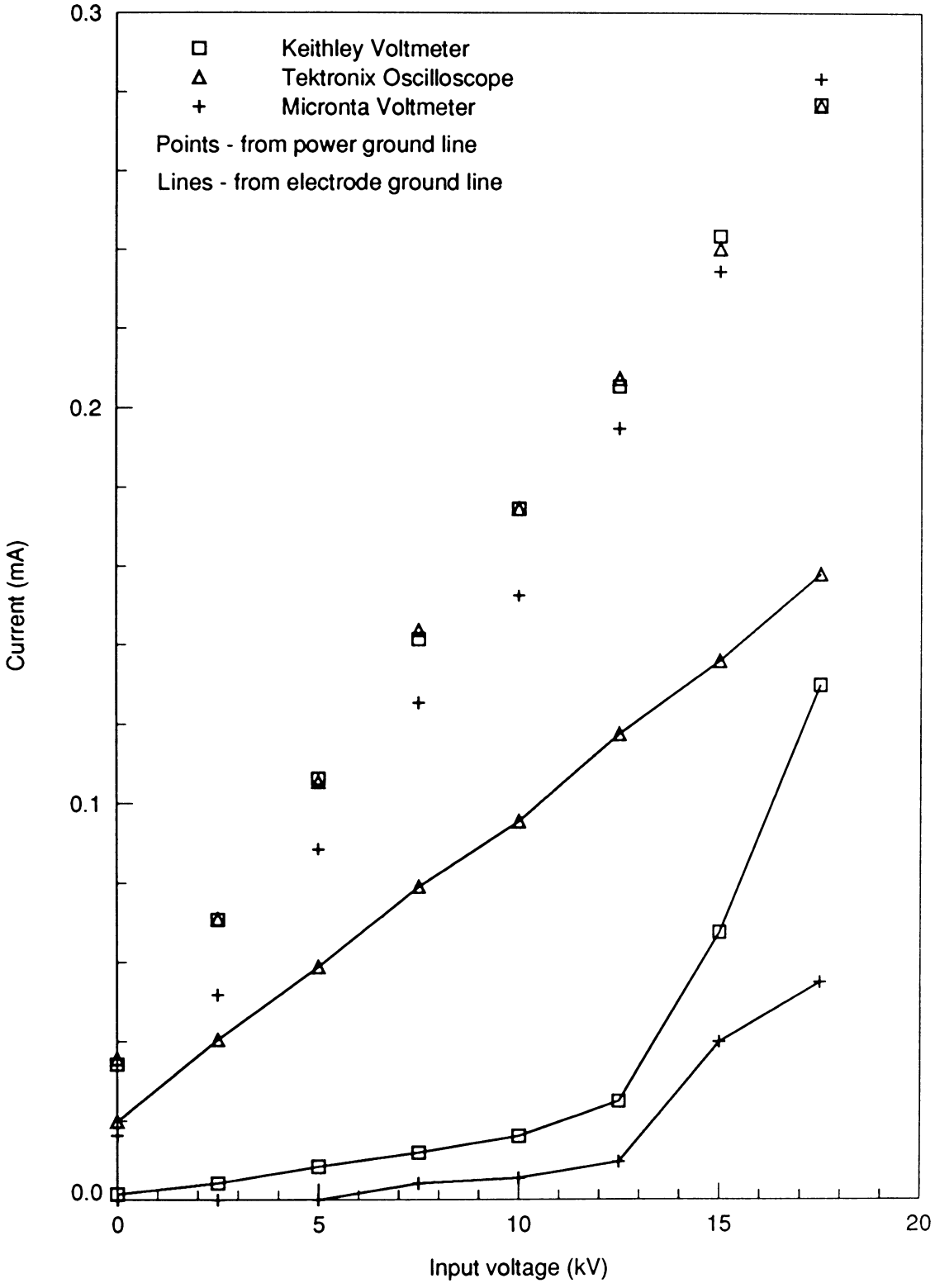

Figure C.2: Voltage vs. Current: Blades

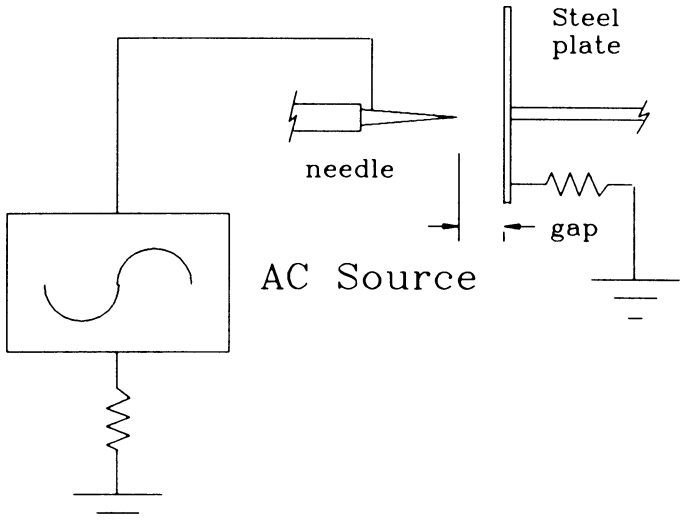

Figure C.3: Current measurement: Needle and flat plate

Table C.3: Current measurement on Needle and flat plate with 10 mm gap: Raw Data

Voltage	Keithley		Tektronix		Micronta	
kV	V_1	V_2	V_1	V_2	V_1	V_2
0.0	0.333	0.013	0.960	0.500	0.130	0.000
2.5	0.617	0.034	1.750	0.960	0.350	0.000
5.0	0.890	0.105	2.500	1.400	0.520	0.000
7.5	1.167	0.280	3.300	1.900	0.780	0.030
10.0	1.450	0.980	4.000	2.350	0.970	0.250

Attempts were made to run all the experiments within the same voltage range, i.e., from 0 to 17.5 kV; however, due to the difference in the geometry of the electrodes, and in the gap between the electrodes, sparks occurred in lower output voltage for the needle-and-plate configuration. Once sparks occurred, the Keithley Digital Multimeter readings were not possible. Therefore, the maximum voltage recorded for this configuration was the maximum voltage before sparking. Figure C.6 and C.7 show the comparison of current measurements.

Table C.4: Current measurement on Needle and flat plate with 10 mm gap: Current

Voltage	Keithley		Tektronix		Micronta	
kV	mA_1	mA_2	mA_1	mA_2	mA_1	mA_2
0.0	0.03426	0.00135	0.03492	0.01838	0.01771	0.00000
2.5	0.06348	0.00353	0.06365	0.03528	0.04767	0.00000
5.0	0.09156	0.01091	0.09093	0.05145	0.07083	0.00000
7.5	0.12006	0.02911	0.12003	0.06983	0.10625	0.00412
10.0	0.14918	0.10187	0.14550	0.08637	0.13213	0.03432

Table C.5: Current measurement on Needle and flat plate with 17 mm gap: Raw Data

Voltage	Keithley		Tektronix		Micronta	
kV	V_1	V_2	V_1	V_2	V_1	V_2
0.0	0.333	0.013	0.960	0.520	0.130	0.000
2.5	0.628	0.033	1.800	1.000	0.340	0.000
5.0	0.904	0.075	2.600	1.420	0.540	0.000
7.5	1.185	0.157	3.400	1.900	0.760	0.000
10.0	1.457	0.280	4.200	2.300	0.980	0.050
12.5	1.698	0.720	4.900	2.800	1.170	0.250
15.0	1.990	1.270	5.700	3.300	1.350	0.550

Table C.6: Current measurement on Needle and flat plate with 17 mm gap: Current

Voltage	Keithley		Tektronix		Micronta	
kV	mA_1	mA_2	mA_1	mA_2	mA_1	mA_2
0.0	0.03426	0.00135	0.03492	0.01911	0.01771	0.00000
2.5	0.06461	0.00343	0.06547	0.03675	0.04631	0.00000
5.0	0.09300	0.00780	0.09457	0.05219	0.07356	0.00000
7.5	0.12191	0.01632	0.12367	0.06983	0.10352	0.00000
10.0	0.14990	0.02911	0.15277	0.08453	0.13349	0.00686
12.5	0.17469	0.07484	0.17823	0.10291	0.15937	0.03432
15.0	0.20473	0.13202	0.20733	0.12128	0.18389	0.07551

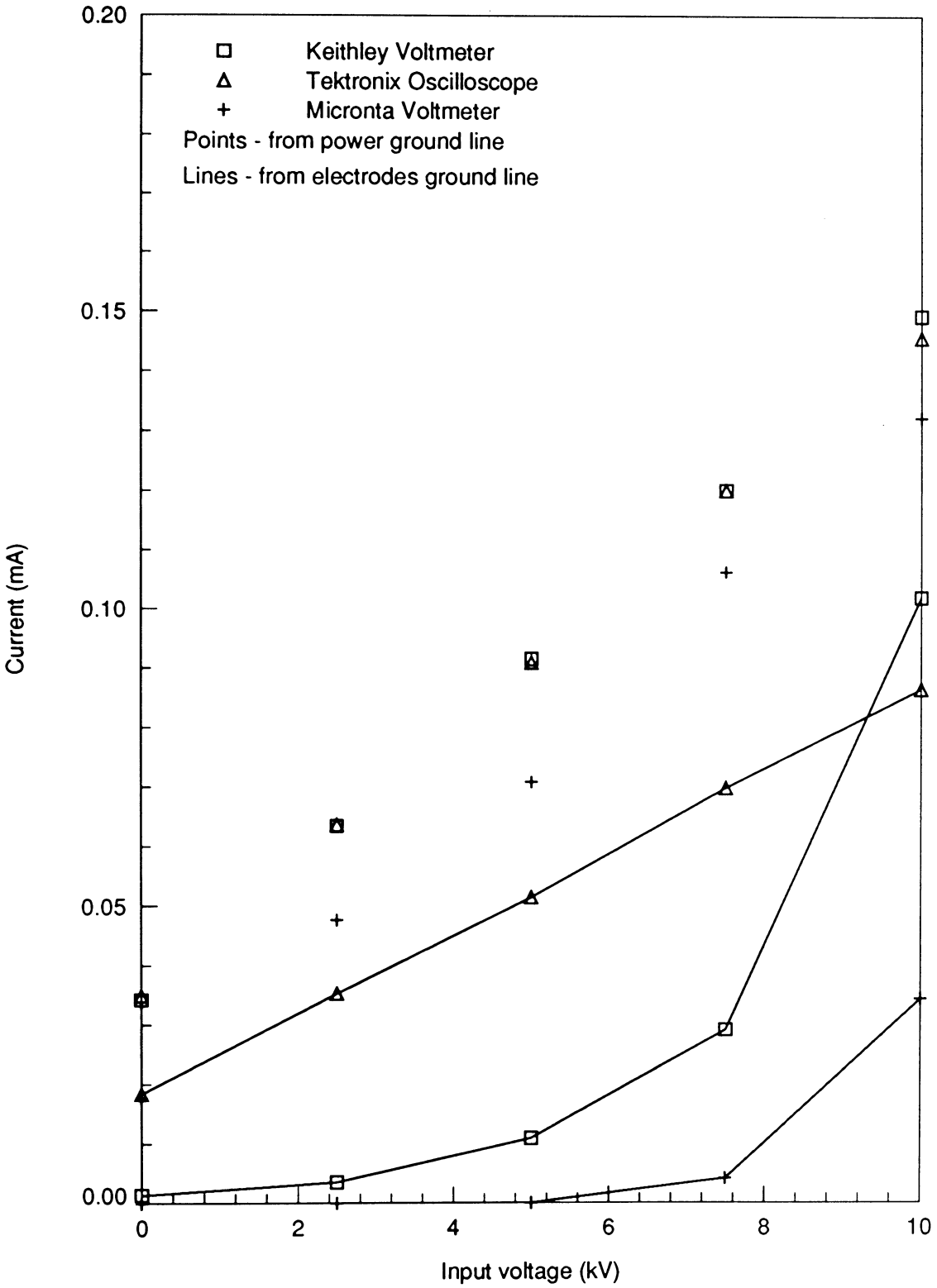

Figure C.4: Voltage vs. Current: Needle-flat plate 10 mm gap

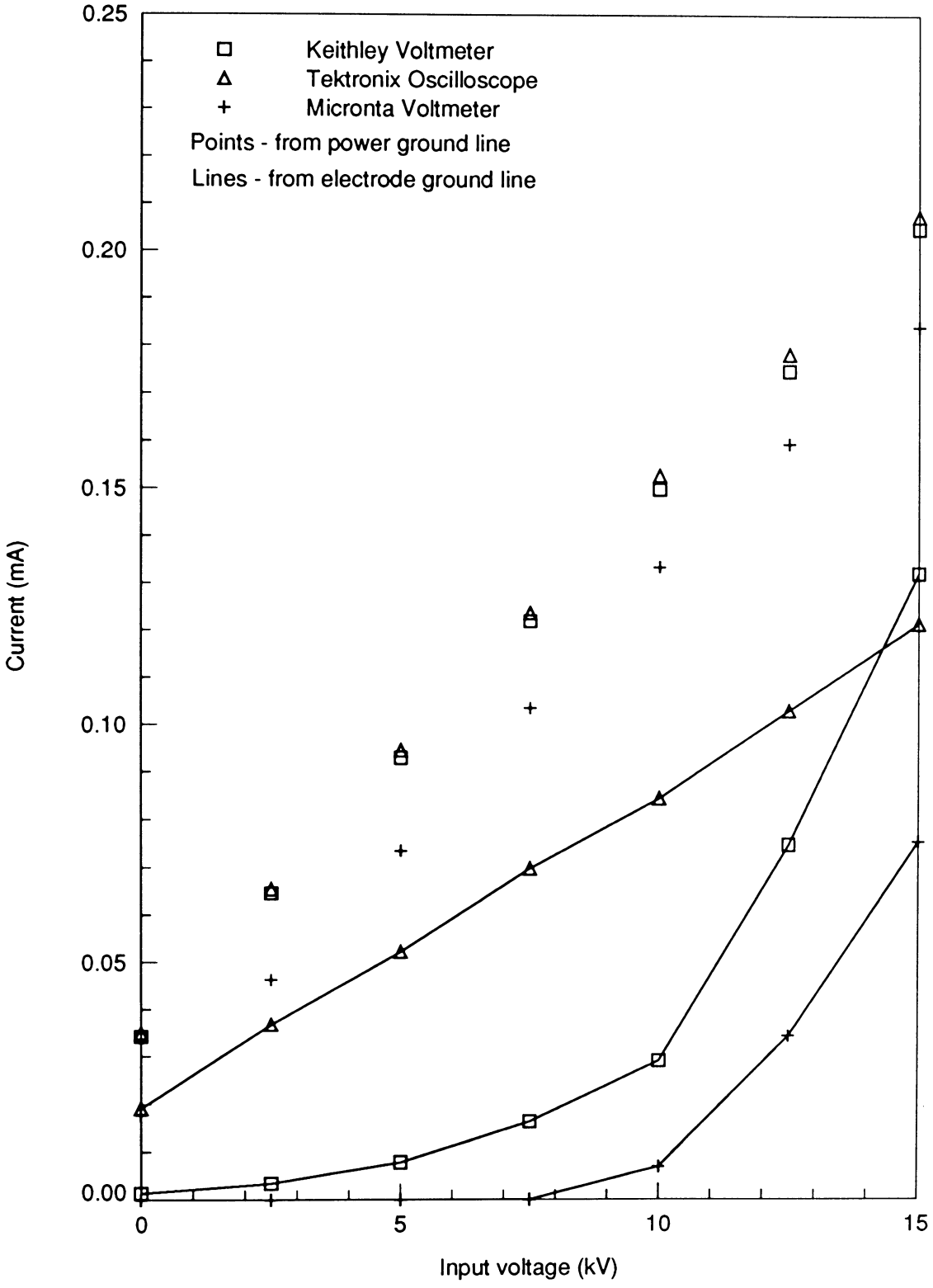

Figure C.5: Voltage vs. Current: Needle-flat plate 17 mm gap

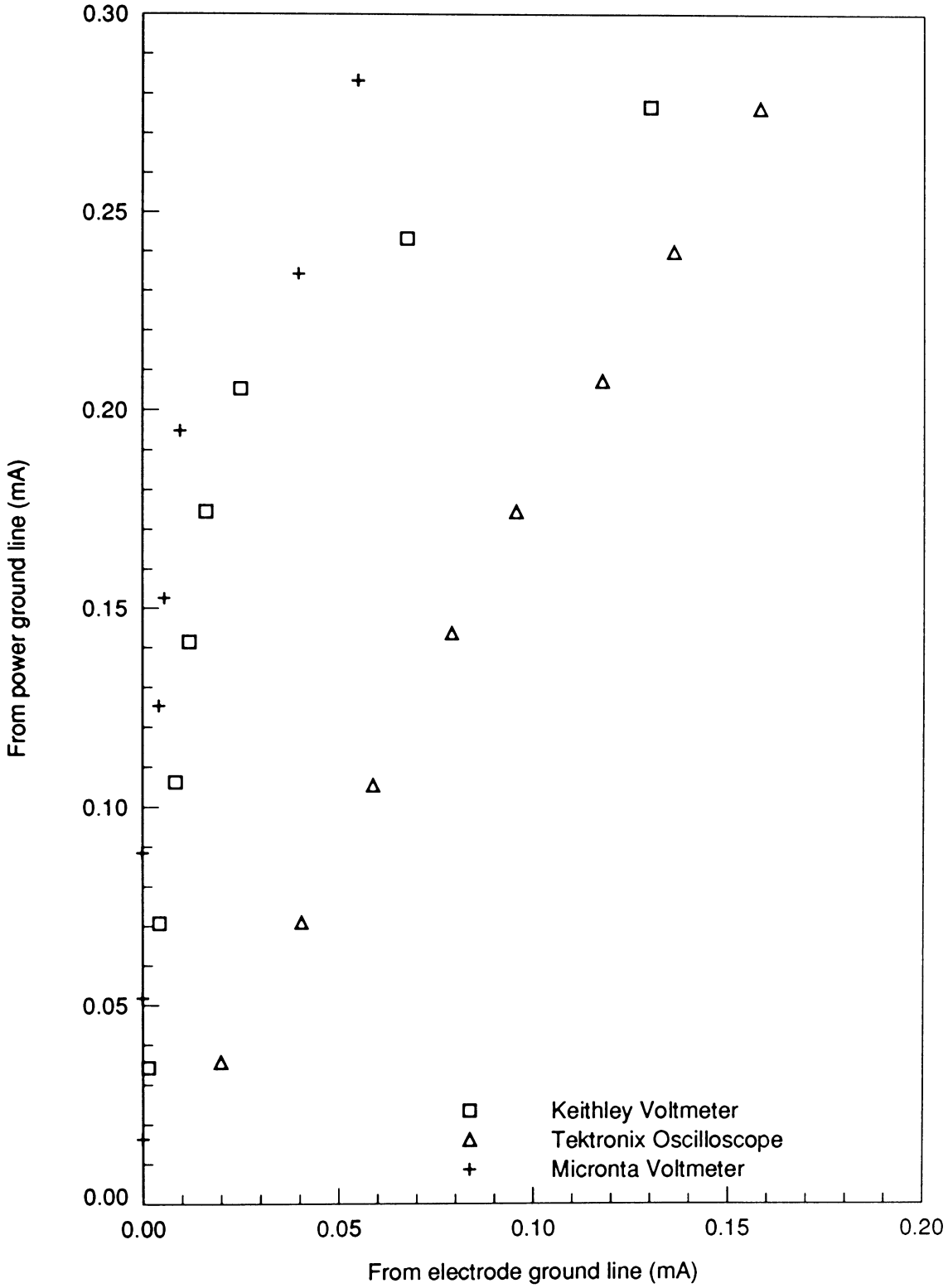

Figure C.6: Current comparison: Blades

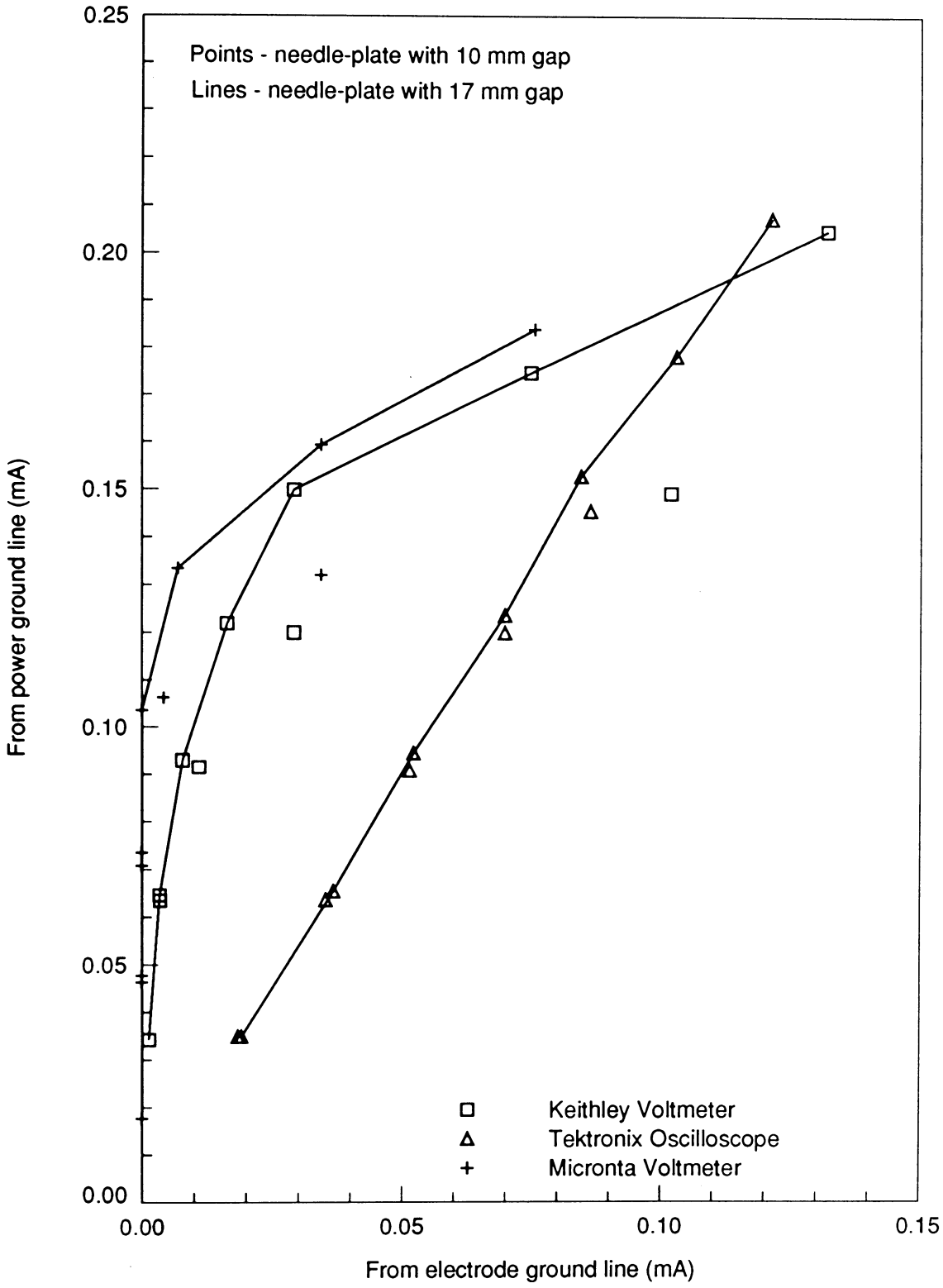

Figure C.7: Current comparison: Needle-flat plate

Ideally, slopes for these lines would be one, means there is no difference between the current measured from the power ground line and the electrode ground line. However, there is a significant difference between these two lines. This difference indicates that some of the current from the power source is discharged to the surrounding, resulting in the *partial-receiving* of the current by the *ground*-electrode. It was decided that the electrode ground line is the better line to measure current.

It can be seen from these data and plots that the *Micronta Voltmeter* was not very accurate, especially for very low voltage, where it recorded zero voltage while the other two instruments were recording relatively higher voltages. It was decided not to use this instrument on subsequent experiments. Another observation on the oscilloscope's screen showed distorted sinusoidal signals which results to some errors when converted to their corresponding *rms* values with Equation C.1. Moreover, it should be noted that the *Keithley Multimeter* is an autoranging digital measuring instrument while the scale of the oscilloscope has to be adjusted manually. A higher scale will give less accuracy. While both *Tektronix Oscilloscope* and *Keithley Multimeter* were used simultaneously throughout the experiments, it should be noted that the *Tektronix* was used mostly to gain confidence on the data as read by the *Keithley*.

APPENDIX D. INTEGRAL METHOD AND BOUNDARY LAYER GROWTH—THEORETICAL ANALYSIS

The momentum integral method was applied to boundary layer growth along a semi-infinite flat plate with an ionic wind. In this method a polynomial velocity profile is assumed that satisfies the boundary and free-stream velocity conditions and integral momentum equation [27]. With the integral method, the momentum equation is not satisfied on a point-by-point basis but on average across the thickness of boundary layer.

Electrostatic body forces resulting from the ionic wind are assumed to act only within the boundary from a discharge line electrode located along the entire leading edge of the flat plate. Convective ion current is neglected in the analysis. Reactive forces from the wind act on the plate through the line electrode. Only dc discharges (ions of one sign) are considered. The ionic wind forces can either aid or oppose the flow depending on the sign of the current, that is, whether the current is directed upstream or downstream. Ionic wind forces of sufficient strength can in fact provide net thrust to the plate, while lesser (aiding) ionic winds can be thought of as decreasing the effective drag on the plate by introducing a slip condition in the outer boundary layer. In fact the skin friction is seen to increase with a downstream directed ionic wind while the effective drag decreases due to net momentum added to the boundary

layer.

With body forces added, the integral momentum equation becomes [27]

$$\frac{d}{dx}\int_0^\delta \rho u(u-U)\,dy + \frac{dU}{dx}\int_0^\delta \rho(u-U)\,dy = \int_0^\delta (f-f')\,dy - \mu\left(\frac{\partial u}{\partial y}\right)_w \qquad \text{(D.1)}$$

where u, U, δ, μ, f, f', and x are the velocity, free stream velocity, boundary layer thickness, fluid viscosity, electrostatic body forces (per volume) within and outside the boundary layer, and distance from the leading edge respectively.

Equation D.1 includes simplifications from the continuity equation and a free stream momentum equation given by

$$\frac{\partial(\rho u)}{\partial x} + \frac{\partial(\rho v)}{\partial y} = 0 \qquad \text{(D.2)}$$

$$\rho U\frac{dU}{dx} = -\frac{\partial p}{\partial x} + f' \qquad \text{(D.3)}$$

where v and p are the y component of velocity and pressure respectively.

The current density J, ion mobility K and electrostatic body force f (per unit volume) are given by the respective equations [20],

$$\begin{aligned} J &= nqV_q \\ K &= \frac{V_q}{E} \\ f &= nqE \end{aligned} \qquad \text{(D.4)}$$

where n, q, V_q are the ion number density, charge and drift velocity, respectively and E is the local electric field strength. As noted previously, in Equation D.4 it is assumed that only ions of a single sign are present (i.e., a dc corona) and that convective ion current is negligible.

Equation D.4 leads to a body force in terms of the current density J and mobility K given by

$$f = \frac{J}{K} \tag{D.5}$$

The body force term in Equation D.1 can be evaluated in terms of the current density using Equation D.5

$$\begin{aligned} \int_0^\delta f\, dy &= \int_0^\delta \frac{J}{K}\, dy \\ \bar{f}\delta &= \frac{I'}{K} \\ \beta f_w \delta &= \frac{I'}{K} \end{aligned} \tag{D.6}$$

where I' is the ion current per unit width of the flat plate and the mean body force $\bar{f}$ over the boundary layer is assumed to be related to the charge body force at the wall f_w through a constant β, (~ 1).

The velocity profile is assumed to be a cubic equation of the form

$$u = a + by + cy^2 + dy^3 \tag{D.7}$$

with boundary conditions

$$\begin{aligned} u(0) = 0; \quad & \frac{\partial^2 u(0)}{\partial y^2} = -\frac{f_w}{\mu} \\ u(\delta) = U; \quad & \frac{\partial u(\delta)}{\partial y} = 0 \end{aligned} \tag{D.8}$$

Casting Equations D.7 and D.8 into dimensionless form, and taking $a = 0$ from the first boundary condition, gives

$$u^* = \frac{u}{U} = b\eta + c\eta^2 + d\eta^3 \tag{D.9}$$

$$u^*(1) = 1 = b + c + d \tag{D.10}$$

$$\frac{du^*(1)}{d\eta} = 0 = b + 2c + 3d \tag{D.11}$$

$$\frac{d^2u^*(0)}{d\eta^2} = 2c = -\frac{f_w\delta^2}{\mu U} = -\left[\frac{I'}{\beta K \mu U}\right]\delta = -j\delta \tag{D.12}$$

and solving for the constants a, b, c, and d from Equations D.8 gives

$$\begin{aligned} a &= 0 \\ b &= \frac{3}{2} + \frac{j\delta}{4} \\ c &= -\frac{j\delta}{2} \\ d &= -\frac{1}{2} + \frac{j\delta}{4} \end{aligned} \tag{D.13}$$

Taking the free stream body force as negligible, $f' = 0$, a constant free stream velocity, $U = constant$, and using Equations D.6, D.9 and D.13 in Equation D.1, and integrating the left hand side leads to a differential equation for the boundary layer thickness δ

$$\rho\bar{U}^2 M(\delta)\frac{d\delta}{dx} = \pm\frac{I'}{K} - \frac{b(\delta)U\mu}{\delta} \tag{D.14}$$

where

$$M(\delta) = \int_0^1 u^*(u^* - 1)\, d\eta = -\frac{39}{280} + \frac{(j\delta)}{560} + \frac{(j\delta)^2}{1680} \tag{D.15}$$

and $b(\delta)$ is given by the second of Equations D.13. Together with Equation D.12, Equation D.14 can be rewritten in the form

$$\frac{\rho\bar{U}M(\delta)}{\mu}\delta\frac{d\delta}{dx} = \pm\beta j\delta - b(\delta) \tag{D.16}$$

Equations D.14 and D.16 show that depending on the magnitude and sign of the ionic wind force term, $I'/K(= \beta j\mu U)$, the boundary layer will either grow, remain constant, or decrease along the plate ($\pm$ values of $j\delta$ emphasize this point

in Equations D.14 and D.16). When the sign of the discharge is negative ($I' < 0$, i.e., an upstream directed wind), the boundary layer will grow more rapidly than without the wind. The ionic wind force is removing momentum from the boundary layer, thus aiding viscosity. A limiting condition in boundary layer growth occurs when the left hand side of Equations D.14 or D.16 is zero. This can happen only for a positive current ($I' > 0$) giving

$$[j\delta]_{max} = \frac{\frac{3}{2}}{\beta - \frac{1}{4}} \approx 2 \tag{D.17}$$

since $\beta \approx 1$.

In the absence of an ionic wind the current I' (and j) is zero. The solution to Equation D.16 then reduces to a standard solution for boundary layer growth along a flat plate [16].

$$\frac{\delta}{x} = \frac{4.64}{\sqrt{\frac{\rho U x}{\mu}}} \tag{D.18}$$

The current-free case gives good results when predicting boundary layer drag and thickness on a flat plate with Equations D.7 and D.18 (e.g., 2.7% error for the former and 7% error for the latter when compared to the Blasius exact solution [16]).

The solution to Equation D.16 for boundary layer growth with ionic wind $j \neq 0$ and $\beta = 1$ is given by

$$x = \begin{cases} \left(\frac{\rho U}{j^2 \mu}\right) \left\{ -\frac{8j\delta}{45} + \frac{(j\delta)^2}{504} + \frac{(j\delta)^3}{3780} - \frac{16ln\left[1-\frac{j\delta}{2}\right]}{45} \right\} & j\delta < 2 \\ \left(\frac{\rho U}{j^2 \mu}\right) \left[\frac{13(j\delta)^2}{280} + \frac{19(j\delta)^3}{1260} + \frac{(j\delta)^4}{180} + \frac{(j\delta)^5}{450} + \ldots \right] & -2 \leq j\delta < 2 \end{cases} \tag{D.19}$$

with the latter reducing to Equation D.18 at zero current $j = 0$. Figure D.1 is a plot of Equation D.19. An increase in boundary layer thickness is apparent for upstream or negative ion currents ($-j$) since momentum is being removed from the boundary

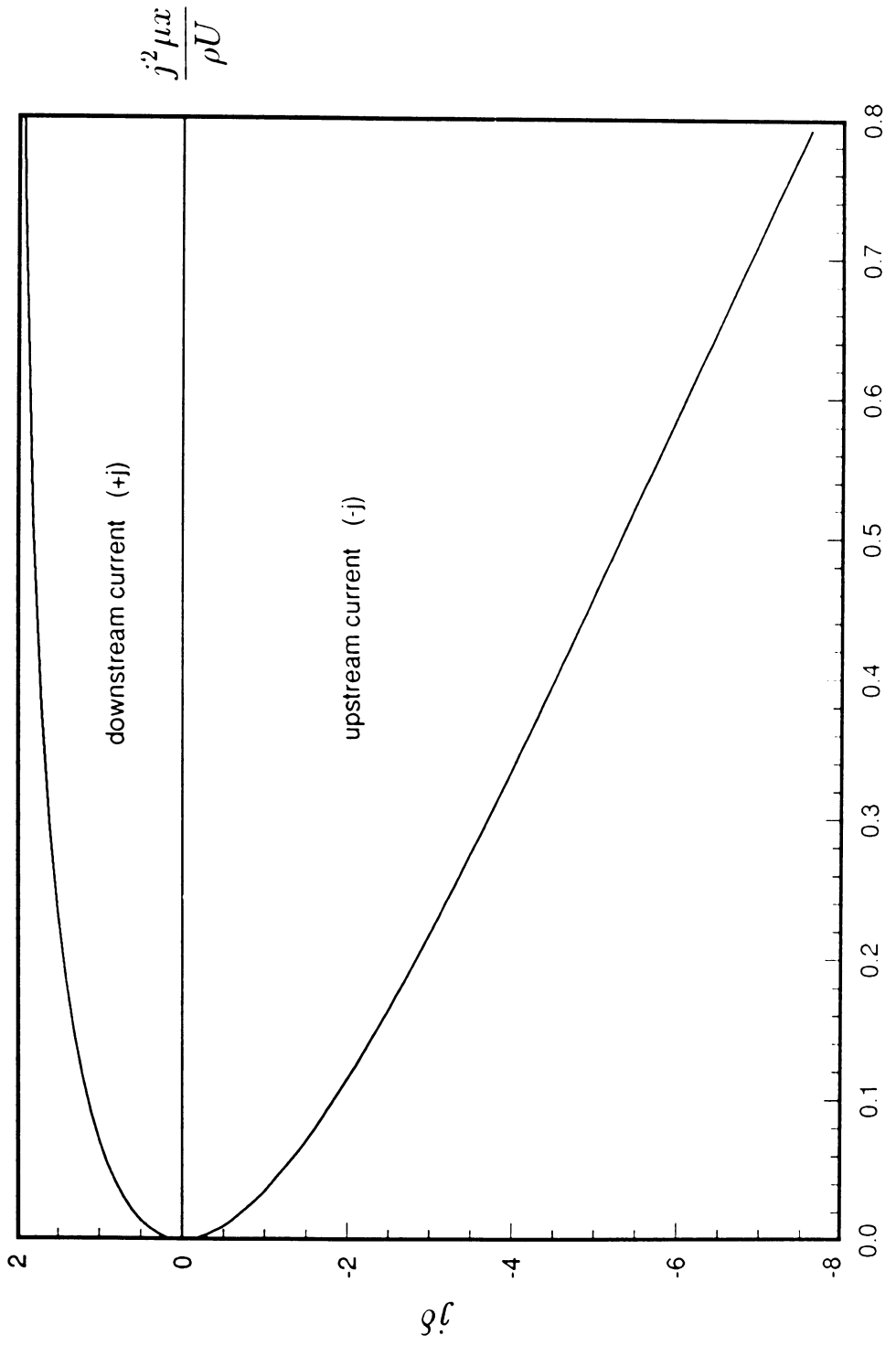

Figure D.1: Plot of Equation D.19 showing boundary layer growth along a flat plate for ion currents with downstream flow ($+j$) and upstream flow($-j$)

layer; whereas, a limiting boundary layer thickness is approached for downstream or positive ion currents ($+j$) indicating a balance has been reached between the momentum loss and gain from viscous and ionic wind effects respectively.

Figure D.2 shows dimensionless velocity profiles for various sign and current values. Inflection points in the profile are seen to occur for negative (upstream) currents from the competing effects of the external flow and the ion forces acting on the boundary layer. The influence of current magnitude is represented by increased velocities above those encountered for zero current. Note that positive values of $j\delta$ greater than 2 will cause the velocity boundary layer thickness to decrease along the plate as discussed previously (Equation D.17).

The force acting on the plate over its entire length from the ionic wind is infinite (as is the force from viscous drag). To consider only finite lengths, one can artificially introduce a second collector electrode that is placed at any distance along the plate and apply the integral momentum equation over this distance to evaluate the wind force. The ionic wind force itself is a reactive force to charges residing on both the line and (fictitious) collector electrodes. The electrodes are taken to be rigidly attached to the plate. Experimentally, the second electrode was a line electrode very similar to the one at the leading edge of the plate.

Using the model just described, the total ionic wind force - F_{ion} on the plate can be evaluated from Equations D.1 or D.5 by integrating f from the leading edge of the plate over the distance x downstream, giving

$$F_{ion,x} = -w\int_0^{\delta(x)} \rho(U^2 - u^2)\,dy + w\int_0^x \mu\left(\frac{\partial u}{\partial y}\right)_w dx = \frac{Ix}{K} \qquad \text{(D.20)}$$

where w is the width of the plate across the flow. The ionic wind force is seen to be proportional to the current and the length of separation between the electrodes, and

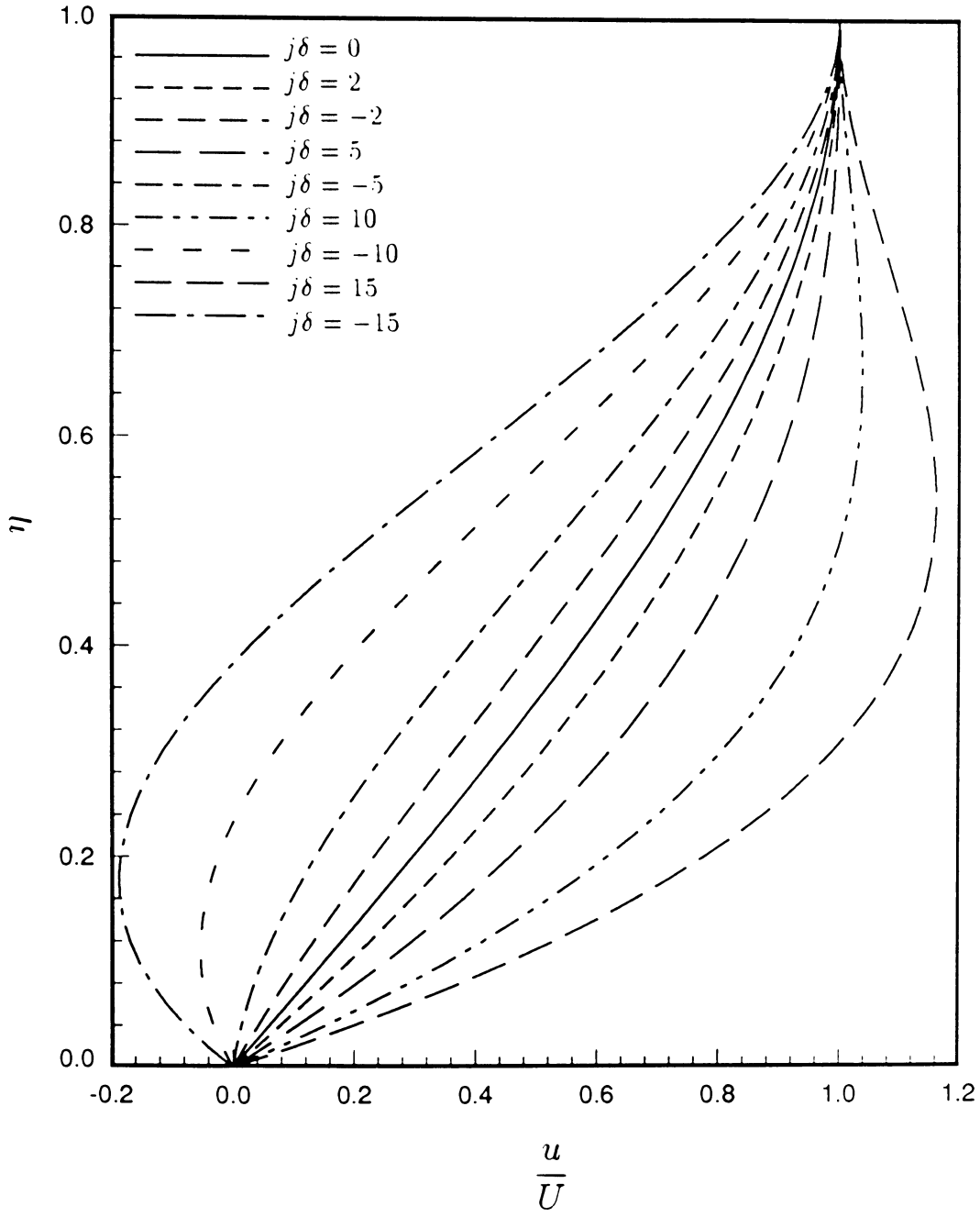

Figure D.2: Plot of Equation D.9 showing effect of current sign ($+j$ is downstream ion current and $-j$ is upstream ion current) and magnitude on velocity profile

inversely related to the ion mobility.

Numerical examples are found by taking a nominal value of the current, $I = 10^{-4}\ A$, along with $x = 2.54 \times 10^{-2}\ m, K = 2.1 \times 10^{-4}\ C.m/N.s, U = 0.67\ m/s, \mu = 1.98 \times 10^{-5} kg/m.s, \rho = 1.1774\ kg/m^3$, and $\beta = 1$. Using Equations D.12, D.17, and D.20 gives $j = 1.4 \times 10^{6}\ m^{-1}, \delta_{max} = 1.43 \times 10^{-6}\ m$, and $F_{ion} = 1.2 \times 10^{-2}\ N$ respectively.

While the ionic force F_{ion} is calculated to be too large ($\sim 10^{-2}\ N$) compared to experimental values ($\sim 10^{-4}\ N$), and the boundary layer thickness appears to be too small, this may be attributed in part to two assumptions. First, all of the current, I is not carried by the gas, and the conductivity of glass must be considered. This decreases F_{ion} in Equation D.20. Secondly, both positive and negative ions are present in the experiment due to the fact that both electrodes are emitters (being sharp razor blades). This decreases f in Equation D.4 (for a given current density J) which effectively increases the ion mobility K (Equation D.5) and decreases F_{ion} in Equation D.20. Both of the above noted effects cause decreases in F_{ion} and increases in δ.

APPENDIX E. ANALYSIS OF VARIANCE

In experiments involving several factors, it is important to determine if the independent variables have some effect on the dependent variables—in this study the independent variables are air speed and high voltage, and the dependent variables are drag force and electric current. Analysis of Variance is a powerful technique to do this task. By this method, the total variation within an experiment can be broken down into variations due to each main factor, interacting factor(s), and residual or experimental error. The significance of each variation is then tested by comparing it to an *F distribution* table value. Reference [21] has the details. This chapter gives a listing of computer program developed from the Analysis of Variance technique, together with some samples of calculation.

Computer Listing

Note: The main program and the subroutine INMAN (to input data data manually) are general purpose programs; while the subroutine INFILE (to read the input data from files) is a special purpose program developed specifically for this study.

```
C PROGRAM ANALYSIS OF VARIANCE
C
C This program constructs an ANOV table for SINGLE-, DOUBLE-, AND
```

```
C   TRIPLE-FACTOR EXPERIMENT
C   The user can provide some input through either file(s) or
C      manually. If file(s) is(are) used, subroutine INFILE has to be
C      created, with arguments (IOPT,NC,NR,NG,NP,X).
C   IOPT - The option of SINGLE-, DOUBLE- or TRIPLE-FACTOR Experiment
C   NC   - Number of column(s)
C   NR   - Number of row(s)
C   NG   - Number of group(s)
C   NP   - Number of replication(s)
C Note: For SINGLE-FACTOR, NR and NG are set = 1
C       For DOUBLE-FACTOR, NG are set = 1
C   X    - The data from the experiment.
C          In this program, the number of data is limited to
C          20x20x20x20 = 160000 or: The number of columns, rows,
C          groups and replications are limited to 20 each
C   CL   - Confidence Level
C   MT   - The F value for certain Confidence Limit and Degrees
C          of Freedom
C
      IMPLICIT REAL (A-C,E-H,M,O-Z)
      IMPLICIT INTEGER (D,I-L,N)
      CHARACTER*11 SRC
      CHARACTER*1 ANSWER
      DIMENSION X(20,20,20,20)
C
      PRINT *,'Type of experiment?'
      PRINT *,'   [1] Single-factor experiment'
      PRINT *,'   [2] Double-factor experiment'
      PRINT *,'   [3] Triple-factor experiment'
   1  READ *,IOPT
      IF (IOPT.LT.1.OR.IOPT.GT.3) THEN
        PRINT *,'Invalid option. Please re-enter:'
        GO TO 1
      ENDIF
C
C Input data
C
   2  PRINT *,'Do you want to enter the data manually? (Y/N)'
      READ (*,3) ANSWER
   3  FORMAT (A1)
```

```
      IF (ANSWER.EQ.'N'.OR.ANSWER.EQ.'n') THEN
        CALL INFILE(IOPT,NC,NR,NG,NP,X)
      ELSE
        CALL INMAN(IOPT,NC,NR,NG,NP,X)
      ENDIF
C
C Calculating the sum of individual element
C   TT   - Total of all observation
C   TC   - Total for each column
C   TR   - Total for each row
C   TG   - Total for each group
C   TCR  - Total for each column-row combination
C   TRG  - Total for each row-group combination
C   TCG  - Total for each column-group combination
C   TCRG - Total for each column-row-group combinati
C   XSQ  - Total squares of each data
C
      NT=NC*NR*NG*NP
      DO 100 I=1,NC
        DO 110 J=1,NR
          DO 120 K=1,NG
            DO 130 L=1,NP
              T1=T1+X(I,J,K,L)
              T2=T2+X(I,J,K,L)
              XSQ=XSQ+X(I,J,K,L)**2
  130       CONTINUE
            TCRG=TCRG+T2*T2
            T3=T3+T2
            T2=0.0
  120     CONTINUE
          TCR=TCR+T3*T3
          T3=0.0
  110   CONTINUE
        TC=TC+T1*T1
        TT=TT+T1
        T1=0.0
  100 CONTINUE
      IF (IOPT.EQ.1) GO TO 210
      DO 135 I=1,NR
      T1=0.0
```

```
      DO 140 J=1,NG
        DO 150 K=1,NC
          T2=0.0
          DO 160 L=1,NP
            T1=T1+X(K,I,J,L)
            T2=T2+X(K,I,J,L)
  160     CONTINUE
          T4=T4+T2
  150   CONTINUE
        TRG=TRG+T4*T4
        T4=0.0
  140 CONTINUE
      TR=TR+T1*T1
  135 CONTINUE
      IF (IOPT.EQ.2) GO TO 210
      DO 170 I=1,NG
        T1=0.0
        DO 180 J=1,NC
          DO 190 K=1,NR
            T2=0.0
            DO 200 L=1,NP
              T1=T1+X(J,K,I,L)
              T2=T2+X(J,K,I,L)
  200       CONTINUE
            T5=T5+T2
  190     CONTINUE
          TCG=TCG+T5*T5
          T5=0.0
  180   CONTINUE
        TG=TG+T1*T1
  170 CONTINUE
C
C Calculating the sum of squares, the degre
C    Square for each source of variation
C
  210 N=NP*NR*NG
      SS1=SS(TC,N,TT,NT)
      DF1=NC-1
      MS1=SS1/REAL(DF1)
      N=1
```

```
SS8=SS(XSQ,N,TT,NT)
DFT=NT-1
IF (IOPT.EQ.1) THEN
  DF8=DFT-DF1
  SSR=SS8-SS1
  GO TO 220
ENDIF
N=NP*NC*NG
SS2=SS(TR,N,TT,NT)
N=NP*NG
SS4=SS(TCR,N,TT,NT)-SS1-SS2
DF2=NR-1
DF4=DF1*DF2
MS2=SS2/REAL(DF2)
IF (IOPT.EQ.2) THEN
  MS3=SS4/REAL(DF4)
  DF8=DFT-DF4-DF2-DF1
  SSR=SS8-SS1-SS2-SS4
  GO TO 220
ENDIF
N=NP*NR*NC
SS3=SS(TG,N,TT,NT)
N=NP*NR
SS5=SS(TCG,N,TT,NT)-SS1-SS3
N=NP*NC
SS6=SS(TRG,N,TT,NT)-SS2-SS3
SS7=SS(TCRG,NP,TT,NT)-SS1-SS2-SS3
DF3=NG-1
DF5=DF1*DF3
DF6=DF2*DF3
DF7=DF4*DF3
MS3=SS3/REAL(DF3)
MS4=SS4/REAL(DF4)
MS5=SS5/REAL(DF5)
MS6=SS6/REAL(DF6)
MS7=SS7/REAL(DF7)
IF (NP.EQ.1) THEN
  DF8=DF4+DF5+DF6+DF7
  SSR=SS4+SS5+SS6+SS7
ELSE
```

```
        DF8=DFT-DF1-DF2-DF3-DF4-DF5-DF6-DF7
        SSR=SS8-SS7-SS6-SS5-SS4-SS3-SS2-SS1
      ENDIF
 220  MS8=SSR/REAL(DF8)
C
C Calculating the Mean-square Ratio, MSR
C
      MSR1=MS1/MS8
      MSR2=MS2/MS8
      MSR3=MS3/MS8
      IF (IOPT.EQ.2) GO TO 225
      MSR4=MS4/MS8
      MSR5=MS5/MS8
      MSR6=MS6/MS8
      MSR7=MS7/MS8
C
C Reading the table value as the Minimum MSR required for factor
C    to be significant
C
  225 PRINT *,'ENTER THE CONFIDENCE LEVEL (IN %)'
      READ *,CI
      CL=1.0-(CI/100.0)
      WRITE (*,230)CL,DF1,DF8
  230 FORMAT (' ENTER THE VALUE OF F(',F5.3,',',I2,',',I2,')')
      READ (*,240)MT1
  240 FORMAT (F8.4)
      IF (IOPT.EQ.1) GO TO 300
      WRITE (*,230)CL,DF2,DF8
      READ (*,240)MT2
      IF (IOPT.EQ.2) THEN
        WRITE (*,230)CL,DF4,DF8
        READ (*,240)MT3
        GO TO 300
      ENDIF
      WRITE (*,230)CL,DF3,DF8
      READ (*,240)MT3
      WRITE (*,230)CL,DF4,DF8
      READ (*,240)MT4
      WRITE (*,230)CL,DF5,DF8
      READ (*,240)MT5
```

```
      WRITE (*,230)CL,DF6,DF8
      READ (*,240)MT6
      WRITE (*,230)CL,DF7,DF8
      READ (*,240)MT7
C
C Constructing the ANOV table
C
  300 WRITE (*,310)
  310 FORMAT (/,1X,'Source of Sum of     Degrees of Mean Square',1X,
     +   'Mean-Square Minimum MSR')
      WRITE (*,320)
  320 FORMAT (1X,'Variation Squares,SS Freedom,DF MS (SS/DF)',2X,
     +   'Ratio,MSR   Required (Table)',/)
      WRITE (*,330)SS1,DF1,MS1,MSR1,MT1
  330 FORMAT (' COLUMNS   ',F10.5,5X,I2,5X,F11.6,1X,F11.6,5X,F8.4)
      IF (IOPT.EQ.1) GO TO 400
      WRITE (*,340)SS2,DF2,MS2,MSR2,MT2
  340 FORMAT (' ROWS      ',F10.5,5X,I2,5X,F11.6,1X,F11.6,5X,F8.4)
      IF (IOPT.EQ.2) THEN
        WRITE (*,350)SS4,DF4,MS3,MSR3,MT3
  350   FORMAT (' COL-ROW   ',F10.5,5X,I2,5X,F11.6,1X,F11.6,5X,F8.4)
        GO TO 400
      ENDIF
      WRITE (*,360)SS3,DF3,MS3,MSR3,MT3
  360 FORMAT (' GROUPS    ',F10.5,5X,I2,5X,F11.6,1X,F11.6,5X,F8.4)
      WRITE (*,361)SS4,DF4,MS4,MSR4,MT4
  361 FORMAT (' COL.-ROW  ',F10.5,5X,I2,5X,F11.6,1X,F11.6,5X,F8.4)
      WRITE (*,362)SS5,DF5,MS5,MSR5,MT5
  362 FORMAT (' COL.-GROUP',F10.5,5X,I2,5X,F11.6,1X,F11.6,5X,F8.4)
      WRITE (*,363)SS6,DF6,MS6,MSR6,MT6
  363 FORMAT (' ROW-GROUP ',F10.5,5X,I2,5X,F11.6,1X,F11.6,5X,F8.4)
      WRITE (*,364)SS7,DF7,MS7,MSR7,MT7
  364 FORMAT (' COL-ROW-GR',F10.5,5X,I2,5X,F11.6,1X,F11.6,5X,F8.4)
  400 WRITE (*,370)SSR,DF8,MS8
  370 FORMAT (' RESIDUAL  ',F10.5,5X,I2,5X,F11.6)
      WRITE (*,380)SS8,DFT
  380 FORMAT (' TOTAL     ',F10.5,5X,I2,//)
C
C The significance of each factor compared with the table value
C
```

```
      SRC='COLUMN'
      IF (MSR1.GT.MT1) THEN
        WRITE (*,410)SRC
410     FORMAT (' The ',A11,' significantly affects the experiment')
      ELSE
        WRITE (*,420)SRC
420     FORMAT (' There is no significant effect of the ',A11)
      ENDIF
      IF (IOPT.EQ.1) GO TO 999
      SRC='ROW'
      IF (MSR2.GT.MT2) THEN
        WRITE (*,410)SRC
      ELSE
        WRITE (*,420)SRC
      ENDIF
      IF (IOPT.EQ.2) THEN
        SRC='INTERACTION'
      ELSE
        SRC='GROUP'
      ENDIF
      IF (MSR3.GT.MT3) THEN
        WRITE (*,410)SRC
      ELSE
        WRITE (*,420)SRC
      ENDIF
      IF (IOPT.EQ.2) GO TO 999
      SRC='COLUMN-ROW'
      IF (MSR4.GT.MT4) THEN
        WRITE (*,410)SRC
      ELSE
        WRITE (*,420)SRC
      ENDIF
      SRC='COL-GROUP '
      IF (MSR5.GT.MT5) THEN
        WRITE (*,410)SRC
      ELSE
        WRITE (*,420)SRC
      ENDIF
      SRC='ROW-GROUP'
      IF (MSR6.GT.MT6) THEN
```

```
        WRITE (*,410)SRC
      ELSE
        WRITE (*,420)SRC
      ENDIF
      SRC='COL-ROW-GRP'
      IF (MSR7.GT.MT7) THEN
        WRITE (*,410)SRC
      ELSE
        WRITE (*,420)SRC
      ENDIF
  999 END
C
      FUNCTION SS(TSQ,N,T,NT)
C Calculates various sum of squares
      INTEGER N,NT
      REAL TSQ,T,SS
      SS=TSQ/REAL(N)-T*T/REAL(NT)
      RETURN
      END
C
      SUBROUTINE INMAN(IOPT,NC,NR,NG,NP,X)
C
C This subroutine is used only if the user want to input the data
C   manually. The maximum numbers of data is 20x20x20x20=160000.
C
      IMPLICIT REAL (A-C,E-H,M,O-Z)
      IMPLICIT INTEGER (D,I-L,N)
      DIMENSION X(20,20,20,20)
C
      PRINT *,'ENTER THE NUMBER OF COLUMN(S) [INTEGER] :'
      READ (*,10)NC
      IF (IOPT.EQ.1) THEN
        NR=1
        NG=1
        GO TO 4
      ENDIF
      PRINT *,'ENTER THE NUMBER OF ROW(S) [INTEGER] :'
      READ (*,10)NR
      IF (IOPT.EQ.2) THEN
        NG=1
```

```
        GO TO 4
      ENDIF
      PRINT *,'ENTER THE NUMBER OF GROUP(S) [INTEGER] :'
      READ (*,10)NG
    4 PRINT *,'ENTER THE NUMBER OF REPLICATIONS [INTEGER] :'
      READ (*,10)NP
   10 FORMAT (I2)
C
C Reading the data
C
      PRINT *,'ENTER THE VALUE(S): '
      DO 100 I=1,NC
        DO 110 J=1,NR
          DO 120 K=1,NG
            DO 130 L=1,NP
              GOTO (5,6,7)IOPT
    5         WRITE (*,20)I,L
   20         FORMAT (' COLUMN ',I2,' REPLICATION ',I2)
              GOTO 50
    6         WRITE (*,30)I,J,L
   30         FORMAT (' COLUMN ',I2,' ROW ',I2,' REPLICATION ',I2)
              GOTO 50
    7         WRITE (*,40)I,J,K,L
   40         FORMAT (' COLUMN ',I2,' ROW ',I2,
     +           ' GROUP ',I2,' REPLICATION ',I2)
   50         READ *,X(I,J,K,L)
  130       CONTINUE
  120     CONTINUE
  110   CONTINUE
  100 CONTINUE
      RETURN
      END
C
      SUBROUTINE INFILE(IOPT,NC,NR,NG,NP,X)
C
C This subroutine is used if the user want to input the data from
C   file(s). The maximum numbers of data is 20x20x20x20=160000.
C   Used specifically to process 'Plate drag with high voltage
C   discharge' experiment
C
```

```
      REAL W,V(6),C(6),X(20,20,20,20)
      INTEGER I,J,NC,NR,NG,NP,NTYPE,IENT
      CHARACTER*10 FINPUT,FIN1,FIN2,FIN3,FIN4,FIN5,FIN6,FIN7,
     +   FIN8,FIN9,FIN10,FIN11,FIN12,FIN13,FIN14
      CHARACTER*3 FTYPE
      CHARACTER*1 FIND
1     FORMAT (A10)
      IF (IOPT.EQ.3) THEN
        PRINT *,'This program does not support TRIPLE-FACTOR'
        PRINT *,'with file(s) as input'
        GOTO 999
      ELSE IF (IOPT.EQ.1) THEN
        PRINT *,'Which file to process? (XXXNN)'
        READ (*,1) FINPUT
        FINPUT=FINPUT(:5)//'.RAW'
        OPEN (10,FILE=FINPUT,STATUS='OLD')
        FTYPE=FINPUT(:3)
        FIND=FINPUT(3:3)
        NR=1
        GOTO 10
      ELSE
        PRINT *,'Which files to process?'
        PRINT *,'  [1] AC - Normal orientation, const. speed'
        PRINT *,'  [2] AC - Reversed orientation, const. speed'
        PRINT *,'  [3] DC - Negative ground, const. speed'
        PRINT *,'  [4] DC - Positive ground, const. speed'
        PRINT *,'  [5] AC - Normal orientation, const. voltage'
        PRINT *,'  [6] AC - Reversed orientation, const. voltage'
        PRINT *,'  [7] DC - Negative ground, const. voltage'
        PRINT *,'  [8] DC - Positive ground, const. voltage'
2       READ *,NTYPE
        IF (NTYPE.EQ.1) THEN
          FTYPE='ACN'
        ELSE IF (NTYPE.EQ.2) THEN
          FTYPE='ACR'
        ELSE IF (NTYPE.EQ.3) THEN
          FTYPE='DNG'
        ELSE IF (NTYPE.EQ.4) THEN
           FTYPE='DPG'
        ELSE IF (NTYPE.EQ.5) THEN
```

```
   FTYPE='ANS'
ELSE IF (NTYPE.EQ.6) THEN
   FTYPE='ARS'
ELSE IF (NTYPE.EQ.7) THEN
   FTYPE='DNS'
ELSE IF (NTYPE.EQ.8) THEN
   FTYPE='DPS'
ELSE
   PRINT *,'Unrecognized answer. Ple
   GOTO 2
ENDIF
IF (NTYPE.GE.5.OR.NTYPE.LE.8) THEN
  FIND='S'
ELSE
  FIND='G'
ENDIF
FIN1=FTYPE//'00.RAW'
FIN2=FTYPE//'02.RAW'
FIN3=FTYPE//'04.RAW'
FIN4=FTYPE//'06.RAW'
FIN5=FTYPE//'08.RAW'
FIN6=FTYPE//'10.RAW'
FIN7=FTYPE//'12.RAW'
FIN8=FTYPE//'14.RAW'
FIN9=FTYPE//'16.RAW'
FIN10=FTYPE//'18.RAW'
OPEN (10,FILE=FIN1,STATUS='OLD')
OPEN (11,FILE=FIN2,STATUS='OLD')
OPEN (12,FILE=FIN3,STATUS='OLD')
OPEN (13,FILE=FIN4,STATUS='OLD')
OPEN (14,FILE=FIN5,STATUS='OLD')
OPEN (15,FILE=FIN6,STATUS='OLD')
OPEN (16,FILE=FIN7,STATUS='OLD')
OPEN (17,FILE=FIN8,STATUS='OLD')
OPEN (18,FILE=FIN9,STATUS='OLD')
OPEN (19,FILE=FIN10,STATUS='OLD')
IF (FTYPE.EQ.'ARS') THEN
  NR=10
  GO TO 9
ENDIF
```

```
        FIN11=FTYPE//'20.RAW'
        OPEN (20,FILE=FIN11,STATUS='OLD')
        NR=11
        IF (FTYPE.EQ.'DPS'.OR.FTYPE.EQ.'DNS') THEN
          FIN12=FTYPE//'22.RAW'
          OPEN (21,FILE=FIN12,STATUS='OLD')
          IF (FTYPE.EQ.'DNS') THEN
            NR=12
            GO TO 9
          ENDIF
          NR=14
          FIN13=FTYPE//'24.RAW'
          FIN14=FTYPE//'26.RAW'
          OPEN (22,FILE=FIN13,STATUS='OLD')
          OPEN (23,FILE=FIN14,STATUS='OLD')
        ENDIF
    9 ENDIF
   10 PRINT *,'Which entity to process?'
      PRINT *,'  [1] Strain (Voltage readings)'
      PRINT *,'  [2] Current (Voltage readings)'
      READ *,IENT
   11 IF (IENT.LT.1.OR.LT.GT.2) THEN
        PRINT *,'Invalid answer. Please re-enter:'
        GO TO 11
      ENDIF
      NC=NDATA(FTYPE)
      NG=1
      NP=6
      M=9
C
C Read file(s)
C
      DO 50 J=1,NR
        M=M+1
        DO 40 I=1,NC
          DO 30 K=1,NG
            IF (FIND.EQ.'S'.OR.FIND.EQ.'s') THEN
              READ (M,14) W,(V(L),L=1,6),(C(L),L=1,6)
   14         FORMAT (1X,F5.3,6(1X,F5.1),6(1X,F5.3))
            ELSE
```

```
              READ (M,15) W,(V(L),L=1,6),(C(L),L=1,6)
   15         FORMAT (F4.1,6(1X,F5.1),6(1X,F5.3))
            ENDIF
            DO 20 L=1,6
              IF (IENT.EQ.1) THEN
                X(I,J,K,L)=V(L)
              ELSE
                X(I,J,K,L)=C(L)
              ENDIF
   20       CONTINUE
   30     CONTINUE
   40   CONTINUE
   50 CONTINUE
  999 RETURN
      END
C
      INTEGER FUNCTION NDATA(FTYPE)
C To obtain numbers of data for individual experiment
      CHARACTER*3 FTYPE
      IF (FTYPE.EQ.'ACR'.OR.FTYPE.EQ.'acr') THEN
        NDATA=10
      ELSEIF (FTYPE.EQ.'DNG'.OR.FTYPE.EQ.'dng') THEN
        NDATA=12
      ELSEIF (FTYPE.EQ.'DPG'.OR.FTYPE.EQ.'dpg') THEN
        NDATA=14
      ELSE
        NDATA=11
      ENDIF
      RETURN
      END
```

Sample Calculation

Single-factor experiment

File of AC Source—normal orientation, at voltage = 0 will be used as an example.

Table E.1: Single-factor experiment: AC Source—normal orientation: no corona

Column Air speed (torr)	Replications Strain (voltage reading) mV	mV	mV	mV	mV	mV	Total of each column
0.000	0.0	0.0	0.0	0.0	0.0	0.0	0.0
0.002	3.0	3.0	2.8	2.8	2.8	2.9	17.0
0.004	5.4	5.4	5.3	5.3	5.4	5.4	32.2
0.006	7.6	7.7	7.7	7.7	7.6	7.6	45.9
0.008	9.5	9.5	9.6	9.6	9.5	9.6	57.3
0.010	11.5	11.5	11.5	11.5	11.5	11.5	69.0
0.012	12.7	12.7	12.7	12.7	12.7	12.8	76.3
0.014	14.7	14.7	14.7	14.7	14.8	14.8	88.4
0.016	16.5	16.5	16.5	16.6	16.6	16.6	99.3
0.018	18.7	18.7	18.7	18.7	18.7	18.7	112.2
0.020	20.5	20.5	20.5	20.5	20.5	20.5	123.0

NC = number of columns (air-speeds) = 11

N = total number of observations = 66

NP = number of replications = 6

$TT = \Sigma x$, where x is the value of each observation, in this case Strain (voltage reading) = 720.9

Σx^2 = summation of squares of all observations = 10450.43

T_C = total of each column

Sums of squares for the sources of variations and the degrees of freedom are computed as follows:

1. Among columns (air-speed):

$$SS_C = \frac{\Sigma T_C^2}{NP} - \frac{TT^2}{N} = \frac{62701.81}{6} - \frac{720.9^2}{66} = 2576.108$$

$$DF_c = NC - 1 = 10$$

2. Total (total variance in the set of observations):

$$SS_{total} = \Sigma x^2 - \frac{TT^2}{N} = 10450.43 - \frac{720.9^2}{66} = 2576.236$$

$$DF_t = N - 1 = 65$$

3. Residual (measure of experimental error or test repeatability):

$$SS_{res} = SS_{total} - SS_c = 2576.236 - 2576.108 = 0.128$$

$$DF_{res} = DF_t - DF_c = 55$$

As shown in Table E.2, the mean-square ratio experimentally determined is much greater than the F ratio for 99.9% confidence, with 10 and 55 degrees of freedom ($F_{0.001;10;55}$). Therefore, it can be concluded with 99.9 % confidence that the air speed significantly affect the drag force.

Table E.2: Analysis-of-variance table for single-factor experiment

Source of variation	Sum of squares SS	Degrees of freedom DF	Mean-square (SS/DF) MS	Mean-square ratio, MSR MS/MS_{res}	Min. MSR required (from table)[a]
Columns	2576.108	10	257.611	110752.961	3.605
Residual	0.128	55	0.002		
Total	2576.236	65			

[a]See Reference [21], Table A-9

Double-factor experiment

The files for the AC source with normal orientation will be used as an example; however, the data will not be presented here, since it consists of 11 files, with each file the size of that of the single-factor experiment. Once again, the air-speeds were taken as the *column*-variation, and the voltages as the *row*-variation.

NR = number of rows = 11

NC = number of columns = 11

NP = number of replications = 6

N = total number of observations = 726

$TT = \Sigma x$, where x is the value of each observation, in this case

voltage reading of strain = -1222.300

$\Sigma {T_c}^2 = 899555.0$

$\Sigma {T_r}^2 = 4619810.0$

$\Sigma {T_{cr}}^2 = 517586.7$

$\Sigma x^2 = 86477.46$

Sums of squares for the sources of variation and degrees of freedom are computed as follows:

1. Among columns (air-speed):

$$SS_c = \frac{\Sigma {T_c}^2}{NP \times NR} - \frac{TT^2}{N} = 11571.746$$

$$DF_c = NC - 1 = 10$$

2. Among rows (high voltage):

$$SS_r = \frac{\Sigma {T_r}^2}{NP \times NC} - \frac{TT^2}{N} = 67939.250$$

$$DF_r = NR - 1 = 10$$

3. Column-row interaction:

$$SS_{cr} = \frac{\Sigma {T_{cr}}^2}{NP} - \frac{TT^2}{N} - SS_c - SS_r = 4695.586$$

$$DF_{cr} = (NR - 1) \times (NC' - 1) = 100$$

4. Total (total variance in the set of observations):

$$SS_{total} = \Sigma {x}^2 - \frac{TT^2}{N} = 84419.586$$

$$DF_t = N - 1 = 725$$

5. Residual:

$$SS_{res} = SS_{total} - SS_c - SS_r - SS_{cr} = 213.008$$

$$DF_{res} = DF_t - (DF_c + DF_r + DF_{cr}) = 605$$

Since all three MSR value for the column, row and interaction are greater than their corresponding table value, it can be concluded with 99.9 % confidence that

Table E.3: Analysis-of-variance table for double-factor experiment

Source of variation	Sum of squares SS	Degrees of freedom DF	Mean square (SS/DF) MS	Mean-square ratio, MSR MS/MS_{res}	Min. MSR required (from table)[a]
Columns	11571.746	10	1157.175	3286.690	2.96
Rows	67939.250	10	6793.925	19296.590	2.96
Column-row Interaction	4695.586	100	46.956	133.367	1.49
Residual	213.008	605	0.352		
Total	84419.586	725			

[a]See Reference [21], Table A-9

the air speed, voltage and interaction between air speed and voltage are significantly affect the experiment.

APPENDIX F. SUPPLEMENTAL COMPUTER PROGRAMS

Several computer programs have been developed to aid computational works and data processing. Listed below are some examples:

Theoretical Drag Coefficient Calculation. To create standard drag curves for a finite flat plate (Chapter 3).

```
      PROGRAM DRAG
C To calculate drag coefficient based on two theoretical solutions
C Imports:
C   Subroutine VELO
C   Function CDTOT
C Variables:
C   PRESS    = air velocity (pressure reading) (torr)
C   VEL      = air velocity (m/sec)
C   RE       = Reynolds number base on length of plate
C   CD(1-4)  = skin-friction drag coefficient
C   CDT(1-4) = drag coefficient total (skin-friction and pressure)
C
      REAL PRESS,VEL,Q,RE,CD1,CD2,CD3,CD4,CDT1,CDT2,CDT3,CDT4
      INTEGER I

C File 'DRAG1.OUT' is Re vs. Cd  based on skin-friction only
C File 'DRAG2.OUT' is Re vs. Cd  total (with pressure drag)
      OPEN (11,FILE='DRAG1.OUT',STATUS='NEW')
      OPEN (12,FILE='DRAG2.OUT',STATUS='NEW')
```

```
      DO 20 I=1,10
        PRESS = REAL(I)*2.0E-03
        CALL VELO(PRESS,VEL,RE,QA)

C Skin-friction drag coefficients:
C Blasius solution
        CD1 = 1.328/SQRT(RE)
C Semi-infinite plate (Imai)
        CD2 = CD1 + 2.326/RE
C Finite flat plate (from Van Dyke)
        CD3 = CD1 + 5.3/RE
C Triple-deck theory
        CD4 = CD1 + 2.661/(RE**(7.0/8.0))

C Total drag coefficient - friction and form drag
        CDT1 = CDTOT(CD1)
        CDT2 = CDTOT(CD2)
        CDT3 = CDTOT(CD3)
        CDT4 = CDTOT(CD4)

C Output - Theoretical drag coefficient
        WRITE (11,11) RE,CD1,CD2,CD3,CD4
        WRITE (12,11) RE,CDT1,CDT2,CDT3,CDT4
  11    FORMAT (1X,5(E10.4,1X))
  20  CONTINUE
      END
```

Experimental Drag Coefficient Calculation. To calculate drag force and dra coefficient from experimental data.

```
      PROGRAM DRAG
C To calculate drag coefficient based on experimental data
C Imports:
```

```
C    Subroutine VELO
C    Function FORCE1
C    Function FORCE2
C    Function WIRE1
C    Function WIRE2
C    Function CUR
C Variables:
C    PRESS = Velocity (pressure reading) (torr)
C    X     = Strain (voltage reading) (mV)
C    C     = Current (voltage reading) (mV)
C    VEL   = Velocity (m/s)
C    QA    = Dynamic pressure x area
C    RE    = Reynolds number
C    FW    = Wire drag
C    FREF  = Reference force (at no air speed)
C    FABS  = Absolute force
C    FP    = Drag force on the plate
C    CD    = Drag coefficient
C
      REAL PRESS,VEL,X(3),C(3),P0,X0(3),C0(3),FABS,RE,
     +  FW1,FW2,FWT,FREV,FP,CD,CURRENT,FACTOR
      INTEGER I,J
      CHARACTER*10 FIN,FOUT
      CHARACTER*3 TYPE
      CHARACTER*1 ANSWER
      COMMON FACTOR

C Input File, from experimental data
   1  PRINT *,'ENTER THE INPUT FILE NAME (no specifier)
      READ (*,2)FIN
   2  FORMAT (A8)
      TYPE=FIN(:3)
      IF (TYPE.EQ.'ACN'.OR.TYPE.EQ.'acn') THEN
        FACTOR=1.0
      ELSE IF (TYPE.EQ.'ACR'.OR.TYPE.EQ.'acr') THEN
        FACTOR=-1.0
      ELSE IF (TYPE.EQ.'DNG'.OR.TYPE.EQ.'dng') THEN
        FACTOR=1.0
      ELSE
        FACTOR=1.0
```

```
      ENDIF
      FIN=FIN(:6)//'.DAT'
      OPEN (10,FILE=FIN,STATUS='OLD')

C Output File, calculated drag data
      FOUT=FIN(:5)//'D.DAT'
      OPEN (13,FILE=FOUT,STATUS='NEW')

C Read first data (no air flow) as a reference
      READ (10,10) P0,(X0(J),J=1,3),(C0(J),J=1,3)
  10  FORMAT (1X,E9.2,3(1X,F7.3),3(1X,F5.3))
      FREF=FORCE2(X0(1))
      DO 20 I=2,11
        READ (10,10) PRESS,(X(J),J=1,3),(C(J),J=1,3)

C Wire drag
        FW1 = WIRE1(PRESS)*FACTOR
        FW2 = WIRE2(PRESS)*FACTOR
        FWT = FORCE1(FW1)+FORCE1(FW2)
C Drag Force on the plate
        FABS = FORCE2(X(1))-FWT
        FP = FABS-FREF
C Subroutine VEL0
        CALL VEL0(PRESS,VEL,RE,QA)
        CD = FP/QA
CURRENT = CUR(C(1))

C Output - Experimental plate drag
        WRITE (13,13) VEL,RE,FP,CD,FABS,CURRENT
  13    FORMAT (1X,F6.4,5(1X,E10.4))

  20  CONTINUE
      PRINT *,'Do you want to process another file? (Y
      READ (*,22)ANSWER
  22  FORMAT (A1)
      IF (ANSWER.EQ.'Y'.OR.ANSWER.EQ.'y') GOTO 1
      END
```

Subroutine and Functions.

```
      SUBROUTINE VELO(PR,VEL,RE,QA)

C This subroutine calculates velocity, Reynolds number, and dynamic
C pressure to be used in drag coefficient computation
      REAL RHO,MU,L,B,D,AF,AP,Q,QA,RE,PR,VEL
      COMMON /AREA/ AF,AP
C Variables:
C   PR    = air velocity (pressure reading) (torr) as the input
C   RHO   = air density (kg/m3)
C   MU    = dynamic viscosity (Ns/m2)
C   L,B,D = plate's dimension (length, width, height)
C   AF    = area subjected to skin-friction
C   AP    = area subjected to pressure drag
C   VEL   = air velocity (m/sec)
C   Q     = dynamic pressure (N/m2)
C   QA    = dynamic pressure x area
C   RE    = Reynolds number base on length of plate
C
C Constants
      RHO = 1.225
      MU = 1.79E-05
      L = 25.0E-03
      B = 75.0E-03
      D = 1.0E-03
      AF= 2.0*B*L
      AP= B*D

C Velocity is calculated using Bernoulli equation on the pitot-static
C tube, with conversion from torr to Pa.
      VEL = SQRT(2.0*PR*1.33322E+02/RHO)

C Reynolds Number
      RE = RHO*VEL*L/MU

C Dynamic pressure
```

```
      Q = 0.5*RHO*(VEL**2)
      QA = Q*(AF+AP)
      RETURN
      END

      FUNCTION CDTOT(X)
C Theoretical drag, total
      REAL X,AF,AP
      COMMON /AREA/ AF,AP
      CDTOT = (X*AF+1.9*AP)/(AF+AP)
      RETURN
      END

      FUNCTION CUR(C)
C This function calculates Current from experimental voltage
C    reading data
      REAL C,R
C Resistance (k-Ohm)
      R = 9.77875
      CUR=C/R
      RETURN
      END

      FUNCTION FORCE1(X)
C Converts voltage reading to force from Appendix A,
C calibration on tip of one wire.
      REAL X
      COMMON FACTOR
      IF (X.GE.0.0) THEN
        FORCE1 = 6.6313E-06*X-5.0823E-06
      ELSE
        X = X*(-1.0)
        FORCE1 = (4.7252E-06*X-4.7348E-06)*(-1.0)*FACTOR
      ENDIF
      RETURN
      END

      FUNCTION FORCE2(X)
C Function FORCE2 - converts voltage reading to force
C from Appendix A, calibration on tip of two wires.
```

```
      REAL X
      COMMON FACTOR
      IF (X.GE.0.0) THEN
        FORCE2 = 2.6743E-05*X-3.6444E-07
      ELSE
        X = X*(-1.0)
        FORCE2 = (1.9226E-05*X+8.6235E-07)*(-1.0)*FACTOR
      ENDIF
      RETURN
      END

      FUNCTION WIRE1(X)
C Function WIRE1 - calculate voltage reading to wire drag force
C (w/o wake effect) based on a 2-degree polynomial curve fit
      REAL X
      WIRE1 = -1.5786E+03*X**2+7.5410E+02*X+2.2247
      RETURN
      END

C Function WIRE2 - calculate voltage reading to wire drag force
C (w/ wake effect) based on a 2-degree polynomial curve fit
      FUNCTION WIRE2(X)
      REAL X
      WIRE2 = 1.8847E+02*X**2+7.2907E+02*X+1.1611
      RETURN
      END
```

Sample data.

The experiment was done by holding the air speed constant, while varying the high voltage discharge. Therefore, the results were a set of *Voltage vs. Strain and Current* tables for different air-speeds. An example of this type of table is shown in Table F.1. Later on these tables were altered to produce a set of *Air speed vs. Strain and Current* tables for different voltages. An example is shown in Table F.2. Another computer program was developed for this purpose. Listed below is an example of

such program, used specifically to alter a set of data taken from AC Source—normal orientation.

```
      PROGRAM ALTER
C This program alters set of files of Voltage VS Strain to
C Air speed VS Strain
      REAL VOLT(0:13),SPEED(0:10),X(0:10,0:13,6),C(0:10,0:13,6)
      INTEGER I,J,K,M,N
C Files ACN##.RAW are the files of Voltage VS Millivolt reading
C for certain AIR SPEED
C Example: 'ACN02.RAW' is for Air Speed of 2.0E-3 torr
      OPEN (7,FILE='ACN00.RAW',STATUS='OLD')
      OPEN (8,FILE='ACN02.RAW',STATUS='OLD')
      OPEN (9,FILE='ACN04.RAW',STATUS='OLD')
      OPEN (10,FILE='ACN06.RAW',STATUS='OLD')
      OPEN (11,FILE='ACN08.RAW',STATUS='OLD')
      OPEN (12,FILE='ACN10.RAW',STATUS='OLD')
      OPEN (13,FILE='ACN12.RAW',STATUS='OLD')
      OPEN (14,FILE='ACN14.RAW',STATUS='OLD')
      OPEN (15,FILE='ACN16.RAW',STATUS='OLD')
      OPEN (16,FILE='ACN18.RAW',STATUS='OLD')
      OPEN (17,FILE='ACN20.RAW',STATUS='OLD')
C Files ANS##.RAW are the files of Air Speed (in torr) VS
C Millivolt reading for certain VOLTAGE
C Example: 'ANS02.RAW' is for constant voltage of 2 kV
      OPEN (18,FILE='ANS00.RAW',STATUS='NEW')
      OPEN (19,FILE='ANS02.RAW',STATUS='NEW')
      OPEN (20,FILE='ANS04.RAW',STATUS='NEW')
      OPEN (21,FILE='ANS06.RAW',STATUS='NEW')
      OPEN (22,FILE='ANS08.RAW',STATUS='NEW')
      OPEN (23,FILE='ANS10.RAW',STATUS='NEW')
      OPEN (24,FILE='ANS12.RAW',STATUS='NEW')
      OPEN (25,FILE='ANS14.RAW',STATUS='NEW')
      OPEN (26,FILE='ANS16.RAW',STATUS='NEW')
      OPEN (27,FILE='ANS18.RAW',STATUS='NEW')
      OPEN (28,FILE='ANS20.RAW',STATUS='NEW')
C Read all data from Voltage VS Millivolt reading files
```

```
      N=6
C The set of input data consists of 11 files with 11 data each
      DO 30 K=0,10
        N=N+1
        DO 20 I=0,10
          READ (N,7)VOLT(I),(X(K,I,J),J=1,6),(C(K,I,J),J=1,6)
 7        FORMAT (F4.1,6(1X,F5.1),6(1X,F5.3))
20      CONTINUE
        SPEED(K)=REAL(K)*2.0E-03
30    CONTINUE

C Alter the file
      M=17
C The set of output data consists of 11 files with 11 data each
      DO 50 I=0,10
      M=M+1
        DO 40 K=0,10
          WRITE (M,18)SPEED(K),(X(K,I,J),J=1,6),(C(K,I,J),J=1,6)
18        FORMAT (1X,F5.3,6(1X,F5.1),6(1X,F5.3))
40      CONTINUE
50    CONTINUE
      PRINT *,'ALTERATION COMPLETED ....'
      END
```

These sets of six raw data were then averaged and written to another set of files, together with the maximum and minimum values of each set to be processed by the drag computation program. Table F.3 and F.4 show examples of such files.

All plots were created using CABAL on EVAX system.

Table F.1: Sample data from AC Source—normal orientation, with 0.002 torr pressure reading: constant air speed

Voltage	Strain (voltage reading)					
kV	mV	mV	mV	mV	mV	mV
0.0	3.0	3.0	2.8	2.8	2.8	2.9[a]
2.0	2.5	2.5	2.3	2.3	2.2	2.4
4.0	1.3	1.2	1.0	1.0	1.0	1.2
6.0	-0.4	-0.3	-0.6	-0.6	-0.8	-0.5
8.0	-3.9	-4.1	-5.0	-4.8	-4.9	-4.7
10.0	-10.5	-10.1	-9.7	-9.1	-9.6	-9.1
12.0	-12.5	-14.5	-14.7	-14.6	-14.0	-14.8
14.0	-13.2	-14.0	-14.2	-12.8	-13.6	-13.2
16.0	-13.6	-13.8	-14.6	-14.3	-14.9	-16.0
18.0	-13.8	-13.2	-12.8	-9.5	-11.1	-10.0
20.0	-13.1	-11.5	-11.8	-10.5	-11.4	-11.2

Table F.2: Sample data from AC Source—normal orientation, with 2 kV high voltage discharge: constant high voltage discharge

Air speed	Strain (voltage reading)					
torr	mV	mV	mV	mV	mV	mV
0.000	-0.5	-0.4	-0.5	-0.5	-0.6	-0.6
0.002	2.5	2.5	2.3	2.3	2.2	2.4
0.004	4.8	4.9	4.7	4.8	4.9	4.9
0.006	6.9	7.2	7.1	7.2	7.2	7.1
0.008	8.9	9.0	9.1	9.0	8.9	9.0
0.010	10.9	10.8	10.9	10.9	10.8	10.9
0.012	12.0	12.1	12.1	12.0	12.0	12.2
0.014	14.0	14.1	14.1	14.2	14.1	14.3
0.016	15.8	16.0	15.8	16.0	15.9	16.0
0.018	18.0	18.1	18.2	18.2	18.2	18.2
0.020	19.8	19.8	19.9	19.9	19.8	19.9

[a]The actual files consist of 6 strain-data and 6 current-data; however, due to the text-width limitation, only the strain-data are presented here. Also in the constant high voltage discharge table.

Table F.3: Sample data from AC Source—normal orientation with voltage 2 kV: average, maximum and minimum

Air speed	Strain (voltage reading)			Current (voltage reading)		
	average	max.	min.	average	max.	min.
torr	mV	mV	mV	V	V	V
0.00E+00	-0.517	-0.400	-0.600	0.012	0.012	0.011
0.20E-02	2.367	2.500	2.200	0.012	0.012	0.011
0.40E-02	4.833	4.900	4.700	0.012	0.012	0.011
0.60E-02	7.117	7.200	6.900	0.012	0.012	0.011
0.80E-02	8.983	9.100	8.900	0.012	0.012	0.011
0.10E-01	10.867	10.900	10.800	0.012	0.012	0.011
0.12E-01	12.067	12.200	12.000	0.012	0.012	0.011
0.14E-01	14.150	14.300	14.000	0.012	0.012	0.011
0.16E-01	15.917	16.000	15.800	0.012	0.012	0.011
0.18E-01	18.150	18.200	18.000	0.012	0.012	0.011
0.20E-01	19.850	19.900	19.800	0.012	0.012	0.011

Table F.4: Sample data from AC Source—normal orientation, with voltage 2 kV: drag data

Velocity	Re	Drag force	Drag Coef.	Abs. force	Current
(m/s)		N		N	mA
0.6598	0.1129E+04	0.4182E-04	0.4100E-01	0.3101E-04	0.1227E-02
0.9331	0.1596E+04	0.8821E-04	0.4324E-01	0.7740E-04	0.1227E-02
1.1428	0.1955E+04	0.1298E-03	0.4242E-01	0.1190E-03	0.1227E-02
1.3196	0.2258E+04	0.1603E-03	0.3929E-01	0.1495E-03	0.1227E-02
1.4754	0.2524E+04	0.1913E-03	0.3752E-01	0.1805E-03	0.1227E-02
1.6162	0.2765E+04	0.2042E-03	0.3336E-01	0.1934E-03	0.1227E-02
1.7457	0.2987E+04	0.2407E-03	0.3371E-01	0.2299E-03	0.1227E-02
1.8662	0.3193E+04	0.2688E-03	0.3295E-01	0.2580E-03	0.1227E-02
1.9794	0.3387E+04	0.3095E-03	0.3372E-01	0.2987E-03	0.1227E-02
2.0865	0.3570E+04	0.3360E-03	0.3294E-01	0.3252E-03	0.1227E-02